8-2015

Timing and Extent of the Little Ice Age Glacial Advances in the Eastern Tian Shan, China

Yanan Li

University of Tennessee - Knoxville, yli49@vols.utk.edu

To the Graduate Council:

I am submitting herewith a dissertation written by Yanan Li entitled "Timing and Extent of the Little Ice Age Glacial Advances in the Eastern Tian Shan, China." I have examined the final electronic copy of this dissertation for form and content and recommend that it be accepted in partial fulfillment of the requirements for the degree of Doctor of Philosophy, with a major in Geography.

Yingkui Li, Major Professor

We have read this dissertation and recommend its acceptance:

Henri D. Grissino-Mayer, Carol P. Harden, Jon Harbor, David G. Anderson

Accepted for the Council:
Dixie L. Thompson

Vice Provost and Dean of the Graduate School

(Original signatures are on file with official student records.)

**Timing and Extent of the Little Ice Age Glacial Advances in
the Eastern Tian Shan, China**

A Dissertation Presented for the
Doctor of Philosophy
Degree
The University of Tennessee, Knoxville

Yanan Li
August 2015

Dedication

To my dear husband, Xiaoyu Lu, for his company, sacrifice, patience, humor, tolerance, encouragement, and everything he did for me.

To my parents, for their unconditional love and support along the way I grow.

To my advisor, for his countless hours of painstaking work to help me in my pursuit of knowledge.

To my friends, for sharing fun and pain together.

Acknowledgments

I would like to express my deepest appreciation to my advisor, Dr. Yingkui Li, for his inspiration during the years of my doctoral program. He evoked my interests in glacial geomorphology. This work would not have been possible without his guidance, encouragement, and patience. As his first Ph.D. student, I feel that I benefit so much from his careful and thoughtful cultivation. His wide range of research expertise, his intelligence in problem solving, his enthusiasm in field investigations, his open mind to new knowledge, and his down-to-earth personality make me so grateful to working with him. I appreciate his positive attitudes, which motivated me when I had doubts in myself. For my every piece of achievements, he cheered heartedly; for my more frequent unsatisfactory results or barriers, he helped me find the outlet, or more importantly, taught me how to find the outlet. Dr. Li provided me great help in this dissertation work, from carrying rock samples in the field to rehearsing presentations at conferences, from details of lab operations to manuscript revisions.

I also want to thank my great group of committee members, Drs. Carol Harden, Henri Grissino-Mayer, Jon Harbor, and David Anderson. Each of them intellectually stimulates me with their immense knowledge and valuable experience. I appreciate the help and opportunities that they provided me throughout my graduate tenure, and also the cooperative participation that made my every key step towards the graduation achieved. Their expertise in different areas of natural sciences often inspires me with ideas to expand and deepen the current research interests.

This dissertation work in Tian Shan was based on an international collaboration of Drs. Li and Harbor and other scholars from many institutes with a goal to reconstruct past glaciations across major transects of Central Asia. In 2010, I was introduced to the group during the glacial/fluvial geomorphology expedition in Tian Shan, supported by the National Science Foundation of China (No. 41328001). In spring 2012, I received a National Geographic Young

Abstract

Located in Central Asia, one of the most continental regions on Earth, the Tian Shan's glaciers contribute critical fresh water to populated areas in the lowland. These glaciers are sensitive to climate change, and knowledge of contemporary glaciers and their changes in the past is of critical importance for sustainable development in this region. Constraining glacial fluctuations in recent centuries will fill a gap in numerical constraints on glacial history and paleoclimate information, and provide important evidence on the spatio-temporal changes of the climate systems in the Tian Shan. This doctoral dissertation investigates the timing and extent of Little Ice Age (LIA) glacial advances in the eastern Tian Shan. In particular, I conducted: 1) the mapping of glacial extents during the LIA and around 2010 using Google Earth high-resolution imagery and ArcGIS; 2) statistical analyses to examine relationships between local topographic/geometric factors and glacier change parameters; and 3) cosmogenic ^{10}Be [beryllium 10] surface exposure dating of presumed LIA moraines.

The major contributions of this dissertation include: 1) a total of 1173 contemporary glaciers with their corresponding presumed LIA extents were delineated in the eastern Tian Shan; 2) glacier area and mean elevation are the two major local factors that affect glacier area changes, but topographic/geometric factors cannot well explain changes in equilibrium line altitudes; 3) three major LIA advances occurred at 730±300 yr BP, 370±100 yr BP, and 210±50 yr BP were constrained based on ^{10}Be surface exposure ages, and the maximum LIA extent (about 700–900 m beyond glacier termini) was reached asynchronously in different sub-regions; 4) presumed LIA moraines in front of small, thin glaciers yielded widely scattered and much older ages than LIA ages. The glacial deposits in front of such glaciers might have formed prior to the LIA and have been reworked during non-erosive glacial transport in LIA. This suggests

that inheritance could be a more significant problem than degradation in the exposure age scatter of young glacial event. More dating work is needed to extend our knowledge on LIA glacial advances, and to better understand the influence of climate systems on glacier changes.

Table of Contents

List of Tables

List of Figures

xi

Chapter 1

Introduction

1.1. Research Overview

The concept of the Little Ice Age (LIA) was first introduced by Matthes (1939) to describe glacial advances to an extensive position after the warm epoch of mid-Holocene and before the 20th century, but controversy exists over whether this cold event occurred synchronously and worldwide (Jones and Bradley 1992; Landsberg 1985). Although the concept of the LIA is now widely accepted as a cold period from approximately AD 1300 to 1850, the exact ages of the LIA period vary from place to place. Most evidence for the LIA was assembled in Europe and North America in early studies (e.g. Grove 2001; Mann 2002; Karlen 1988; Fagan 2000; Appleby 1980; Matthews and Briffa 2005; Pfister 1980). Over the past decades, studies have been expanded around the world to reconstruct the climate signal and to identify the extent of glacial advances during the LIA (e.g. Barclay, Wiles, and Calkin 2009; Benedict 1968; Bräuning 2006; Koch and Kilian 2005; Luckman 2000; Mosley-Thompson et al. 1990; Schaefer et al. 2009; Xu and Yi 2014). However, few glacial chronologies have been established to constrain the glacial advances during the LIA across the Tian Shan, where glaciers supply critical freshwater to arid and semi-arid Central Asia (Koppes et al. 2008; Li et al. 2014; Solomina, Barry, and Bodnya 2004; Yi et al. 2004). The motivation for this research comes from the need for direct dating of presumed LIA moraines in the Tian Shan in paleoenvironmental studies, as well as an interest in examining the controlling factors that underlie the spatio-temporal pattern of glacial retreat after the LIA.

In this doctoral dissertation, I investigated the extent and timing of the LIA glacial advances in the eastern Tian Shan using [10]Be surface exposure dating and mapping the LIA and contemporary glacial extents in Google Earth. Understanding the spatio-temporal pattern of LIA glacial advances provides insights into the variations in climate controls of glacial activities and

the impact of local topographic and geometric factors, such as glacier area, slope, aspect, shape, hypsometry, and elevation, on glacier changes. Maps of glacial extents during the LIA and the most recent decade can also provide a dataset for documenting the status of glaciers. Because glaciers serve as important freshwater resource in this region of Central Asia, studying the response of glaciers to climate change during past centuries is of critical importance for better estimating future glacial and environmental changes that might have significant impacts on water availability and water security in this rapidly developing region.

1.2. Tian Shan and Related Studies

1.2.1. Regional context: geographic, climate, and socio-economic settings

The Tian Shan ("Heavenly Mountains" in Chinese) is one of the largest mountain ranges in Central Asia (Figure 1-1). It stretches from the western boundary of Kyrgyzstan across Xinjiang Uighur Autonomous Region in China, and almost reaches Mongolia, with a WSW-ENE orientation and a length of about 2500 km. It was formed by the collision of the Indian and Eurasian continental plates about 40 to 50 million years ago (Yin and Harrison 2000). The Tian Shan comprises many individual ranges, most of which reach about 4000 m above sea level (a.s.l.). The highest peak is Mt. Tumur (also known as the Victory Peak, Jengish Chokusu, or Peak Pobeda, 7439 m a.s.l.), located along the border of Kyrgyzstan, Kazakhstan, and China. The Tian Shan is bounded by the Taklimakan Desert to the south and the Gurbantonggut Desert to the north, characterized with a sharp contrast of landscapes of high mountains and intervening valleys/basins.

The Tian Shan has a continental climate, with high aridity and extreme contrasts in seasonal and diurnal temperatures. For example, at a height around 3500 m a.s.l. in the central Tian Shan, monthly mean temperatures are −16 to −13 ℃ in winter months (December–

3

Feburary), and 3 to 5 ℃ in summer months (June–August) (Ye et al. 2005). Two climate systems control this region: the moisture-bearing mid-latitude westerlies and the Siberian High pressure system (Aizen et al. 2001; Aizen et al. 1997; Gong and Ho 2002; Sorg et al. 2012). The Tian Shan acts as a mountain barrier to air masses moving toward them, and is an important control of the climate patterns in surrounding areas. This orographic effect leads to a sharp precipitation gradient, with precipitation decreasing from west to east. On the windward northwestern mountain slopes, the annual precipitation at high elevations can be up to 1500 to 2000 mm; while, to the east and in the interior regions, it is as low as <100 mm (Sorg et al. 2012). Most precipitation in the eastern Tian Shan occurs during the summer (Aizen et al. 1997). The Asian Monsoon systems hardly penetrate into the Tian Shan area due to the orographic barriers of the Himalayas and the Tibetan Plateau (Chen et al. 2008).

Glaciers develop at high elevations in the Tian Shan and play an important role in the hydrologic cycle, water balance, ecosystems, and socio-economic development of Central Asia. Meltwater from glaciers feeds into rivers, including the Syr Darya River, the Ili River, the Kaidu River, and the Urumqi River (Figure 1-1), providing essential water supply for ecosystems and human beings in surrounding areas. For example, the ancient trade route, the Silk Road, was established because of the existence of civilizations that were closely associated with the oases nourished by melting glaciers and mountain snow (Liu et al. 2014). Today, meltwater from glaciers in the Tian Shan provides the water supply for a population of approximately 50 million in the Central Asian countries. Due to the rapid urbanization, agriculture, and industrial development, these countries are facing intensive stress in water supply (Varis 2014). Thus, glaciers are an important freshwater source and should be carefully documented and investigated for the present and future water management in this region.

1.2.2. Documenting the presence of glaciers

Glaciers in the Tian Shan are commonly found at elevations between 2800 m a.s.l. and 7500 m a.s.l. Aizen et al. (2006) mapped glaciers in the Kyrgyz Tian Shan based on remote sensing data and identified 7590 glaciers with a total area of 13271 km^2 and an estimated 1840 km^3 volume of ice. An inventory of glaciers in the Chinese Tian Shan was compiled by Chinese glaciologists in the 1970s based on field investigations, topographic maps, and aerial photographs. The inventory was published by Wang et al. (1986) in Chinese and by Shi (2008) in English. They reported 9035 glaciers in the Chinese Tian Shan, which covered an area of 9225 km^2 with an estimated ice volume of 1011 km^3 (Shi, Liu, and Kang 2009).

The Global Land Ice Measurement from Space (GLIMS) project aims to establish a glacier inventory of the whole world (Cogley 2010; Ohmura 2009; Raup et al. 2007). With their free accessibility, standardization, worldwide contribution, and high percent of coverage, the GLIMS data are often considered to accurately represent the status of glaciers. The glacier inventory of Shi, Liu, and Kang (2009) in the Chinese Tian Shan has been incorporated into the GLIMS data. This inventory advanced our knowledge of Tian Shan glaciers, but the fact that glaciers have been continuously retreating in recent decades hampers the use of this dataset as an appropriate representation of present glaciers. In addition, glacier boundaries determined in the original study might have a high level of uncertainty due to data sources and techniques used in the 1970s.

In the past decade, Google Earth has become a popular platform in Earth surface studies. The high-resolution satellite images assembled from a variety of sources in this platform enhance interpretations of land features. Google Earth has been used in many glacial studies to check modern glaciers and glacial landforms (e.g. Kassab, Wang, and Harbor 2013; She et al. 2014;

Stroeven et al. 2013), but few studies have been conducted to directly map glaciers with Google Earth for a large region like the eastern Tian Shan. Although manual delineation of glaciers and their related landforms can be time consuming, Google Earth-based mapping provides a relatively high accuracy that may not be achieved using other data sources and methods (Yu and Gong 2012). Maps of contemporary and LIA glaciers provide not only a visualization of glacial retreat pattern, but also an updated dataset of glacier information in the region.

1.2.3. How to determine whether a glacial advance occurred in the Little Ice Age?

Glaciers might have advanced during the LIA and produced distinct glacial landforms in front of present-day glaciers. Matthes (1939) noted that many of the small cirque glaciers in the mountain ranges in the western U.S. are fronted "… by very fresh-looking terminal moraines arranged in compact concentric series or combined into one or two massive compound embankments…" He later noted that, "Indeed, there already is considerable evidence indicating that the glacier-oscillations of the last few centuries have been among the greatest that have occurred during the 4000-year period, …" (Matthes 1939). In early studies, the period of glacial advances in the latter half of the Holocene was commonly recognized as the Neoglacial period (e.g. Benedict 1968; Mosley-Thompson et al. 1990; Moss 1951; Porter and Denton 1967); but, with more detailed studies and advances in dating techniques, the LIA has been identified as a separated period of glacial expansions that occurred in the past several centuries (Grove 2004). Evidence has revealed high variability in the timing and extent of LIA glacial advances around the world, indicating that the LIA was probably not a globally synchronous cold event (Bradley and Jones 1993; Chenet et al. 2010; Kreutz et al. 1997; Luthi 2014; Mann 2002; Mann, Bradley, and Hughes 1999).

To determine when a glacier reached its maximum extent during the LIA, one needs to know the time when its LIA moraine was deposited. As described in Matthes (1939) and later studies (e.g. Shi and Ren 1990; Su and Shi 2002; Xu and Yi 2014; Owen 2009), moraines formed during the LIA look fresh, have massive loose boulders piled on their tops and steep sides, and are located hundreds of meters to a few kilometers away from the present-day glacier terminus. A variety of methods applied to date LIA moraines have been based on proxy materials, such as buried wood, trees, and lichens. Radiocarbon dating of organic matter in or underlying the moraine has been used to estimate the formation time of the presumed LIA moraines in many places (e.g. Derbyshire et al. 1984; Jiao et al. 2005; Matthews 1991). Dendrochronological methods are frequently used to estimate the moraine deposition age if either 1) trees were killed or disturbed by an ice margin advance, or 2) new trees growing on the moraine are present. Dating the last year of dead trees or the first year of the new growing trees has helped identify LIA glacial events (e.g. Bräuning 2006; Koch and Kilian 2005; Luckman 2000; Viereck 1967; Wiles, Barclay, and Calkin 1999). Another method used to date LIA moraines is lichenometric dating (e.g. Solomina, Barry, and Bodnya 2004; Loso, Doak, and Anderson 2014; Matthews and Shakesby 1984; Winkler 2000), in which moraine ages are derived using the growth curve of the largest lichen on the moraine. These methods provide valuable tools for constraining the formation ages of presumed LIA moraines (Figure 1-2). However, in regions like the eastern Tian Shan, the lack of organic material or trees at high elevations restricts the use of these methods. A few studies have attempted to date moraines using lichenometry and radiocarbon dating of inorganic carbonate coatings on moraine clasts in the eastern Tian Shan. For example, Chen (1989) dated three moraines in front of the Glacier No.

1 to 412±20 yr BP[1], 173±20 yr BP, and 79±20 yr BP, using lichenometry. Yi et al. (2004) used

AMS ^{14}C dating of inorganic carbonate coating from the same outermost moraine and obtained

ages of 400±120 yr BP and 430±120 yr BP (recalculated in Xu and Yi 2014).

Since the early 1990s, the development of the in-situ-produced cosmogenic nuclide (CN)

dating technique has allowed great progress in dating glacial landforms. A rapid increase of

publications associated with this technique reflects its recent popularity (Figure 1-3). This dating

method is based on the fact that cosmogenic nuclides are produced predictably over time when

minerals became exposed to and bombarded by cosmic rays. The rock surface accumulates a

certain cosmogenic nuclide at a production rate which depends on latitude/longitude location,

altitude, and depth below the surface (Balco 2011). Thus, by measuring the concentration of such

nuclide and knowing the production rate at a sample site, the time of exposure can be determined

for the sample surface. With an assumption of zero surface erosion, the exposure time can be

resolved using equation (1),

$$t = -\frac{1}{\lambda}ln[1 - \frac{\lambda N}{P}] \tag{1}$$

where t is the exposure time; N is the nuclide concentration (in atoms g^{-1}); P is the production

rate (atoms g^{-1} yr^{-1}); λ is the decay constant, which equals 4.99×10^{-7} yr^{-1} for ^{10}Be (Balco 2011;

Gosse and Phillips 2001; Ivy-Ochs and Kober 2008; Lal 1991; Li and Harbor 2009).

Currently the cosmogenic nuclides used in Quaternary geochronology and landscape

evolution studies include radioactive nuclides ^{10}Be, ^{26}Al, ^{36}Cl, and ^{14}C, and stable noble gases

^{3}He and ^{21}Ne. Among them, ^{10}Be is the most widely used nuclide in glacial chronology because

of its low detection limit and relatively well-constrained production rate (Balco 2011). Another

---

[1]BP: before present (1950 AD).

advantage of ^{10}Be CN dating is that the primary target mineral, quartz, is almost ubiquitous in glacial environments and resistant to chemical weathering (Gosse and Phillips 2001).

The time range of ^{10}Be CN dating usually spans from 10^3 to 10^6 years, but with technical improvements, studies have successfully applied it to date events on timescales of 10^2 years (Kelly et al. 2008; Owen et al. 2010; Schimmelpfennig et al. 2014; Finkel et al. 2003; Koppes et al. 2008; Li et al. 2014; Owen et al. 2005; Schaefer et al. 2009; Seong et al. 2009). For example, a high-resolution glacial chronology with five events during the last millennium was developed for the Southern Alps of New Zealand (Schaefer et al. 2009). The youngest glacial fluctuation during the LIA was dated to 105±30 yr BP, while the LIA maximum extent was dated to 515±70 yr BP (Schaefer et al. 2009). Koppes et al. (2008) measured two ^{10}Be ages for the LIA moraines in the Ala Archa Valley of the Kyrgyz Tian Shan. Li et al. (2014) constrained four clustered LIA ages of 340±40 yr BP for Glacier No. 1 in the eastern Tian Shan. Chen et al. (2015) obtained six ages dated to 730±300 yr BP in the Karlik Range of the easternmost Tian Shan.

1.2.4. Factors controlling glacier change

Climate is the major factor driving glacial advance or retreat. Increased precipitation and/or decreased temperature usually lead to glacier growth; in contrast, decreased precipitation and/or increased temperature may cause glacier retreat. The balance between ice accumulation and ablation on glacier surface is measured by mass balance, an important indicator of how glaciers respond to climate variability (Hagen and Reeh 2003). A positive mass balance at a location of glacier surface represents that the supply of mass mainly by snow deposition exceeds the loss of mass mainly by snow/ice melting, and vice versa. In arid regions like Central Asia, sublimation is another major factor affecting glacier surface mass balance. Low air humidity, high solar radiation, and strong winds lead to large sublimation rates (Gascoin et al. 2013). In the

eastern Tian Shan, these climate conditions might play a key role in glacier changes and spatial pattern of different changing magnitudes.

Different responses of glaciers can be used to examine influences of climate systems in different regions. In the Tian Shan, the surface mass balance of glaciers is mainly controlled by the interaction of the westerlies and the Siberian High (Aizen et al. 2006; Benn and Owen 1998; Sorg et al. 2012; Gong and Ho 2002). Zech (2012) proposed that moisture advected by the westerlies contributed to glacial advances that occurred during Marine Oxygen Isotope Stages (MIS) 3 in the Kyrgyz Tian Shan and southern Pamir mountain ranges. The relatively restricted glacial advances during the global Last Glacial Maximum (LGM, which occurred during MIS 2) in the Tian Shan have been explained as a consequence of reduced moisture advection via the westerlies due to lee effects behind the massive Fennoscandian Ice Sheet and/or blocking of the westerlies by a strong Siberian High, resulting in an arid condition during MIS 2 (Abramowski et al. 2006; Koppes et al. 2008; Narama et al. 2007; Zech 2012; Zech et al. 2005). The Siberian High, formed on the northeastern part of the Eurasia, brings intensive cold air masses and high pressure to Central Asia (Aizen et al. 2001; Gong and Ho 2002). It may have relatively stronger impact on the eastern section than on the western section of the Tian Shan. Changes in equilibrium line altitude (ELA), as an indicator of glacier change, were examined by Li et al. (2014) for MIS 4, 3, and 2 glacial advances across the Tian Shan, and no spatial pattern was found in magnitudes of ELA changes. They suggested that the cold conditions enhanced by the Siberian High might favor glacier development in the eastern Tian Shan and counteract the diminishing effect of the moisture-bearing westerlies.

In addition to the climate controls, local topographic and geometric factors, such as slope, area, aspect, and shape, also function as important drivers for different glacier changes. Small

glaciers have changed more significantly in size than large ones in recent decades because of less favorable topographic settings (e.g. Bhambri et al. 2011; Li et al. 2011; Liu et al. 2003). Most glaciers that are preserved today in middle and high latitudes have poleward aspects because glaciers with these aspects receive less solar radiation than glaciers with other aspects (Evans 2006). Kerr (2013) argued for the possibility of overestimating the contribution of glacial melting to sea level rise because most glaciers that glaciologists can access easily are located on relatively gentle terrain and are more vulnerable to climate change, compared to the relatively stable glaciers located on rough terrain, which are usually not easy to access. However, only limited studies have been conducted to examine the relationship between local topographic/geometric factors and glacier changes. It is possible that the topographic setting, the characteristics of a glacier itself, and changes of climate conditions interact together to drive glacier change over time and space.

Debris cover in the ablation zone also affects ice melt rates and responses of a glacier to climate change because the heat conduction is modified by the debris layer, and in particular, the ablation rate increases with increasing debris thickness once a critical thickness is exceeded (e.g. Kayastha et al. 2000; Östrem 1959; Scherler, Bookhagen, and Strecker 2011). Since most glaciers in the eastern Tian Shan are clean-ice glaciers, this factor is not considered in this research.

1.3. Research Hypotheses and Objectives

This study focuses on mapping, dating, and investigating climate and topographic controls on LIA glacial advances in the eastern Tian Shan, China. Although Tian Shan glaciers have received significant attention, quantitative constraints for the timing of glacial advances during the LIA are still limited. One main goal of this study is to investigate the extent and

timing of the maximum LIA glacial advances in the study region using ^{10}Be CN dating, which can fill a gap in paleoclimate information for this critical region. In addition, the spatial pattern of glacier change from the LIA to present is examined. Based on Google Earth mapping of contemporary glaciers and LIA glacial extents, glacier change can be visually examined, and indicators of glacier change can be derived for statistical analyses. The dynamics of clean-ice glaciers in the eastern Tian Shan are assumed to be mainly controlled by topography and climate (Owen et al. 2005; Pedersen and Egholm 2013). Based on the assumption that glaciers have experienced similar climate influence at a relatively small region, variations in individual glacier changes can be interpreted as reflecting the influences of local topographic and geometric parameters of glaciers. In a large area, such as the study region of the eastern Tian Shan, different climate conditions would affect the spatial pattern of glacier changes along with the local topographic and geometric factors.

Overall, this dissertation research aims to test the following hypotheses:

1) Area and mean elevation are the most significant topographic and geometric factors compared to other factors, including slope, aspect, shape, and hypsometry, to glacier changes in the eastern Tian Shan at a local scale.

2) The outermost moraine of the presumed LIA moraine sets was formed during the LIA.

3) The timing of the maximum LIA glacial advance was not synchronous among various sites in the eastern Tian Shan.

The major objectives of this study are:

1) to map the maximum extent of the LIA glacial advances over the eastern Tian Shan (Chapter 2);

2) to examine statistical relationships between local topographic and geometric factors and changes in glacier area and equilibrium line altitude since the LIA (Chapter 3); and

3) to date the presumed LIA moraines using ^{10}Be CN dating and examine the influence of climate and local factors on the spatio-temporal pattern of the LIA glacial advances in the eastern Tian Shan (Chapter 4).

1.4. Research Significance

Most glacial studies in the Tian Shan have focused on either the most recent decades or paleo-glaciations before the Holocene, whereas relatively few studies have examined glacier changes during the past several centuries. In particular, little is known about glacial fluctuations since the LIA. This study is the first to investigate the timing and controlling factors of LIA glacial advances across a large region in Central Asia. Cosmogenic ^{10}Be ages of the presumed LIA moraines can not only help interpret if glacial advances in fact occured during the LIA, but can also provide a unique opportunity for comparing results derived from various dating methods, including lichenometry or radiocarbon dating. Deciphering the timing and extent of LIA advances is critical to understanding past climate conditions in the Tian Shan because transitional regions are particularly sensitive to changes in shifting dominance of climate systems. Knowledge gained in this study will be useful for building and testing climate models to predict future climate scenarios, not only in Central Asia, but also in other parts of Asia affected by the same atmospheric circulations. In addition, the updated maps of contemporary glaciers and the maximum LIA glacial extents produced by this work can provide valuable information about the distribution of glaciers that can be directly used by other scholars.

1.5. Organization of the Dissertation

This dissertation is organized in a manuscript format that includes three manuscripts targeted for different journals.

Chapter 2 focuses on mapping contemporary glaciers and the maximum LIA glacial extents in the eastern Tian Shan. A total of 1173 modern glaciers and their corresponding presumed LIA extents were manually delineated using Google Earth. Although uncertainties and limitations exist, this approach takes advantages of the repository of high-resolution satellite imagery in Google Earth, which is freely accessible, and demonstrates its potential for glacier mapping. I estimated the areal reduction of glaciers in three sub-regions from their assumed LIA maximum extent to their positions in the 2010s. The map product is attached at the end of Chapter 2. The glacier datasets are provided separately in Appendices.

In Chapter 3, I examine the relationship between the topographic/geometric factors and glacier changes since the LIA. One sub-region with a confined area was selected. Using the 30-m Advanced Spaceborne Thermal Emission and Reflection Radiometer (ASTER) global digital elevation model (DEM), I quantified six topographic/geometric parameters for each glacier and estimated the ELA change and the relative area change since the LIA. The relationships between the local factors and glacier changes were established using a stepwise regression model.

In Chapter 4, I present ^{10}Be exposure ages of boulder samples collected from five glacial valleys at two study areas in the eastern Tian Shan. These ages were used to determine whether the assumed LIA moraines had formed during the LIA. I reconstructed the sequence of glacial advances during the LIA along with other available ^{10}Be ages in the region, and compared the timing and extent of the maximum LIA extent at different sites. I also examined the possible causes for the age scatter. Using the topographic maps of the 1960s, I analyzed the glacial history

of advances and retreats since the LIA. Finally, I discussed potential climate and local factors that could drive the spatio-temporal pattern of LIA glacier changes across the eastern Tian Shan.

I summarize the major findings about the LIA glacial advances in the eastern Tian Shan in Chapter 5 and discuss the potential tasks for future work. The data associated with this research are provided in Appendices.

References

Abramowski, U., A. Bergau, D. Seebach, R. Zech, B. Glaser, P. Sosin, P. W. Kubik, and W. Zech. 2006. Pleistocene glaciations of Central Asia: results from [10]Be surface exposure ages of erratic boulders from the Pamir (Tajikistan), and the Alay-Turkestan range (Kyrgyzstan). *Quaternary Science Reviews* 25(9–10): 1080–1096.

Aizen, E. M., V. B. Aizen, J. M. Melack, T. Nakamura, and T. Ohta. 2001. Precipitation and atmospheric circulation patterns at mid-latitudes of Asia. *International Journal of Climatology* 21(5): 535–556.

Aizen, V. B., E. M. Aizen, D. R. Joswiak, K. Fujita, N. Takeuchi, and S. A. Nikitin. 2006. Climatic and atmospheric circulation pattern variability from ice-core isotope/geochemistry records (Altai, Tien Shan and Tibet). *Annals of Glaciology* 43: 49–60.

Aizen, V. B., E. M. Aizen, J. M. Melack, and J. Dozier. 1997. Climatic and hydrologic changes in the Tien Shan, Central Asia. *Journal of Climate* 10(6): 1393–1404.

Appleby, A. B. 1980. Epidemics and famine in the Little Ice Age. *The Journal of Interdisciplinary History* 10(4): 643–663.

Balco, G. 2011. Contributions and unrealized potential contributions of cosmogenic-nuclide exposure dating to glacier chronology, 1990–2010. *Quaternary Science Reviews* 30(1–2): 3–27.

Barclay, D. J., G. C. Wiles, and P. E. Calkin. 2009. Holocene glacier fluctuations in Alaska. *Quaternary Science Reviews* 28(21): 2034–2048.

Benedict, J. B. 1968. Recent glacial history of an alpine area in the Colorado Front Range, USA. II: Dating the glacial deposits. *Journal of Glaciology* 7(49): 77–87.

Benn, D. I., L. A. Owen. 1998. The role of the Indian summer monsoon and the mid-latitude westerlies in Himalayan glaciation: review and speculative discussion. *Journal of the Geological Society* 155: 353–363.

Bhambri, R., T. Bolch, R. K. Chaujar, and S. C. Kulshreshtha. 2011. Glacier changes in the Garhwal Himalaya, India, from 1968 to 2006 based on remote sensing. *Journal of Glaciology* 57(203): 543–556.

Bradley, R. S., and P. D. Jones. 1993. 'Little Ice Age' summer temperature variations: Their nature and relevance to recent global warming trends. *The Holocene* 3(4): 367–376.

Bräuning, A. 2006. Tree-ring evidence of 'Little Ice Age' glacier advances in southern Tibet. *The Holocene* 16(3): 369–380.

Chen, F., Z. Yu, M. Yang, E. Ito, S. Wang, D. B. Madsen, X. Huang, Y. Zhao, T. Sato, H. J. B. Birks, I. Boomer, J. Chen, C. An, and B. Wuennemann. 2008. Holocene moisture evolution in arid central Asia and its out-of-phase relationship with Asian monsoon history. *Quaternary Science Reviews* 27(3–4): 351–364.

Chen, J. 1989. Preliminary researches on lichenometric chronology of Holocene glacial fluctuations and on other topics in the headwater of Urumqi River, Tianshan Mountains. *Science in China Series B-Chemistry* 32(12): 1487–1500.

Chen, Y., Y. Li, Y. Wang, M. Zhang, Z. Cui, C. Yi, and G. Liu. 2015. Late Quaternary glacial history of the Karlik Range, easternmost Tian Shan, derived from [10]Be surface exposure and optically stimulated luminescence datings. *Quaternary Science Reviews* 115: 17–27.

Chenet, M., E. Roussel, V. Jomelli, and D. Grancher. 2010. Asynchronous Little Ice Age glacial maximum extent in southeast Iceland. *Geomorphology* 114(3): 253–260.

Cogley, J. G. 2010. A more complete version of the World Glacier Inventory. *Annals of Glaciology* 50(53): 32–38.

Derbyshire, E., J. Li, F. Perrott, S. Xu, and R. Waters. 1984. Quaternary glacial history of the Hunza Valley, Karakoram mountains, Pakistan. *The International Karakoram Project* 2: 456–495.

Dong, H. L., H. C. Jiang, B. S. Yu, and X. Q. Liu. 2010. Impacts of environmental change and human activity on microbial ecosystems on the Tibetan Plateau, NW China. *GSA Today* 20(6): 4–10.

Evans, I. S. 2006. Local aspect asymmetry of mountain glaciation: A global survey of consistency of favoured directions for glacier numbers and altitudes. *Geomorphology* 73(1–2): 166–184.

Fagan, B. M. 2000. *The Little Ice Age: How climate made history, 1300–1850*: Basic Books. 246 pp.

Finkel, R. C., L. A. Owen, P. L. Barnard, and M. W. Caffee. 2003. Beryllium-10 dating of Mount Everest moraines indicates a strong monsoon influence and glacial synchroneity throughout the Himalaya. *Geology* 31(6): 561–564.

Gascoin, S., S. Lhermitte, C. Kinnard, K. Bortels, and G. E. Liston. 2013. Wind effects on snow cover in Pascua-Lama, Dry Andes of Chile. *Advances in Water Resources* 55: 25–39.

Gong, D. Y., and C. H. Ho. 2002. The Siberian High and climate change over middle to high latitude Asia. *Theoretical and Applied Climatology* 72(1–2): 1–9.

Gosse, J. C., and F. M. Phillips. 2001. Terrestrial in situ cosmogenic nuclides: theory and application. *Quaternary Science Reviews* 20(14): 1475–1560.

Grove, A. T. 2001. The "Little Ice Age" and Its Geomorphological Consequences in Mediterranean Europe. In *The Iceberg in the Mist: Northern Research in pursuit of a "Little Ice Age,"* eds. A. J. Ogilvie and T. Jónsson, 121–136: Springer Netherlands.

Grove, J. M. 2004. Little ice ages: ancient and modern (2 volumes): Routledge, London. 718 pp.

Hagen, J. O., and N. Reeh. In situ measurement techniques: land ice. In *Mass balance of the cryosphere: observations and modelllinbg of contemporary and future changes*, eds, J. L. Bamber and A. J. Payne, 11–41: Cambridge University Press.

Ivy-Ochs, S., and F. Kober. 2008. Surface exposure dating with cosmogenic nuclides. *Eiszeitalter und Gegenwart* 57(1/2): 179–209.

Jiao, K. Q., S. Iwata, T. D. Yao, Z. F. Jing, and Z. Q. Li. 2005. Variation of Zepu Glacier and environmental change in the eastern Nyainqentanglha range since 3.2 ka BP. *Journal of Glaciology and Geocryology* 27(1): 74–79.

Jones, P. D., and R. S. Bradley. 1992. Climatic variations over the last 500 years. In *Climate since AD*, 649–665.

Karlen, W. 1988. Scandinavian glacial and climatic fluctuations during the Holocene. *Quaternary Science Reviews* 7(2): 199–209.

Kassab, C., J. Wang, and J. Harbor. 2013. Glacial geomorphology of the Dalijia Shan region, northeastern Tibetan Plateau. *Journal of Maps* 9(1): 98–105.

Kayastha, R. B., Y. Takeuchi, M. Nakawo, and Y. Ageta. 2000. Practical prediction of ice melting beneath various thickness of debris cover on Khumbu Glacier, Nepal, using a positive degree-day factor. In *Debris-Covered Glaciers*, eds. M. Nakawo, C. F. Raymond and A. Fountain, 71–81.

Kelly, M. A., T. V. Lowell, B. L. Hall, J. M. Schaefer, R. C. Finkel, B. M. Goehring, R. B. Alley, and G. H. Denton. 2008. A [10]Be chronology of lateglacial and Holocene mountain glaciation in the

Scoresby Sund region, east Greenland: implications for seasonality during lateglacial time. *Quaternary Science Reviews* 27(25–26): 2273–2282.

Kerr, R. A. 2013. Melting glaciers, not just ice sheets, stoking sea-level rise. *Science* 340: 798–798.

Koch, J., and R. Kilian. 2005. 'Little Ice Age' glacier fluctuations, Gran Campo Nevado, southernmost Chile. *The Holocene* 15(1): 20–28.

Koppes, M., A. R. Gillespie, R. M. Burke, S. C. Thompson, and J. Stone. 2008. Late Quaternary glaciation in the Kyrgyz Tien Shan. *Quaternary Science Reviews* 27(7/8): 846–866.

Kreutz, K., P. Mayewski, L. Meeker, M. Twickler, S. Whitlow, and I. Pittalwala. 1997. Bipolar changes in atmospheric circulation during the Little Ice Age. *Science* 277: 1294–1296.

Lal, D. 1991. Cosmic ray labeling of erosion surfaces: in situ nuclide production rates and erosion models. *Earth and Planetary Science Letters* 104(2): 424–439.

Landsberg, H. E. 1985. Historic weather data and early meteorological observations. In *Palaeoclimatic Analysis and Modelling*, ed. A. D. Hecht, 27–70: Wiley, New York.

Li, K. M., H. L. Li, L. Wang, and W. Y. Gao. 2011. On the relationship between local topography and small glacier change under climatic warming on Mt. Bogeda, eastern Tian Shan, China. *Journal of Earth* Science 22(4): 515–527.

Li, Y. K., and J. Harbor. 2009. Cosmogenic nuclides and geomorphology: Theory, limitations, and applications. In *Geomorphology and Plate Tectonics*, eds. D. M. Ferrari and A. R. Guiseppi, 1–33: Nova Science Publishers, Inc. Hauppauge, New York.

Li, Y. K., G. N. Liu, Y. X. Chen, Y. N. Li, J. Harbor, A. P. Stroeven, M. Caffee, M. Zhang, C. C. Li, and Z. J. Cui. 2014. Timing and extent of Quaternary glaciations in the Tianger Range, eastern Tian Shan, China, investigated using [10]Be surface exposure dating. *Quaternary Science Reviews* 98: 7–23.

Li, Y. K., G. N. Liu, P. Kong, J. Harbor, Y. X. Chen, and M. Caffee. 2011. Cosmogenic nuclide constraints on glacial chronology in the source area of the Urumqi River, Tian Shan, China. *Journal of Quaternary Science* 26(3): 297–304.

Liu, S. Y., W. X. Sun, Y. P. Shen, and G. Li. 2003. Glacier changes since the Little Ice Age maximum in the western Qilian Shan, northwest China, and consequences of glacier runoff for water supply. *Journal of Glaciology* 49(164): 117–124.

Liu, Y., F. Tian, H. Hu, and M. Sivapalan. 2014. Socio-hydrologic perspectives of the co-evolution of humans and water in the Tarim River basin, Western China: the Taiji-Tire model. *Hydrology and Earth System Sciences* 18(4): 1289–1303.

Loso, M. G., D. F. Doak, and R. S. Anderson. 2014. Lichenometric dating of Little Ice Age glacier moraines using explicit demographic models of lichen colonization, growth, and survival. *Geografiska Annaler: Series A, Physical Geography* 96(1): 21–41.

Luckman, B. H. 2000. The Little Ice Age in the Canadian Rockies. *Geomorphology* 32(3–4): 357–384.

Luthi, M. P. 2014. Little Ice Age climate reconstruction from ensemble reanalysis of Alpine glacier fluctuations. *Cryosphere* 8(2): 639–650.

Mann, M. E. 2002. Little Ice Age. *Encyclopedia of Global Environmental Change* 1: 504–509.

Mann, M. E., R. S. Bradley, and M. K. Hughes. 1999. Northern hemisphere temperatures during the past millennium: inferences, uncertainties, and limitations. *Geophysical Research Letters* 26(6): 759–762.

Matthes, F. E. 1939. Report of committee on glaciers, April 1939. *Eos, Transactions American Geophysical Union* 20(4): 518–523.

Matthews, J. A. 1991. The late Neoglacial ('Little Ice Age') glacier maximum in southern Norway: New ^{14}C-dating evidence and climatic implications. *The Holocene* 1(3): 219–233.

Matthews, J. A., and K. R. Briffa. 2005. The 'Little Ice Age': Re-evaluation of an evolving concept. *Geografiska Annaler: Series A, Physical Geography* 87(1):17–36.

Matthews, J. A., and R. A. Shakesby. 1984. The status of the 'Little Ice Age' in southern Norway: relative-age dating of Neoglacial moraines with Schmidt hammer and lichenometry. *Boreas* 13(3): 333–346.

Mosley-Thompson, E., L. G. Thompson, P. M. Grootes, and N. Gundestrup. 1990. Little Ice Age (neoglacial) paleoenvironmental conditions at Siple Station, Antarctica. *Annals of Glaciology* 14: 199–204.

Moss, J. H. 1951. Early man in the Eden Valley. In *University of Pennsylvania Museum Monograph*, 9–92: Philadelphia.

Narama, C., R. Kondo, S. Tsukamoto, T. Kajiura, C. Ormukov, and K. Abdrakhmatov. 2007. OSL dating of glacial deposits during the last glacial in the Terskey-Alatoo Range, Kyrgyz republic. *Quaternary Geochronology* 2(1–4): 249–254.

Ohmura, A. 2009. Completing the World Glacier Inventory. *Annals of Glaciology* 50(53): 144–148.

Östrem, G. 1959. Ice melting under a thin layer of moraine, and the existence of ice cores in moraine ridges. *Geografiska Annaler* 41(4): 228–230.

Owen, L. A. 2009. Latest Pleistocene and Holocene glacier fluctuations in the Himalaya and Tibet. *Quaternary Science Reviews* 28(21–22): 2150–2164.

Owen, L. A., R. C. Finkel, P. L. Barnard, H. Z. Ma, K. Asahi, M. W. Caffee, and E. Derbyshire. 2005. Climatic and topographic controls on the style and timing of Late Quaternary glaciation throughout Tibet and the Himalaya defined by Be-10 cosmogenic radionuclide surface exposure dating. *Quaternary Science Reviews* 24(12–13): 1391–1411.

Owen, L. A., C. Yi, R. C. Finkel, and N. K. Davis. 2010. Quaternary glaciation of Gurla Mandhata (Naimon'anyi). *Quaternary Science Reviews* 29(15–16): 1817–1830.

Pedersen, V. K., and D. L. Egholm. 2013. Glaciations in response to climate variations preconditioned by evolving topography. *Nature* 493(7431): 206–210.

Pfister, C. 1980. The little ice age: thermal and wetness indices for central Europe. *Journal of Interdisciplinary History* 10(4): 665–696.

Porter, S. C., and G. H. Denton. 1967. Chronology of neoglaciation in the North American Cordillera. *American Journal of Science* 265(3): 177–210.

Porter, S. C. 1979. Glaciologic evidence of Holocene climatic change. In *International Conference on Climate and History*, Review papers volume, 148–179: Norwich, UK.

Raup, B., A. Racoviteanu, S. J. S. Khalsa, C. Helm, R. Armstrong, and Y. Arnaud. 2007. The GLIMS geospatial glacier database: A new tool for studying glacier change. *Global and Planetary Change* 56(1–2): 101–110.

Schaefer, J. M., G. H. Denton, M. R. Kaplan, A. Putnam, R. C. Finkel, D. J. A. Barrell, B. G. Andersen, R. Schwartz, A. Mackintosh, T. Chinn, and C. Schluchter. 2009. High-frequency Holocene glacier fluctuations in New Zealand differ from the Northern signature. *Science* 324(5927): 622–625.

Scherler, D., B. Bookhagen, and M. R. Strecker. 2011. Spatially variable response of Himalayan glaciers to climate change affected by debris cover. *Nature Geoscience* 4(3): 156–159.

Schimmelpfennig, I., J. M. Schaefer, N. Akcar, T. Koffman, S. Ivy-Ochs, R. Schwartz, R. C. Finkel, S. Zimmerman, and C. Schluechter. 2014. A chronology of Holocene and Little Ice Age glacier culminations of the Steingletscher, Central Alps, Switzerland, based on high-sensitivity beryllium-10 moraine dating. *Earth and Planetary Science Letters* 393: 220–230.

Seong, Y. B., L. A. Owen, C. L. Yi, R. C. Finkel, and L. Schoenbohm. 2009. Geomorphology of anomalously high glaciated mountains at the northwestern end of Tibet: Muztag Ata and Kongur Shan. *Geomorphology* 103(2): 227–250.

She, J. F., Y. F. Zhang, X. G. Li, and Y. N. Chen. 2014. Changes in snow and glacier cover in an arid watershed of the western Kunlun Mountains using multisource remote-sensing data. *International Journal of Remote Sensing* 35(1): 234–252.

Shi, Y. 2008. *Concise glacier inventory of China*: Shanghai Popular Science Press, Shanghai, China.

Shi, Y., and J. Ren. 1990. Glacier recession and lake shrinkage indicating a climatic warming and drying trend in central Asia. *Annals of Glaciology* 14: 261–265.

Shi, Y. F., C. H. Liu, and E. Kang. 2009. The Glacier Inventory of China. *Annals of Glaciology* 50(53): 1–4.

Solomina, O., R. Barry, and M. Bodnya. 2004. The retreat of Tien Shan glaciers (Kyrgyzstan) since the Little Ice Age estimated from aerial photographs, lichenometric and historical data. *Geografiska Annaler Series A: Physical Geography* 86(2): 205–215.

Sorg, A., T. Bolch, M. Stoffel, O. Solomina, and M. Beniston. 2012. Climate change impacts on glaciers and runoff in Tien Shan (Central Asia). *Nature Climate Change* 2(10): 725–731.

Stroeven, A. P., C. Hattestrand, J. Heyman, J. Kleman, and B. M. Moren. 2013. Glacial geomorphology of the Tian Shan. *Journal of Maps* 9(4): 505–512.

Su, Z., and Y. Shi. 2002. Response of monsoonal temperate glaciers to global warming since the Little Ice Age. *Quaternary International* 97–98: 123–131.

Varis, O. 2014. Curb vast water use in central Asia. *Nature* 514: 27–29.

Viereck, L. A. 1967. Botanical dating of recent glacial activity in western North America. In *Arctic and Alpine Environments*, eds. H. E. Wright and W. H. Osburn, 189–204: Indiana University Press.

Wang, Y. S., C. H. Liu, L. F. Ding and 7 others, eds. 1986. Glacier inventory of China (III): Tien Shan mountains (interior drainage area of scattered flow in east)., Science Press, Beijing. Academia Sinica, Lanzhou Institute of Glaciology and Geocryology. [In Chinese.]

Wiles, G. C., D. J. Barclay, and P. E. Calkin. 1999. Tree-ring-dated 'Little Ice Age' histories of maritime glaciers from western Prince William Sound, Alaska. *The Holocene* 9(2): 163–173.

Winkler, S. 2000. The 'Little Ice Age' maximum in the Southern Alps, New Zealand: preliminary results at Mueller Glacier. *The Holocene* 10(5): 643–647.

Xu, X., and C. Yi. 2014. Little Ice Age on the Tibetan Plateau and its bordering mountains: Evidence from moraine chronologies. *Global and Planetary Change* 116: 41–53.

Yang, B., J. S. Wang, A. Brauning, Z. B. Dong, and J. Esper. 2009. Late Holocene climatic and environmental changes in and central Asia. *Quaternary International* 194: 68–78.

Ye, B., D. Yang, K. Jiao, T. Han, Z. Jin, H. Yang, and Z. Li. 2005. The Urumqi River source Glacier No. 1, Tianshan, China: Changes over the past 45 years. *Geophysical Research Letters* 32(21): L21504. doi: 10.1029/2005GL024178.

Yi, C., K. Liu, Z. Cui, K. Jiao, T. Yao, and Y. He. 2004. AMS radiocarbon dating of late Quaternary glacial landforms, source of the Urumqi River, Tien Shan—a pilot study of ^{14}C dating on inorganic carbon. *Quaternary International* 121(1): 99–107.

Yin, A., and T. M. Harrison. 2000. Geologic evolution of the Himalayan-Tibetan orogen. *Annual Review of Earth and Planetary Sciences* 28(1): 211–280.

Yu, L., and P. Gong. 2012. Google Earth as a virtual globe tool for Earth science applications at the global scale: progress and perspectives. *International Journal of Remote Sensing* 33(12): 3966–3986.

Zech, R. 2012. A late Pleistocene glacial chronology from the Kitschi-Kurumdu Valley, Tien Shan (Kyrgyzstan), based on ^{10}Be surface exposure dating. *Quaternary Research* 77(2): 281–288.

Zech, R., B. Glaser, P. Sosin, P. W. Kubik, and W. Zech. 2005. Evidence for long-lasting landform surface instability on hummocky moraines in the Pamir Mountains (Tajikistan) from ^{10}Be surface exposure dating. *Earth and Planetary Science Letters* 237(3): 453–461.

Appendix for Chapter 1
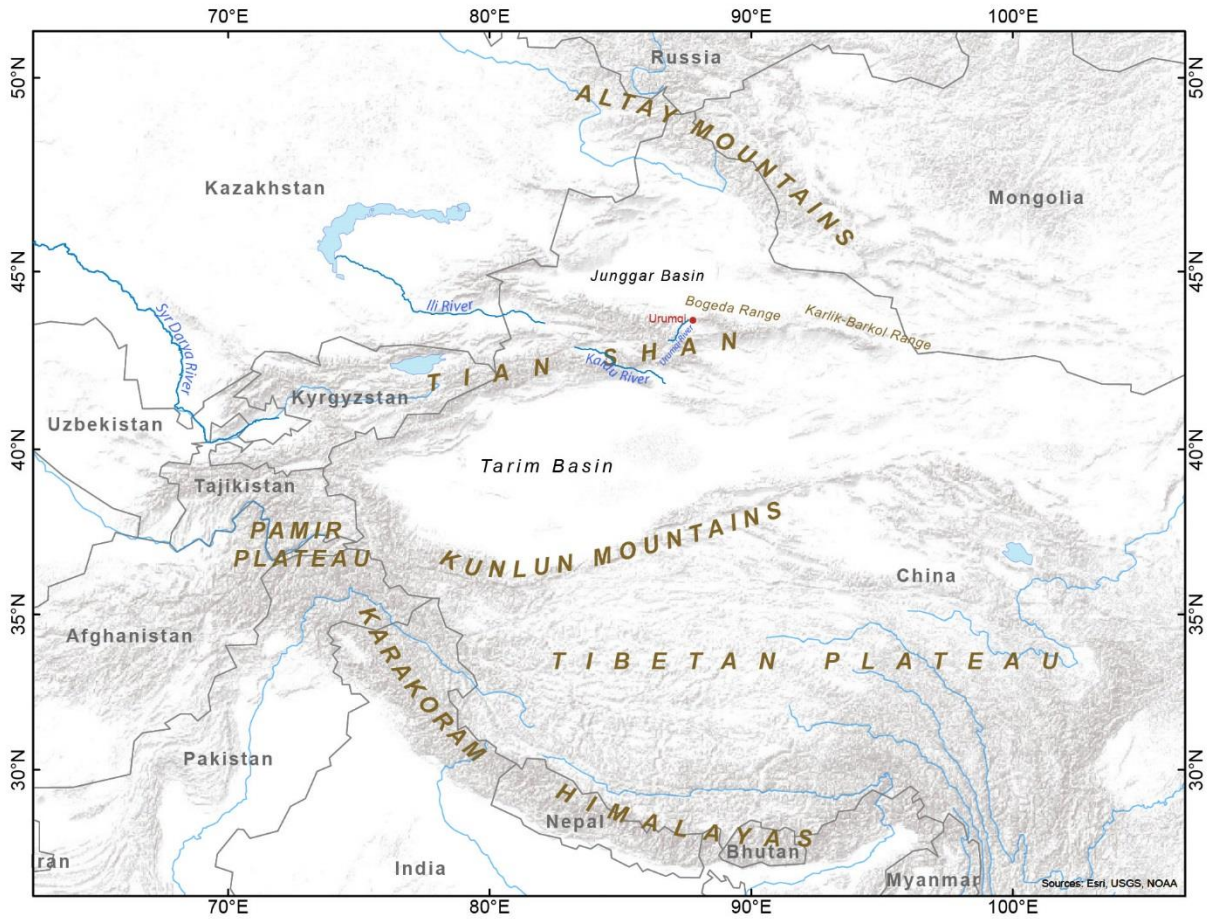
Figure 1-1. Location of Tian Shan and other high mountains in Central Asia.
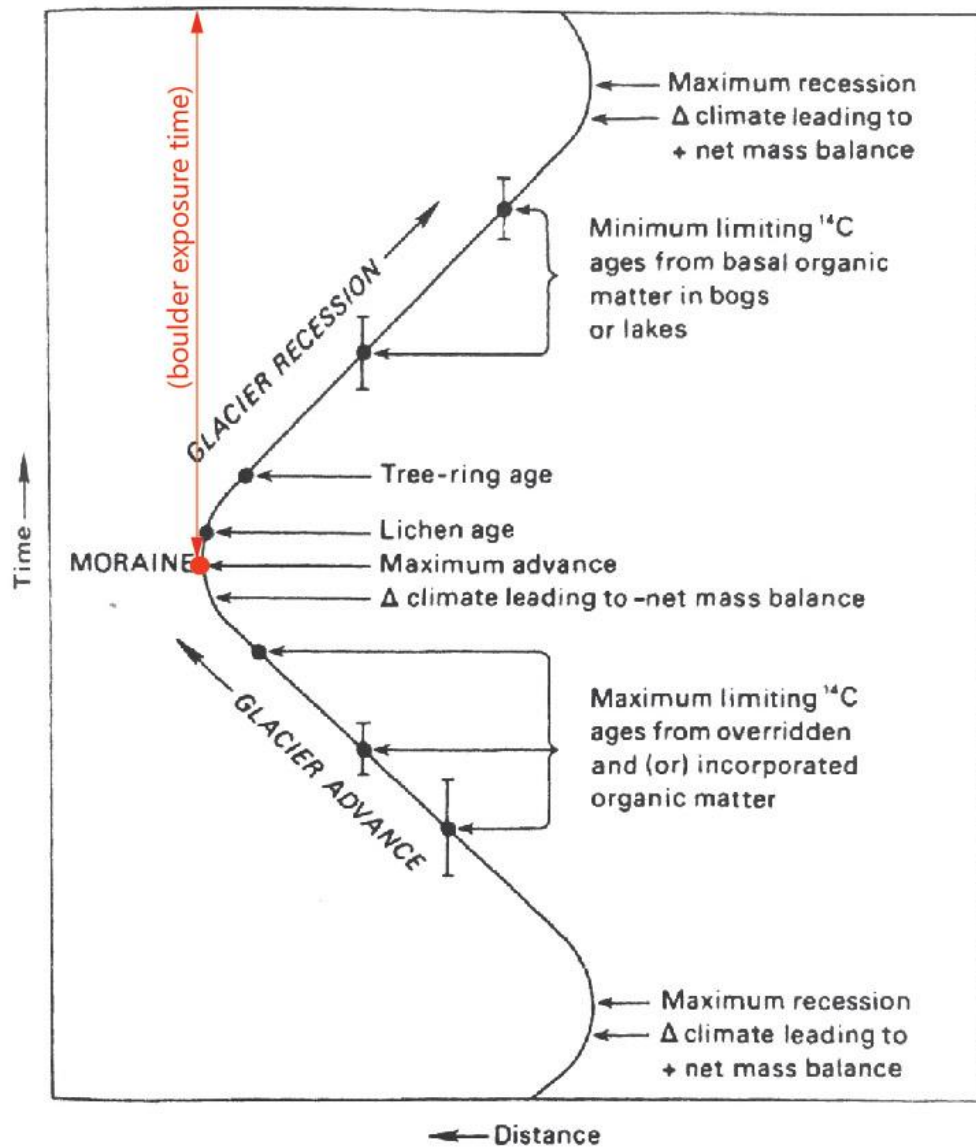
Figure 1-2. The relationship between glacial advance and recession caused by climate changes and possible methods of dating the moraine (originally from Porter 1979; modified from Grove 2004).
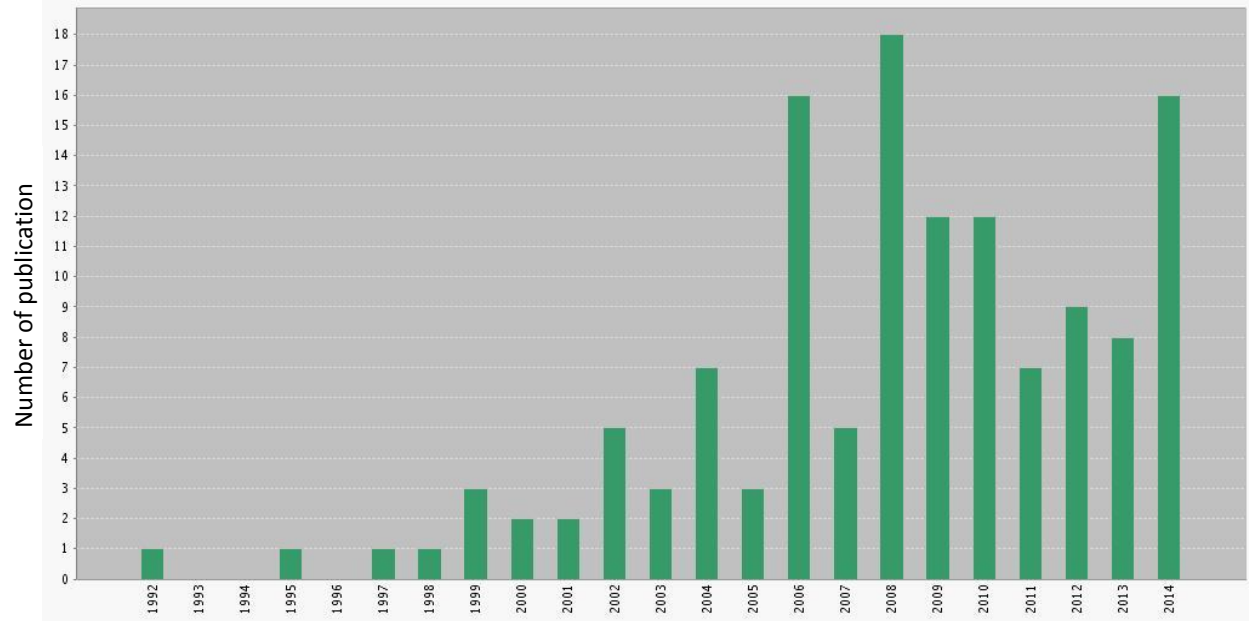
Figure 1-3. Number of publications from 1992 to 2014 (n=132) returned in an ISI Web of Science search, which have key words "Cosmogenic nuclide" and "Little Ice Age".

Chapter 2

Google Earth-Based Mapping of Contemporary and Little Ice Age Glacial Extents in the Eastern Tian Shan, China

This chapter is a manuscript submitted to *Journal of Maps*. According to the author's guidelines, articles in this journal should be short (~2000 words), and it is mandatory to have a separate map file, as well as the Software and Map Design sections at the end of the maintext. The format of this chapter follows the requirements of this journal. The use of "we" in this chapter refers to co-author, Dr. Yingkui Li, and myself. As the first author, I did the mapping and wrote the manuscript.

Abstract

Mountain glaciers across the Tian Shan provide critical freshwater resources for the arid and semi-arid areas in Central Asia. Glacial retreat since the Little Ice Age (LIA) has been investigated in some individual valleys, but its spatial characteristics across a large region still remain unclear. We mapped 1173 contemporary glaciers and their corresponding maximum LIA extents for three sub-regions, the Boro-Eren, the Bogeda, and the Barkol-Karlik Ranges in the eastern Tian Shan, based on Google Earth imagery and an Advanced Spaceborne Thermal Emission and Reflection Radiometer (ASTER) global digital elevation model (DEM). Mapped glaciers in these ranges are mainly valley glaciers, hanging glaciers, and small cirque glaciers. The total area of glaciers decreased from 796.5 km^2 during the LIA Maximum to 582.6 km^2 by the early 2010s, with an area loss of 35.7%. This study provides a useful dataset to document glacier changes since the LIA in the eastern Tian Shan.

2.1. Introduction

Melt water from glaciers provides critical freshwater resources in arid and semi-arid regions of Central Asia. Understanding the extent and timing of glacial fluctuations is of critical importance to water supply for approximately 50 million people in this region (Aizen, 2011). The Tian Shan, known as the "Water Tower of Central Asia" (Sorg et al., 2012), is a series of WSW-ENE trending mountain ranges (about 2500 km long), stretching from the western boundary of Kyrgyzstan across Xinjiang in China, and almost reaching Mongolia (Figure 2-1). A

widely used glacier inventory in the Tian Shan was compiled in the 1970s using topographic maps and aerial photographs acquired in the 1960s (Shi et al., 2010). This inventory contains about 11,000 glaciers in the Chinese section of the Tian Shan and has been archived in the Global Land Ice Measurements from Space (GLIMS), a glacier database funded by NASA (Shi et al., 2010; GLIMS and NSIDC, 2005). Although glacier-related studies in this region have attracted extensive attention (e.g. Liu and Han, 1992; Solomina et al., 2004; Aizen et al., 2007; Sorg et al., 2012), most studies are site specific, and a documentation of glacial fluctuations with reliable timing and extent constraints across a large area is still lacking.

This paper focuses on mapping contemporary and Little Ice Age (LIA) glacial extents in the eastern Tian Shan, China. The LIA is a well-recognized cold event that occurred during the last millennium, between approximately AD 1300 and 1850 (Grove, 2004; Matthews and Briffa, 2005). With the development of various dating techniques and the availability of high-resolution satellite imagery, more accurate glacial landform mapping has become possible for large areas. In the eastern Tian Shan, lichenometry and radiocarbon dating techniques have been used to constrain the timing of the LIA glacial advances (Chen, 1989; Yi et al., 2004). Recently, we constrained the maximum LIA glacial advance to 340±70 yr BP[1] at the source area of the Urumqi River using cosmogenic ^{10}Be surface exposure dating (Li et al., 2014). These studies have suggested the existence of the LIA glacial advances in the eastern Tian Shan. The spatial pattern of glacier changes since the LIA can be illustrated by delineating glacial landforms similar to these dated moraines, assuming they were formed in a similar period. Stroeven et al. (2013) published a geomorphological map of a set of glacial landforms across the Tian Shan based on Landsat ETM+, Google Earth imagery, and the Shuttle Radar Topography Mission

---

[1]BP: before present (1950 AD).

(SRTM) DEM. However, their map did not include glacial landforms associated with the LIA, and the contemporary glaciers, adopted from the GLIMS dataset with some revisions, still represented the glacier coverage in the 1960s. Updated glacier boundaries are needed because studies have revealed that glacier recession has accelerated in the Tian Shan during recent decades (Khromova et al., 2003; Narama et al., 2010; Bolch et al., 2012; Sorg et al., 2012). The purpose of this paper is to present our manually delineated maps of contemporary and LIA glacial extents in the eastern Tian Shan using Google Earth imagery and the Advanced Spaceborne Thermal Emission and Reflection Radiometer (ASTER) 30-m global digital elevation model version 2 (GDEM V2). We also estimated the changes in glacier coverage from the LIA to around 2010. These maps document glacier changes between the LIA and the present (around 2010) in this critical region.

2.2. Geographical Settings of the Study Area

Our mapping area ranges from approximately 85˚40'E to 94˚50'E and from 42˚40'N to 44˚00'N, stretching about 800 km in length with an area of ca. 154 000 km^2. Glaciers are distributed discretely in different mountain ranges, with terminal elevations ranging from 3000 to 4000 m above sea level (a.s.l.). We defined three sub-regions from west to east (Figure 2-1). The first sub-region is the Boro-Eren Range, which includes the eastern Borohoro and the Eren Habirga ranges. In this sub-region, meltwater from glaciers in the Daxi Valley serves as a water source for the regional capital city of Urumqi, a rapid developing city with 3 million people (Figure 2-2A). The Tian Shan Glaciological Station was established by the Chinese Academy of Sciences in 1959 at the head of the Daxi Valley to regularly monitor Glacier No. 1 and surrounding glaciers (Figure 2-2B). The second sub-region is the Bogeda Range, located in the north of the Turpan Depression and 50 km east of Urumqi (Figure 2-1). The Bogeda Range is

28

one of the key sites in Chinese Tian Shan listed on the World Heritage by UNESCO (United Nations Educational, Scientific and Cultural Organization, http://whc.unesco.org/en/list/1414). In summer 2012, we investigated a valley glacier in the Heigou Valley on the southern slope of the Bogeda Range and recorded a GPS track on the LIA moraine to check the landforms we mapped in Google Earth (Figure 2-2C). The third sub-region, the Barkol-Karlik Range, located at the easternmost Tian Shan, includes the Barkol and the Karlik ranges (Figure 2-1). These two WSW-ENE trending mountain ranges contain glaciers at high elevations (above ~3500 m a.s.l.). The highest peaks in these three sub-regions are Mt. Heyuan (5298 m a.s.l.), Mt. Bogeda (5445 m a.s.l.), and Mt. Tomurty (4886 m a.s.l.), respectively.

2.3. Methods

2.3.1. Data sources

Advances in remote sensing and Geographic Information System (GIS) techniques offer the potential to map and monitor glaciers in remote mountain areas (Paul et al., 2004; Bhambri and Bolch, 2009). Although the accuracy of the glacier delineation is affected by imagery sources, imagery availability, and glacier properties (Paul et al., 2013), many studies have applied satellite images, including products of Landsat Thematic Mapper (TM) and Enhanced TM+ (ETM+), ASTER, SPOT, GeoEye, Quickbird, and Worldview, to automatically or semi-automatically delineate glacial extents. In recent years, Google Earth has become a popular platform for visualizing various types of remote sensing data, such as Landsat, SPOT, IKONOS, GeoEye, Quickbird, and Worldview, in a 3D and interactive manner (Yu and Gong, 2012; Sun et al., 2012). The enhanced 3D and interactive visualization make Google Earth a unique platform for landform mapping, even though the date and spatial resolution of the imagery may vary from place to place (Butler, 2006). Google Earth also provides historical imagery, allowing for the

examination of temporal glacier changes and the identification of clear images for glacier boundary delineation. In this study, Google Earth high-resolution images in 2011–2013 from regions with limited cloud or snow cover were used as the major source to delineate present glacial extents and the LIA glacial extents. We also downloaded the ASTER GDEM V2 from the NASA Land Processes Distributed Active Archive Center (LPDAAC) using Global Data Explorer (http://gdex.cr.usgs.gov/gdex/). This one arc-second ASTER GDEM provides approximately 30-m resolution in this area and can be used to help identify glacial landforms and make maps.

2.3.2. Mapping procedure

LIA moraines in the Tian Shan are commonly identified as fresh, bouldery, and sharp-crested moraines located within a few hundreds of meters to a few kilometers away from the present glacier terminus (Shi and Ren, 1990; Solomina, 2004). These moraines usually include two or three lateral/terminal moraine ridges, thought to represent multiple glacial advances during the LIA (Shi and Ren, 1990; Liu et al., 2003). Various numerical dating techniques have been used to constrain the ages of these moraines, especially at the source area of the Urumqi River in the first sub-region. Chen (1989) dated three recessional moraines in front of Glacier No. 1 to 412±20 yr BP, 173±20 yr BP, and 79±20 yr BP, respectively, using lichenometry. Yi et al. (2004) used AMS ^{14}C dating of inorganic carbonate coating from the same moraine and obtained ages of 400±120 yr BP and 430±120 yr BP. Four cosmogenic [10]Be ages of 300±40 yr BP, 370±50 yr BP, 350±100 yr BP, and 340±50 yr BP were obtained at the same site by Li et al. (2014) (Figure 2-2B1). In the Turgan Valley of the Karlik Range (the third sub-region), Chen et al. (2015) provided six [10]Be ages clustered around 700 yr BP for the outermost LIA moraine.

These ages indicated that these fresh moraines were formed during the LIA. We defined the outermost moraine as the maximum glacial extent during the LIA.

The mapping procedure is illustrated in Figure 2-3. The contemporary and LIA glacial extents were digitized in Google Earth and then imported to ArcGIS. We used a Wacom LCD Tablet® to digitize glacier boundaries in Google Earth. This tablet has a pressure-sensitive pen to allow the user to directly draw features on the LCD screen. We delineated outlines for contemporary glaciers and the LIA moraines in Google Earth and stored these outlines as KMZ files. Then, we converted these KMZ files to shapefiles in ArcGIS and overlapped them with the ASTER GDEM to check the delineated features. Contemporary glacier outlines were modified to remove rocks exposed amidst glacier surface. Each LIA moraine outline was converted to a polygon based on the delineated LIA outline and its corresponding contemporary glacier boundary. All shapefiles and DEMs were projected into the WGS1984 UTM projection, and information about each glacier is associated or calculated in the attribute table, including glacier ID, Google Earth imagery date, glacial feature (clean-ice, debris-covered, or potential rock glacier), glacier area, perimeter, and latitude/longitude of its centroid position (Appendix 1). We also calculated the relative area change, based on total areas of contemporary glaciers and LIA glacial extents, for each sub-region and for the eastern Tian Shan.

2.3.3. Accuracy assessment

We used GPS measurements as the ground truth to quantify the accuracy of the delineated glacier boundaries in Google Earth. A revised automated proximity and conformity analysis (R-APCA) (Li et al., 2008) was applied to quantify the offset between GPS measurements and delineated glacier boundaries. During field seasons in 2010 and 2012, we recorded a total of 15 GPS coordinates on top of the LIA moraines in front of three glaciers at

31

the source area of the Urumqi River (Figure 2-2B1). The distances between these 15 points and their corresponding delineated boundaries range from 1.8 m to 18.8 m, with an average of 10.5 m. In addition, at the Heigou Valley in the Bogeda Range, we tracked a route using handheld GPS by walking along the ridge of a LIA moraine (Figure 2-2C1). The average distance between the GPS track and the delineated boundary is about 9.4 m. Such offsets are within one pixel (30-m) of the Landsat imagery, a commonly used image source for glacier delineation (Paul et al., 2004; Bolch, 2007; Bhambri et al., 2011). Thus, the accuracy of our delineated glacier boundaries (~10 m) is comparable with accuracies of maps of glaciers derived from Landsat or other satellite imagery.

2.4. Glacier Characteristics and Glacier Change

2.4.1. Contemporary glaciers

We mapped 1173 glaciers in the eastern Tian Shan. The total glacier area is 582.6 km^2. Among these 1173 glaciers, the area of a single glacier ranges from 0.002 km^2 (in the Boro-Eren sub-region) to 8.8 km^2 (also in the Boro-Eren sub-region), and the longest glaciers are about 6 km from head to toe in all three sub-regions. Valley glaciers are mostly situated around high elevations in the U-shaped valleys, while hanging glaciers and cirque glaciers are frequently found dispersing close to mountain ridges, often with steep terrain. Because most mapped glaciers are north-facing, they receive less incoming solar radiation and preserve snow/ice better than glaciers in south-facing slopes.

The Boro-Eren sub-region contains 818 contemporary glaciers. Large valley glaciers in this region are primarily distributed in the west around Mt. Heyuan (5298 m a.s.l.), while most other glaciers are small glaciers and hanging glaciers along mountain ridges. The Bogeda Range includes 227 contemporary glaciers. Large valley glaciers are concentrated around Mt. Bogeda

(5445 m a.s.l.), with glacier tongues located approximately above 3300 m. In the Barkol-Karlik sub-region, a total of 128 contemporary glaciers were mapped. The Barkol Range, located northwest of the Karlik, has only 11 glaciers. The Karlik Range contains more well-developed, clean-ice glaciers. Unlike glaciers in the other two sub-regions, the glacier areas in the Barkol-Karlik Range are relatively uniform, with an average of around 1.0 km^2. Basic descriptions of glaciers in three sub-regions are listed in Table 2-1.

2.4.2. Glacier changes between LIA and present

In this study, the total area of the delineated LIA glacial extent is approximately 796.5 km^2. The difference in area of contemporary glaciers compared to the maximum glacial extent during the LIA is 284.4 km^2, or about 35.7% of the maximum LIA extent. Specifically, the glaciers in the Boro-Eren Range have receded the most, about 42.3%; glacier recession in the Bogeda Range has been less, about 31.2%; and the retreat in the Barkol-Karlik Range is the least, about 20.4%.

The difference in the percentage of area changes in these sub-regions might suggest a W-E pattern of climate influence or topographic settings that affect glaciers. One possible explanation is related to the precipitation conditions during the LIA in Central Asia. Studies in the Tian Shan and surrounding areas have suggested a relatively wet period during the LIA based on climate proxy data (e.g. Qin and Shi, 1992; Yao et al., 1996; Wu et al., 2005). Strengthened, equatorward-shifted westerlies and a weakened Asian Monsoon during the LIA have been hypothesized and simulated in climate models that explained the wet LIA conditions in Central Asia (Raible et al., 2007; Chen et al., 2010). As abundant moisture was transported from west to east by the westerlies, more extensive glacial advances might have occurred in the west than in

the east because of mountain blocking. Thus, during the warming period after the LIA, more glacier mass was lost in the west than in the east.

Local topographic/geometric factors might also affect glacier recession. Studies have indicated that glacier area and mean elevation have a significant negative correlation with the relative area change of glaciers from the LIA to the present (Li and Li, 2014). Glaciers in the Barkol-Karlik Range are larger and distributed at higher elevations (Table 2-1) compared to the glaciers in the other two sub-regions, probably leading to less relative area change. Further analyses are necessary to examine the dominating factors that affect the pattern of glacier change.

2.5. Uncertainties and Limitations

Google Earth provides freely available high-resolution imagery that can be used to map glaciers and identify glacial landforms. The average offsets between our delineated glacier boundaries and the GPS ground measurement are about 10 m. This positional accuracy is comparable to or higher than the accuracy of glacier mapping using Landsat or other satellite imagery (Bhambri et al., 2011; Narama et al., 2010). More "ground truth" measurements are necessary to improve the accuracy of the mapping.

In addition to the positional uncertainty, other uncertainties and limitations can be caused by human error, the availability of data, data quality, or other factors. The interpretation of the landforms and the completeness of the glacier dataset may be affected by differences in image quality, including resolution, map projection, cloud/snow cover, and season. For example, we did not delineate glaciers or moraines covered by cloud. We also had trouble to identify the LIA moraines in low-resolution images. All of these would cause errors in glacier mapping and probably underestimate glacier coverage in different sub-regions. In some cases, Google Earth

imagery may not be georeferenced accurately, causing some boundary shifts at different times. The uncertainties and bias can also be introduced by the subjectivity and experience of the investigators. For example, different boundaries may be interpreted for glaciers that are partially covered by debris.

2.6. Conclusions

In this study, we created a map of contemporary glaciers and the Little Ice Age glacial extents in the eastern Tian Shan, focusing on three sub-regions: the Boro-Eren Range, the Bogeda Range, and the Barkol-Karlik Range. We manually delineated the boundaries of 1173 contemporary glaciers and their corresponding maximum LIA glacial extents within Google Earth. The contemporary glaciers are distributed at elevations above 3000 m a.s.l. and are mainly valley glaciers, cirque glaciers, and hanging glaciers. The offsets between our delineated glacier boundaries and the GPS ground measurement are about 10 m on average, an acceptable accuracy level in glacier mapping studies.

The comparison between the extent of contemporary and LIA glaciers allows for the quantification of glacier area change in these sub-regions. Since the LIA to present (~2010), the total glacier areas in the mapped area have decreased from 796.5 km^2 to 512.1 km^2, by 35.7%. Specifically, the glacier areas have decreased by 42.3% in the Boro-Eren Range, 31.2% in the Bogeda Range, and 20.4% in the Barkol-Karlik Range, respectively. This pattern of glacier ice loss, decreasing from west to east, may be related to the precipitation pattern associated with westerlies, or to local topographic and geometric characteristics.

Software

We used *Google Earth* to delineate the glaciers and glacial landforms. Mapped features in Google Earth (KMZ files) were imported into *ArcGIS 10.1* for processing and mapping. *Adobe Illustrator CS6* was used to produce the final layout of the map.

Map Design

The map is designed to include four main components. An overview map is provided to illustrate the mapping location in the world and in the mountain range. To better illustrate mapped features, we enlarged three sub-regions as separate components. Each component has its own scale and elevation range. The Barkol Range was designed as an inset map in the third sub-region because it is distant from the Karlik Range. The title, legend, data sources, and the statistics of glacier change (as a table) are illustrated on the top.

Acknowledgments

References

Aizen, V.B., Kuzmichenok, V.A., Surazakov, A.B., & Aizen, E.M. (2007). Glacier changes in the Tien Shan as determined from topographic and remotely sensed data. *Global and Planetary Change, 56*, 328–340.

Aizen, V. (2011). "Tian Shan Glaciers" Encyclopedia of Earth Sciences Series: *Encyclopedia of Snow, Ice and Glaciers*. Ed. Singh, V.P., Singh, P., & Haritashya, U.K. Springer Netherlands.

Bhambri, R., & Bolch, T. (2009) Glacier mapping: a review with special reference to the Indian Himalayas. *Progress in Physical Geography*, 33(5), 672–704.

Bhambri, R., Bolch, T., Chaujar, R.K., & Kulshreshtha, S.C. (2011). Glacier changes in the Garhwal Himalaya, India, from 1968 to 2006 based on remote sensing. *Journal of Glaciology*, 57(203), 543–556.

Bolch, T. (2007). Climate change and glacier retreat in northern Tien Shan (Kazahkstan /Kyrgyzstan) using remote-sensing data. *Global and Planetary Change*, 56(1–2), 1–12.

Butler, D. (2006). The web-wide world. *Nature*, 439, 776–778.

Chen, F.H., Chen, J.H., Holmes, J., Boomer, I., Austin, P., Gates, J.B., Wang, N.L., Stephen, J.B., & Zhang, J.W. (2010) Moisture changes over the last millennium in arid central Asia: a review, synthesis and comparison with monsoon region. *Quaternary Science Reviews*, 29, 1055–1068.

Chen, J.Y. (1989). The preliminary studies of several problems on lichenometry of glacial variation in the Holocene at the headwaters of the Urumqi River. *Science in China (Series B)*, 1, 95–104.

Chen, Y.X., Li, Y.K., Wang, Y., Zhang, M., Cui, Z.J., Yi, C.L., & Liu, G.N. (2015) Late Quaternary glacial history of the Karlik Range, easternmost Tian Shan, derived from [10]Be surface exposure and optically stimulated luminescence datings. *Quaternary Science Reviews*, 115, 17-27.

GLIMS and NSIDC. (2005, updated 2013). *Global Land Ice Measurements from Space glacier database*. Compiled and made available by the international GLIMS community and the National Snow and Ice Data Center, Boulder CO, U.S.A.

Grove, J.M. (2004). *Little Ice Ages, Ancient and Modern*. Loudon: Routledge.

Khromova, T.E., Dyurgerov, M.B., & Barry, R.G. (2003). Late-twentieth century changes in glacier extent in the Ak-shirak Range, Central Asia, determined from historical data and ASTER imagery. *Geophysical Research Letters*, 30(16), 1863.

Li, Y.N., & Li, Y.K. (2014). Topographic and geometric controls on glacier changes in the central Tien Shan, China, since the Little Ice Age. *Annals of Glaciology*, 55(66), 177–186.

Li, Y.K., Liu, G.N., Chen, Y.X., Li, Y.N., Harbor, J., Stroeven, A.P., Caffee, M., Zhang, M., Li, C.C., & Cui, Z.J. (2014). Timing and extent of Quaternary glaciations in the Tianger Range, eastern Tian Shan, China, investigated using [10]Be surface exposure dating. *Quaternary Science Reviews*, 98, 7–23.

Li, Y.K., Napieralski, J., & Harbor, J. (2008). A revised automated proximity and conformity analysis method to compare predicted and observed spatial boundaries of geologic phenomena. *Computers & Geosciences*, 34, 1806–1814.

Liu, C.H., & Han, T.D. (1992). Relation between recent glacier variations and climate in the Tien Shan Mountains, Central Asia. *Annals of Glaciology*, 16, 11–16.

Liu, W.G., Liu, Z.H., An, Z.S., Wang, X.L., & Chang, H. (2011). Wet climate during the 'Little Ice Age' in the arid Tarim Basin, northwestern China. *Holocene*, 21(3), 409–416.

Matthews, J.A., & Briffa, K.R. (2005). The Little Ice Age: Re-evaluation of an evolving concept. *Geografiska Annaler*, 87(1), 17–36.

Narama, C., Kääb, A., Duishonakunov, M., & Abdrakhmatov, K. (2010). Spatial variability of recent glacier area changes in the Tien Shan Mountains, Central Asia, using Corona (~1970), Landsat (~2000), and ALOS (~2007) satellite data. *Global and Planetary Change*, 71(1–2), 42–54.

Paul, F., Huggel, C., & Kääb, A. (2004). Combining satellite multi-spectral image data and a digital elevation model for mapping debris-covered glaciers. *Remote Sensing of Environment*, 89(4), 510–518.

Paul, F., Barrand, N.E., Baumann, S., Berthier, E., Bolch, T., Casey, K., Frey, H., Joshi, S.P., Konovalov, V., Le Bris, R., Mölg, N., Nosenko, G., Nuth, C., Pope, A., Racoviteanu, A., Rastner, P., Raup, B., Scharrer, K., Steffen, S., & Winsvold, S. (2013) On the accuracy of glacier outlines derived from remote-sensing data. *Annals of Glaciology*, 54(63), 171–182.

Qin, B., & Shi, Y.F. (1992). Changes of inland lakes of Asia since Holocene. In: Shi, Y.F. (Ed.), *Advances on Studies of Climate in China and Sea Level Variation*. China Ocean Press, Beijing. (in Chinese).

Raible, C.C., Yoshimori, M., Stocker, T.F., & Casty, C. (2007). Extreme midlatitude cyclones and their implications for precipitation and wind speed extremes in simulations of the Maunder minimum versus present day conditions. *Climate Dynamics* 28(4), 409–423.

Shi, Y.F., Liu, C.H., & Kang, E.S. (2010). The glacier inventory of China. *Annals of Glaciology*, 50(53), 1–4.

Shi, Y.F., & Ren, J.W. (1990). Glacier recession and lake shrinkage indicating a climatic warming and drying trend in Central Asia. *Annals of Glaciology*, 14, 261–265.

Solomina, O.N., Barry, R., & Bodnya, M. (2004). The retreat of Tien Shan glaciers (Kyrgyzstan) since the Little Ice Age estimated from aerial photographs, lichenometric and historical data. *Geografiska Annaler*, 86(A2), 205– 215.

Sorg, A., Bolch, T., Stoffel, M., Solomina, O.N., & Beniston, M. (2012). Climate change impacts on glaciers and runoff in Tien Shan (Central Asia). *Nature Climate Change*, 2, 1–7.

Stroeven, A.P., Hättestrand, C., Heyman, J., Kleman, J., & Morén, B.M. (2013). Glacial geomorphology of the Tian Shan. *Journal of Maps*, 9(4), 505–512.

Sun, X.J., Shen, S.H., Leptoukh, G.G., Wang, P.X., Di, L.P., & Lu, M.Y. (2012). Development of a web-based visualization platform for climate research using Google Earth. *Computers & Geosciences*, 47, 160–168.

Wu, J.L., Shen, J., Wang, S.M., Jin, Z.D., & Yang, X.D. (2005). Characteristics of an early Holocene climate and environment from lake sediments in Ebinur region, NW China. *Science in China (Series D)*, 48(2), 258–265.

Yao, T.D., Thompson, L.G., Qin, D.H., Tian, L.D., Jiao, K.Q., Yang, Z.H., & Xie, C. (1996). Variations in temperature and precipitation in the past 2000a on the Xizang (Tibet) Plateau - Guliya ice core records. *Science in China (Series D)*, 39(4), 425–433.

Yi, C.L., Liu, K.X., Cui, Z.J., Jiao, K.Q., Yao, T.D., & He, Y.Q. (2004). AMS radiocarbon dating of late Quaternary glacial landforms, the source area of the Urumqi River, Tien Shan: a pilot study of 14C dating on inorganic carbon. *Quaternary International*, 121, 99–107.

Yu, L., & Gong, P. (2012). Google Earth as a virtual globe tool for Earth science applications at the global scale: progress and perspectives. *International Journal of Remote Sensing*, 33(12), 3966–3986.

Appendix for Chapter 2

Table 2-1. Descriptive characteristics of glaciers and percentage of glacier area lost between the LIA (approximately 300–800 yr BP) and present (~2010) in three sub-regions

		Boro-Eren	Bogeda	Barkol-Karlik
Area (km²)	mean	0.378	0.665	0.992
	median	0.164	0.296	0.554
Elevation (m)	mean	3937	3846	4095
	median	3935	3814	4104
No. of glaciers with LIA extent		487	179	81
No. of glaciers*		818	227	128
Relative area change		42.3%	31.2%	20.4%

*Note: Number of glaciers is not the same as the number of glaciers with the LIA extent because some small glaciers do not present LIA glacial moraines that are recognizable in Google Earth.
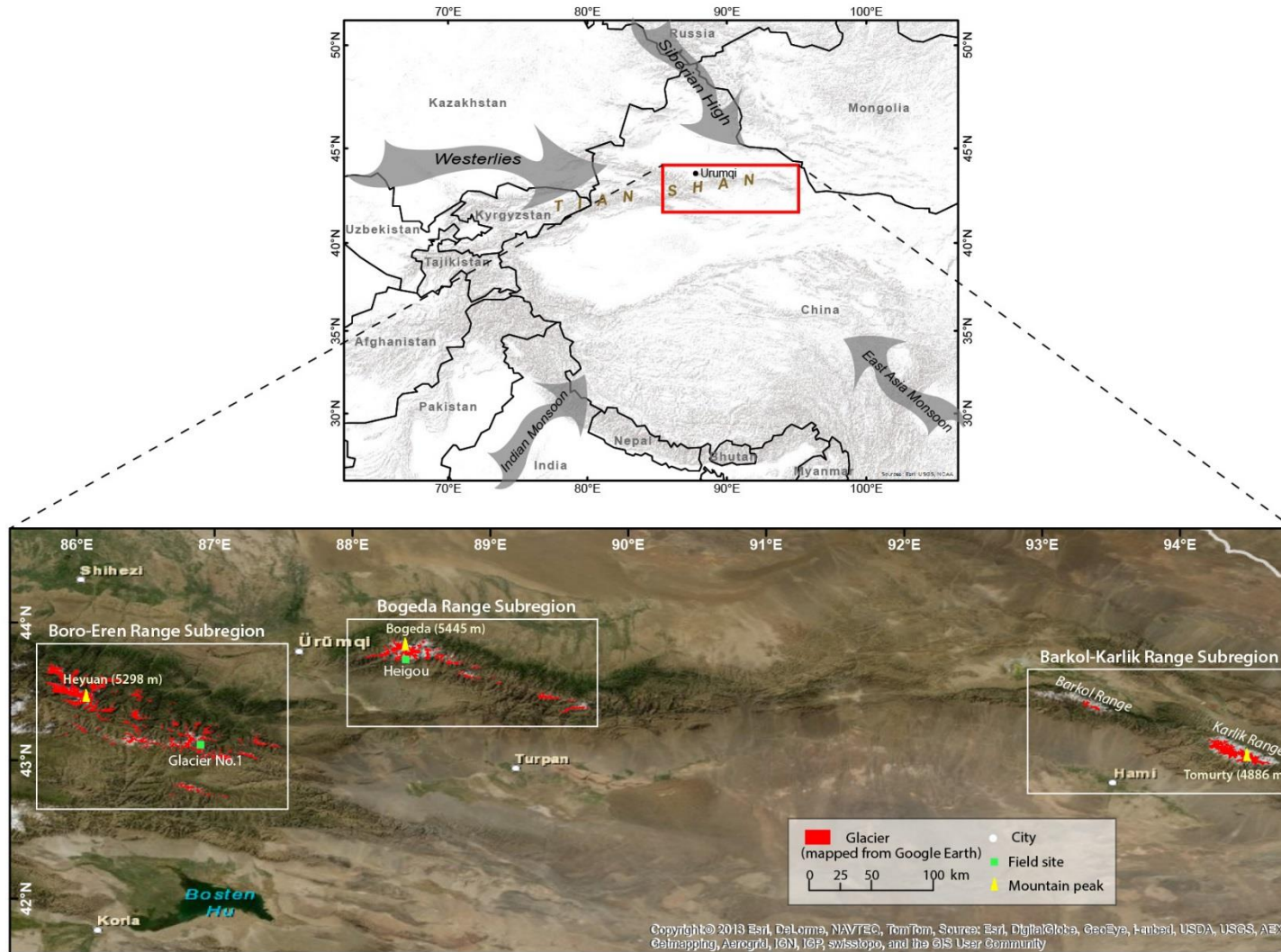
Figure 2-1. Study area of the eastern Tian Shan. Upper: Overview map showing the location of the study area (red box) and surrounding climate systems (grey arrows); Bottom: three sub-regions in the eastern Tian Shan. Field sites of the Urumqi River headwaters and Heigou are illustrated as green dots.
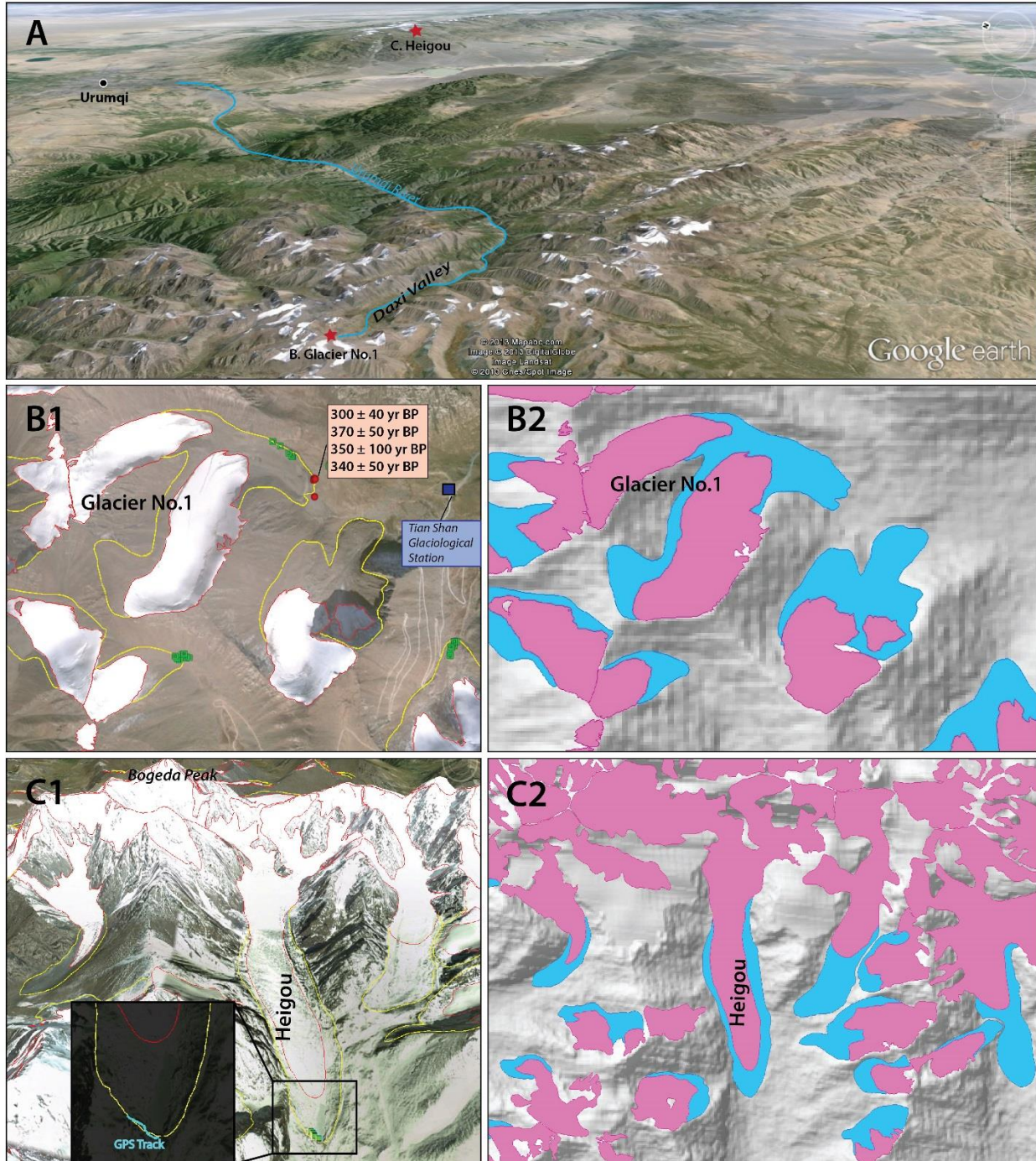
Figure 2-2. **A**: a bird's eye view from Glacier No. 1 in Google Earth; B and C show two examples of glacier mapping: **B1** and **C1** are the Urumqi River headwaters area and Heigou area, respectively, with contemporary (red line) and LIA (yellow line) glacial extents delineated in Google Earth; **B2** and **C2** are the converted polygons denoting corresponding glacial extents (contemporary in pink, LIA in blue) in ArcGIS, draped with semi-transparent hillshaded DEM. Red dots and numbers in the box in B1 are four cosmogenic [10]Be dating results of the LIA moraine (Li et al., 2014); green dots in B1 and C1 are the sample sites on the LIA moraines. Inset graph in C1 shows a field GPS tracking route (in blue) lined up with the LIA glacier boundary (in yellow) drawn from Google Earth.

41
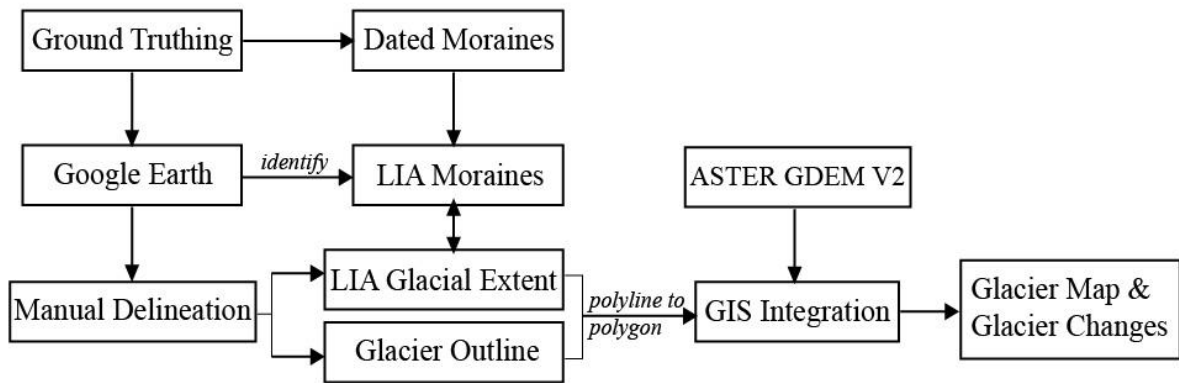
Figure 2-3. Flowchart of the mapping procedure.

Map Screenshot

Google Earth-Based Mapping of Contemporary and Little Ice Age Glacial Extents in the Eastern Tian Shan, China

Yanan Li*, Yingkui Li

Department of Geography, University of Tennessee, Knoxville, TN 37996, USA

* yli49@vols.utk.edu

Legend

- Contemporary glacier
- Contemporary glacier (without LIA extent)
- LIA glacial extent

Mapping was conducted using Google Earth and ASTER global digital elevation model (30 m) in 2011-2013. The Little Ice Age glacial extents are based on numerical dating of the terminal moraines at some sites. Map production is completed in ArcGIS 10.1 and Adobe Illustrator CS6.

Elevation Data
ASTER global DEM v2
(http://gdex.cr.usgs.gov/gdex/)

Map Datum   **Projection**
WGS 84   UTM Zone 45N

	No. of Glaciers	Glacier Area (km²)	LIA Extent (km²)	Area Loss
Boro-Eren Range	818	307.6	460.2	42.3%
Bogeda Range	227	149.1	196.8	31.2%
Barkol-Karlik Range	128	125.9	139.5	20.4%
Total:	1173	582.6	796.5	35.7%
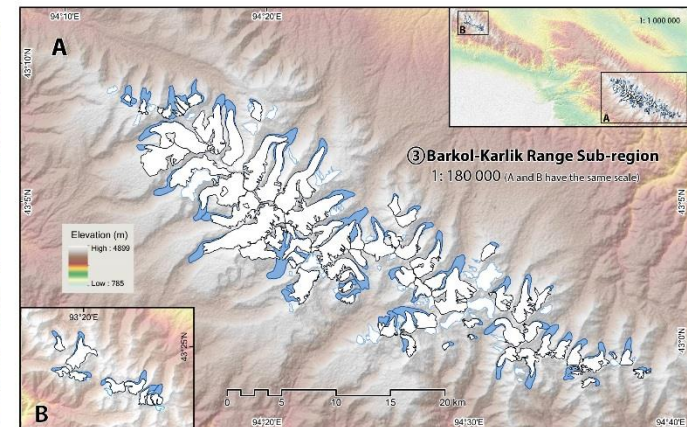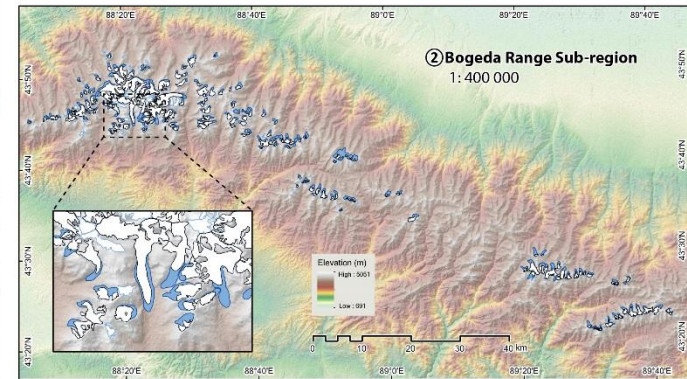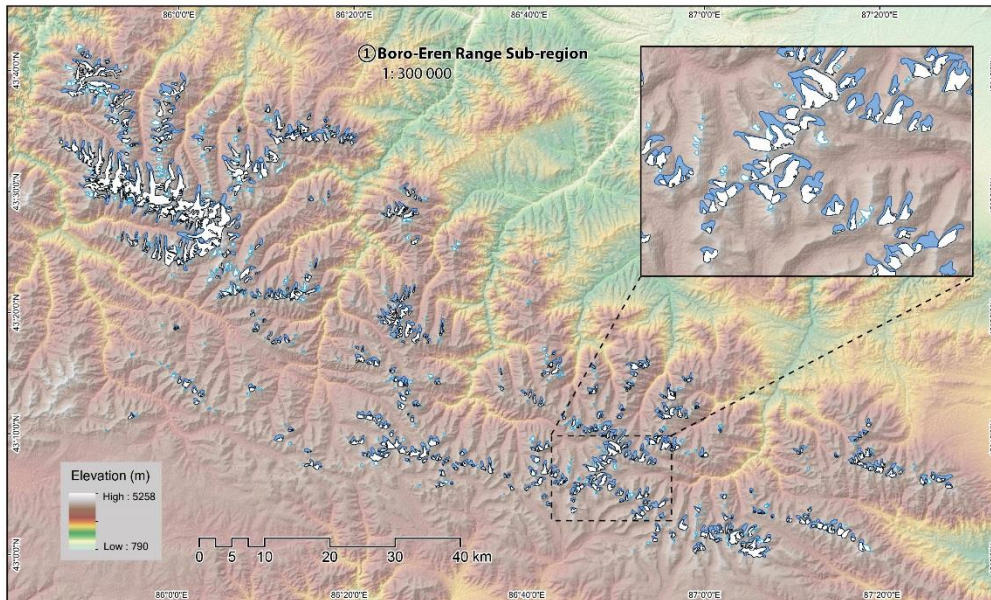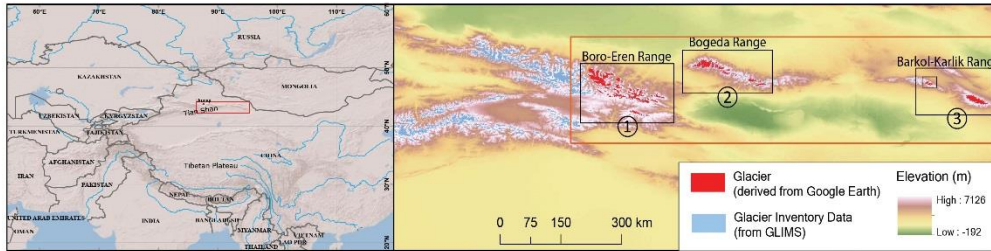
Chapter 3

Topographic and Geometric Controls on Glacier Changes since the Little Ice Age in the Boro-Eren Range, Eastern Tian Shan

This chapter is a slightly modified version of a paper published in a peer-reviewed journal: Li, Y.N., and Y.K. Li. 2014. Topographic and geometric controls on glacier changes in the central Tien Shan, China, since the Little Ice Age. *Annals of Glaciology* 55(66): 177–186. The term "the Central Tian Shan" is re-defined as "the Boro-Eren Range, eastern Tian Shan" in order to be consistent with other parts of the dissertation. The use of "we" is this chapter refers to co-author, Dr. Yingkui Li, and myself. As the first author, I conducted the analyses and wrote the manuscript.

Abstract

We examined the topographic and geometric controls on glacier changes in area and equilibrium line altitude (ELA) since the Little Ice Age (LIA) in the Boro-Eren Range of the eastern Tian Shan, China. We delineated the extents of 487 modern glaciers and their corresponding maximum LIA glacial advances using satellite imagery in Google Earth and analyzed the relationships between the magnitude of glacier changes and a set of local topographic/geometric factors, including glacier area, slope, aspect, shape, hypsometry, and mean elevation. Our results showed that: 1) glacier area decreased from 460.2 km^2 during the LIA to 265.6 km^2 in the 2000s (a loss of 42.3%), with an average ELA increase of ~100 m; 2) relative area changes of glaciers are strongly related with two of these local factors (the glacier area and mean elevation); and 3) ELA change does not show a strong relationship with local factors, suggesting that it may be controlled mainly by climate factors. This study provides important information about the local controls of glacier changes at the centennial time-scale, which are of critical importance to assess future glacier changes in this arid and semiarid region.

3.1. Introduction

Meltwater from glaciers plays an important role in sustaining human habitats and ecosystems, especially for arid and semi-arid regions like Central Asia. Glacier retreat in Central Asia alters moisture-bearing atmospheric circulations, induces glacier-lake outburst floods, and

may ultimately cause desertification, recolonization of plants and animals, and human migration (Chen and others, 2005; Wang, 2010; Gao and others, 2013). Known as the "Water Tower of Central Asia", the Tian Shan possesses a high concentration of mountain glaciers (Liu and Han, 1992; Solomina and others, 2004; Aizen and others, 2007; Sorg and others, 2012). Variations in glacial meltwater may lead to political disputes, since multiple countries with millions of people in Central Asia share the same rare water sources from these glaciers. Reseach on the glacier changes could help better evaluate the change and storage of freshwater source in glaciers and provide scientific support in decision-making process at the management level.

Like many regions in the world, the Tian Shan has been experiencing glacier retreat since the end of the Little Ice Age (LIA) in the mid-19th century, with an accelerated rate in recent decades (Khromova and others, 2003; Narama and others, 2010; Bolch and others, 2012; Sorg and others, 2012). The surface mass balance of glaciers in the Tian Shan is controlled by the interaction of the westerlies and Siberian High. Westerlies bring moist air masses during summer months, and the precipitation from June to August accounts for 32–50% of the annual precipitation in different altitudinal zones of the central Tian Shan (Aizen and others, 1995). In winter (November to February), the Siberian High invades this area, bringing cold and dry air masses with only 8–10% of the annual precipitation (Aizen and others, 1995). In addition, glaciers are affected by local topographic/geometric characteristics. For example, researchers studying mountain glaciers in northwestern China and the Himalayas suggested that small glaciers have changed more significantly than large ones in recent decades (Liu and others, 2003; Bhambri and others, 2011; Li and others, 2011). Statistical analysis of glaciers from the World Glacier Inventory (http://nsidc.org/data/glacier_inventory/) revealed that most glaciers in mid-high latitudes have poleward aspects due to limited solar radiation (Evans, 2006). A recent study

found that the contribution of glacial melting to sea level rise on a global scale, determined by the measurements of monitored glaciers, might be overestimated because these monitored glaciers, which are relatively easy to access, are also more vulnerable to climate change, whereas relatively stable glaciers distributed in the rough terrains are usually hard to reach (Kerr, 2013). However, only limited studies have been conducted to systematically examine the relationship between local topographic/geometric factors and glacier changes.

Most glacial studies in the Tian Shan have focused on either the most recent decades or paleo-glaciations before the Holocene, whereas few studies have been conducted on the centennial time scale. In particular, little is known about glacial fluctuations since the LIA. The LIA was a cold period during the last millennium, approximately between 1550 and 1850 AD (Grove, 2004). Geomorphic evidence of several glacial advances in recent centuries confirmed its occurrence, and the LIA moraines in the Tian Shan are empirically identified as fresh, bouldery, and sharp-crested moraines within hundreds of meters to a few kilometers away from the modern glacier terminus (Shi and Ren, 1990; Solomina, 2000). The timing of the LIA glacial advances in the Tian Shan has been constrained, using lichenometry and radiocarbon dating, to have ranged from 430±120 to 79±20 yr BP[1] (Chen, 1989; Yi and others, 2004; Yi and others, 2008).

In the work presented here, we delineated 487 modern glaciers and their corresponding LIA extents from the satellite imagery in Google Earth to evaluate the topographic/geometric controls on glacier changes in the eastern Tian Shan. We derived glacier area directly from the delineated glacier polygon. We also calculated five other local factors, including slope, aspect, shape, hypsometry, and mean elevation, using the Advanced Spaceborne Thermal Emission and

---

[1]BP: before present (1950 AD).

Reflection Radiometer (ASTER) global digital elevation model version 2 (GDEM V2, 30-m

resolution). Statistical analysis was used to examine the relationship between the magnitude of

glacial retreat and these local factors. We assumed that glaciers have been affected by similar

changes in climate conditions within this confined area from the LIA to the present. This study

provided the first regional view of glacial retreat since the LIA in the eastern Tian Shan.

3.2. Study Area

The Tian Shan is a series of mountain ranges with a WSW-ENE trend about 2500 km

long, from the western boundary of Kyrgyzstan across Xinjiang Uighur Autonomous Region in

China, and almost reaching Mongolia (Figure 3-1). Most of these mountain ranges reach about

4000 m above sea level (a.s.l.), with the highest peaks over 7000 m a.s.l. along the boundary

between China and Kyrgyzstan (Xu and others, 2010). It is one of the driest regions in the world,

located in the center of the Eurasian continent. The barrier effects of the terrain lead to a

decreasing gradient in precipitation from northwest (annual precipitation of 1500–2000 mm) to

southeast (~100 mm) (Grove, 2004; Sorg and others, 2012). Our study area is located in the

eastern sector of the Tian Shan, particularly including the eastern part of the Borohoro Range and

the Eren Habirga Range (85˚40'E–87˚22'E, 43˚38'N–42˚55'N; use Boro-Eren Range for

reference). Large valley glaciers are distributed around the highest peak of Mt. Heyuan (5289 m

a.s.l.), whereas cirque glaciers, hanging glaciers, and small valley glaciers are dispersed across

the rest of the study area (Figure 3-1). Abundant U-shaped valleys and other glacial landforms

indicate that this area was extensively glaciated in the past. One well-studied site in this region is

the Urumqi River headwaters, where Chinese Academy of Sciences established a glaciological

station in 1959 to monitor the dynamics of glaciers. The station includes a meteorological

observation field, a hydrological station, and a cold area plant testing field. Since 1959, the

glaciological station has conducted long-term continuous monitoring of glacier physics, chemistry, and energy characteristics (mainly for Glacier No. 1), as well as various studies associated with glacial geomorphology, hydrology, and ecology (e.g., Li and others, 2001, 2011; Ye and others, 2005; Gao and others, 2013). Meltwater from the glaciers around this station provides fresh water for over 3 million people in the city of Urumqi.

3.3. Data and Methods

3.3.1. Satellite imagery and glacier outline delineation

Google Earth has become one of the most popular virtual globes with free access to high-resolution imagery covering the whole world (Yu and Gong, 2012). It integrates satellite imagery, aerial photographs, and digital maps into a three-dimensional interactive platform (Sun and others, 2012). The resolution of Google Earth imagery (DigitalGlobe®) in some regions can be as fine as 0.6-m (Frankl and others, 2013). The high-resolution imagery for some remote areas and convenient interactive visualization operations of Google Earth make it possible to map glacier changes in those areas with a relatively high accuracy. We used Google Earth to identify and delineate the extents of modern glaciers and their corresponding LIA moraines in the Boro-Eren Range of the Tian Shan in China. In our study area, the dates of the imagery span from 2002 to 2012, but most are from around 2010 (see the BE glaciers in Appendix 1). The outlines of modern and LIA glaciers were delineated as polygon features. LIA glacial advances in the Tian Shan are usually represented by two or three lateral-terminal moraines (Shi and Ren, 1990; Liu and others, 2003). We regarded the outermost moraine as the maximum extent of LIA glacial advances. Debris cover was not a major issue in delineating glacier boundaries because most glacier surfaces in this area are clean. We excluded a few glaciers that were partially covered by

clouds. In total, we manually delineated 487 modern glaciers and their corresponding LIA Maximum extents in Google Earth.

3.3.2. Field measurements and validation of the delineation

Fieldwork was conducted in the Urumqi River headwaters in 2010 and 2012. In 2010, we collected four boulder samples on top of the outermost LIA moraine of Glacier No. 1 and obtained tightly clustered ^{10}Be ages from 300±40 to 370±50 yr BP with a weighted mean of 340±70 yr BP (Li and others, 2014; Figure 3-2). These ages are consistent with the age of 412±20 yr BP, obtained using lichenometry (Chen, 1989) and the ages of 400±120 and 430±120 yr BP based on AMS ^{14}C dating of inorganic carbonate coatings from the same moraine (Yi and others, 2004; Li and others, 2011). These ages indicated that the fresh moraines close to modern glaciers were formed during the LIA in this area. In 2012, we recorded additional GPS coordinates from the top of LIA moraines in this area to evaluate the accuracy of the delineation from Google Earth. A total of 15 GPS coordinates on the ridge of the outermost LIA moraines in front of three individual glaciers were used as "ground truth" to assess the accuracy of our delineation by examining the proximity between the delineated outlines and GPS measurements (Li and others, 2008; Figure 3-2).

3.3.3. Indicators of glacier changes since the LIA

A variety of indicators have been used to quantify glacial advance/retreat, including changes in glacier area (Narama and others, 2010; Kamp and others, 2011), glacier length (Cook and others, 2005; Huybers and Roe, 2009), the equilibrium line altitude (ELA) (Benn and Lehmkuhl, 2000; Asahi, 2010), and glacier volume (Liu and others, 2003; Bliss and others, 2013). Change in glacier area is a commonly used indicator because it can be derived relative easily from glacial extents at different times. Comparisons of the relative magnitude of glacier

change among different regions does not account for the changes in ice thickness; thus, may not reflect the actual total mass lost. ELA is an indicator of glacier mass balance, and ΔELA has been widely used in paleoclimate research to reconstruct past temperature and/or precipitation (e.g., Yang and others, 2008; Asahi, 2010). We selected the relative area change and ΔELA as two major indicators to quantify the glacier changes since the LIA.

Relative area change

Glacier area (m^2) can be derived directly from the delineated glacier outline (polygon). The relative change of glacier area (as a percentage) can be determined using the following equation:

$$\Delta A = (1 - \frac{\sum A_M}{A_{LIA}}) * 100 \tag{1}$$

where *ΔA* is the percentage of change in glacier area; A_M is the area of modern glacier, and A_{LIA} is the glacier area during the LIA. If several glaciers coalesced during the LIA, we assigned the same percentage to each modern glaciers, determined as shown in Equation (1).

ELA estimation

Benn and Lehmkuhl (2000) introduced six methods that have been commonly used to estimate ELAs of past glaciations: the balance ratio (BR), the accumulation-area ratio (AAR), the maximum elevation of lateral moraines (MELM), the toe-to-headwall altitude ratio (THAR), the toe-to-summit altitude (TSAM), and the cirque-floor altitude. We used the TSAM in our study. TSAM determines the ELA by calculating the mean elevation between the highest peak within the glacier catchment and the terminus of each glacier at a certain period (Benn and Lehmkuhl, 2000). Maisch (1992) compared the directly measured ΔELA since 1850 AD with the change in the elevation of the terminus, calculated from 684 glaciers in the Alps, and concluded

that half of the terminus elevation change, which is the same value derived using the TSAM if assuming a constant summit elevation, is about the same as the measured ΔELA. The TSAM has also been applied to estimate ΔELAs for >1000 glaciers in the Tibetan Plateau and Mongolia (Benn and Lehmkuhl, 2000). We used the elevations of glacier terminus derived from GDEM V2 to determine the ELA change since the LIA Maximum for each glacier.

3.3.4. Local topographic/geometric factors

We derived the following topographic/geometric parameters in GIS: (1) Glacier area, as mentioned above, was derived directly from the delineated glacier outline. (2) Slope (in degrees between 0 and 90) was determined as the mean slope of each raster cell (30-m $\times$ 30-m) within the glacier outline. (3) Aspect is the direction of the steepest slope, in degrees counted from north (0˚) and increasing clockwise. We determined the average aspect for each glacier by calculating the directional mean of the aspect from each raster cell within the glacier outline after converting angle units to radians. (4) Shape index (SI) was derived from the equation:

$$SI = sqrt(4\pi*A/P^2) \tag{2}$$

where A is the area and P is the perimeter of the glacier outline. SI ranges from 0 to 1 with a value of 1 for a circular polygon. (5) Mean elevation represents the absolute altitudinal location of a glacier on the mountain. It was derived by averaging the elevations of all DEM cells within the glacier outline. (6) Hypsometric integral (HI), also called the "elevation-relief ratio", was calculated using the difference between the mean and minimum elevations divided by the local relief (max elevation–min elevation) within the glacier outline (Pike and Wilson, 1971). HI ranges from 0 to 1, with smaller value indicating a concave hypsometric curve (more ice distributed in low elevations).

3.3.5. Statistical analysis

We first explored the descriptive statistics of each factor to examine the overall characteristics of these 487 glaciers, including the mean, median, standard deviation, minimum, and maximum values. Histograms were used to examine the data distribution, and data transformation was applied when necessary, to guanrantee a normal distribution. For example, glacier area was transformed into its logarithmic value in the regression because of the apparent diminishing trend in its frequency distribution (Figure 3-3a). Then, we conducted multivariate stepwise regression to quantify the relationships between glacier changes (both relative area change and ΔELA) and these local topographic/geometric factors. We treated relative glacier area change and ΔELA as dependent variables for each regression and six factors (glacier area, slope, aspect, shape, hypsometry, and mean elevation) as independent variables. The R^2 value was used to evaluate the goodness of fit and p value to determine the significance level of the statistics. We also used scatter plot and Pearson correlation to examine the relationships between glacier changes and the statistically significant factors. All statistical analyses were excuted in RStudio software package.

3.4. Results and Discussion

3.4.1. Accuracy of delineated glacier outlines in Google Earth

We used 15 field-measured GPS coordinates from the top of the outermost LIA moraines in the Urumqi River headwaters to assess the accuracy of the delineations. The offsets between these GPS coordinates and their corresponding delineations range from 1.8 m to 18.8 m, with an average of 10.5 m. The minimum offset occurs at a lateral moraine, whereas the maximum from a terminal moraine (Figure 3-2). This difference is probably caused by the fact that the ridges of lateral moraines in this area are constrained by topography to be relatively sharp and narrow, and

the ridges of terminal moraines are relatively flat and wide. Nonetheless, all these offsets are within one pixel (30-m) of the Landsat imagery that has been commonly used to delineate glacier outlines (Paul and others, 2004; Bolch, 2007; Bhambri and others, 2011). Therefore, the delineated glacier outlines in Google Earth are relatively accurate compared with most glacier maps derived from Landsat imagery.

3.4.2. Glacier characteristics and glacier changes since the LIA

The total contemporary (around 2010) area of the 487 glaciers we delineated in the Boro-Eren Range is 265.6 km^2. Most glaciers have an area <1.0 km^2 (430 out of 487, 88.3%) (Figure 3-3a), and the glacier with the maximum area of 8.8 km^2 is located near the Heyuan Peak. The slopes of these 487 glaciers have a mean value of 33.6˚ (Figure 3-3b), which is about 10 degrees steeper than the mean slope of the 488 glaciers in the eastern Himalayas (Racoviteanu and others, 2011), but similar to the mean slope of 29.4˚ in the Bogeda Range, the eastern Tian Shan (Li and others, 2011). We divided the aspect of glaciers into eight 45˚ intervals. Most glaciers (90.3%) are north-facing (N, NW, and NE) (Figure 3-3c). However, during the delineation process, we did observe some LIA moraines, without corresponding modern glaciers, on the southern slopes, indicating the existence of south-facing glaciers that have disappeared since the LIA. The shape index values of mapped glaciers range from 0.26 to 0.95 with the mean and median around 0.60 (Figure 3-3d). Elongated glaciers concentrate around the Heyuan Peak, but most glaciers do not extend far in the valley. Small hanging and mountaintop glaciers tend to have round shapes. The hypsometric integral values show a normal distribution, with a mean of 0.49 (Figure 3-3e). The mean elevations of most glaciers are between 3800 and 4100 m a.s.l., with an average of 3937 m a.s.l. (Figure 3-3f). The present-day ELAs we derived using TSAM are similar to these mean elevations.

The total glacial coverage we delineated during the LIA Maximum is about 460.2 km^2, indicating a reduction in area of approximately 42.3% through this three-to-four-hundred-year period. Relative area change of individual glaciers has a wide range, of 8.4–98.2%, and 261 of 487 glaciers have lost more than 50% of their LIA area (Figure 3-4a). ΔELAs of these glaciers show a positively skewed distribution with a mean of 101 m and a median of 81 m (Figure 3-4b). Our derived mean ΔELA since the LIA in the eastern Tian Shan is within the ΔELA range of 100–150 m in the same period estimated by Porter (1970), using the AAR method, for the temperate zone of the Northern Hemisphere. The ΔELA since the LIA, estimated using TSAM in the Kyrgyz Tian Shan, is about 75–100 m (Solomina and others, 2004).

3.4.3. Relationships between glacier changes and topographic/geometric factors

Relationship between ΔELA and local factors

The R^2 value in the regression between ΔELA and six local factors is 0.162 (Table 3-1). Although t-tests for aspect, slope, shape, and the whole regression all passed the significance level of 0.001 (p < 0.001, Table 3-1), this low R^2 value means that only 16.2% of the variation in ΔELA are explained by these local factors, and indicates that they are not the main drivers for ΔELA. The spatial distribution of ΔELA shows a distinct pattern along the W-E and N-S transects with larger ΔELAs occurring in the west and on north-facing slopes, but smaller values in the central-eastern areas and on south-facing slopes (Figure 3-5). Such a pattern is in accordance with the precipitation distribution in the Tian Shan: more precipitation falls in the western and northern ranges and less precipitation on the southern slopes. Although Benn and Lehmkuhl (2000) suggested that local factors such as slope, aspect, hypsometry, and others can contribute to ΔELA for clean and snowfall-fed glaciers, our results suggest that only a small

portion of ΔELA can be explained by local factors in the Boro-Eren Range. Climate factors, such as precipitation and temperature, are more likely causing the spatial differences in ΔELAs.

Relationship between relative area change and local factors

In contrast to ΔELA, we obtained a strong relationship between relative glacial area change and two of these six local factors:

$$\Delta A = 304.468 - 11.286 \times \ln A - 0.028 \times E \tag{3}$$

where ΔA is the relative area change in percentage; lnA is the logarithmic value of the glacier area (m^2) and E is the mean elevation (m). The R^2 value is 0.640 ($p < 0.001$, Table 3-2). The scatter plot illustrates a good fit of the regression (Figure 3-6a). Therefore, our results suggest that the relative area change of a glacier is closely and negatively associated with its area and mean elevation. Glacier area is commonly believed to be a key factor affecting glacier shrinkage (Liu and others, 2003; Khromova and others, 2003; Bhambri and others, 2011; Li and others, 2011). The scatter plot of lnA vs. relative area change, and its high correlation coefficient ($r = -0.766$; $p < 0.001$), indicate that small glaciers tend to have relatively large reduction in area (Figure 3-6b). This finding is consistent with findings of recent decadal glacier changes in other regions such as the European Alps (Paul and others, 2004), northern Kyrgyz Tian Shan (Bolch, 2007), Central Himalayas (Bhambri and others, 2011), and eastern Chinese Tian Shan (Li and others, 2011). Mean elevation is also well correlated with relative area change ($r = -0.405$; $p < 0.001$) (Figure 3-6c), suggesting that glaciers distributed at high elevations tend to recede slowly compared with those at low elevations.

Although other factors did not show significant contributions to glacier change in this area, the correlation analysis suggested that most pair-wise correlations are significant at the 0.001 level (Table 3-3). Glaciers on steeper slopes tend to have lost more area. Glacier shape

index has a negative correlation with ΔELA, but a positive correlation with the relative area change. Such relationships probably indicate that when a glacier is nearly round in shape, it may have become too small to have a large ΔELA, but can still undergo relatively large loss of area. Hypsometric integral has a positive correlation with relative area change but at a relatively low level (r = 0.124; p = 0.006). Our results showed a relatively high percentage in relative area reduction for north-facing glaciers (Figure 3-6d). Most previous studies suggested that south-facing glaciers in the northern hemisphere are prone to have larger area loss due to the greater amount of incoming solar radiation they receive (e.g., Evans, 2006; Li and others, 2011). Our opposite result is probably caused by the intrinsic sampling bias in the study, which unbalanced the binomial frequency distribution of south- and north-facing glaciers and resulted in a non-randomized sampling. Most of the south-facing glaciers have already disappeared, and we were unable to identify the empty glacier basins that should have had experienced 100% glacier area loss. Therefore, the value of 42.3% in glacier area reduction since the LIA is most likely underestimated.

3.4.4. Comparison with nearby regions

Our study showed that glaciers in the Boro-Eren Range of the eastern Tian Shan lost about 42.3% in area, with a mean ELA increase of ~100 m, since the LIA Maximum. Savoskul (1997) reported two retreat patterns since the LIA Maximum from 20 glaciers in the Kyrgyz Tian Shan (~740 km west of our study area) based on 1:100 000 topographic maps: in the warm and humid western frontal ranges, the relative area loss reached 50 to 90% and the ELA increases were 100–200 m (estimated by various methods, including the median elevation, THAR, AAR, and MELM); whereas, in the inner cold and arid ranges, glaciers were more stable, with 3 to 7% reductions in area and 20–50 m ELA increases. The spatial patterns of our calculated relative

area change and ΔELA in the Boro-Eren Range are similar to the pattern reported by Savoskul (1997) of the warm and humid western frontal ranges, but different from the pattern he reported for the inner cold and arid ranges. This difference implies the need to examine detailed changes in glaciers across different regions to fully understand the climate and local controls on glacier changes in the Tian Shan. Solomina (2000) and Solomina and others (2004) examined a large dataset of glacier changes in the Kyrgyz Tian Shan and reported an average ΔELA of 70 m from the LIA Maximum to the 1980s using TSAM, the same method used in our study. Their ΔELA estimate is similar to the value we derived in the eastern Tian Shan. Liu and others (2003) conducted a study on glacier change since the LIA Maximum in western Qilian Shan (~1000 km southeast of our study area) based on aerial photographs from 1956, 1:50 000 topographic maps from the 1970s, and Landsat TM images from 1990. They found that from the LIA to 1990, glacier areas decreased 25–28%, and the ELA of small glaciers rose by 46 m to the 1950s (ΔELA was estimated using the elevations of glacier termini in different periods; Liu and others, 2003). They also found that the decrease in glacier area between 1956 and 1990 was comparable to the decrease between the LIA and 1956, which indicates a much faster shrinking rate in recent decades. Considering the accelerated rate of retreat after 1956 found in their study, the glacier change in western Qilian Shan might have experienced a similar or even larger magnitude of retreat compared to the retreat of glaciers, shown by our results, in the eastern Tian Shan.

Topographic/geometric controls on glacier changes have been examined only for recent decades because of the availability of remote sensing data. Similar to our results in the Boro-Eren Range, studies from the Bogeda Range (Li and others, 2011) and the Garhwal Himalaya, India (Bhambri and others, 2011) also concluded that small glaciers were more sensitive to climate change. In addition, our results indicated that glaciers tended to recede more slowly at

high elevations. This relationship is valid in many regions (Aizen and others, 2007; Li and others, 2011; Racoviteanu and others, 2008), but in some regions an inverse relationship occurs for different glacier types. For example, in Garhwal Himalaya, larger compound glaciers, which extended to lower valleys, have receded at a slower rate, while smaller glaciers, found at higher elevations have receded faster (Bhambri and others, 2011). Previous studies also found fragmentation and disappearance of glaciers over recent decades (Liu and others 2003; Li and others, 2011; Bhambri and others, 2011). The fact that only 4% of glaciers in our study area are facing south may indicate a pattern similar to that shown in other studies that south-facing glaciers have lost more area than north-facing glaciers (Nainwal and others, 2008).

3.4.5. Limitations

Several limitations still exist in our study. First, bias may have been introduced by not counting glaciers that have disappeared (mainly south-facing glaciers). During the delineation, we also excluded some glaciers covered by clouds in satellite imagery, potentially causing additional bias in our analysis. Second, the time range of satellite imagery in Google Earth spans ten years (2002–2012). Therefore, the extents delineated for different glaciers may be not from the same year, causing some minor inconsistency. Finally, the LIA moraines were only dated in one valley, and more absolute geological dating of these moraines from other valleys is needed in the future.

3.5. Conclusions

We conducted a detailed study of local topographic/geometric controls on glacier changes since the LIA Maximum in the Boro-Eren Range, eastern Tian Shan, based on 487 glaciers and their corresponding LIA extents delineated from satellite imagery in Google Earth. Six topographic/geometric factors, including glacier area, slope, aspect, shape, hypsometry, and

mean elevation, were evaluated with two glacier change indicators: relative area change and ΔELA (estimated using TSAM). Our results show that the total glacier area decreased from 460.2 km^2 during the LIA to 265.6 km^2 in the 2000s (42.3%) with an average ELA increase of ~100 m. These estimates are comparable with those obtained in other studies in nearby regions of Central Asia. The relationship between ΔELA and these local factors is not significant (R^2 = 0.162), indicating that ΔELA is probably affected mainly by climate rather than local settings. In contrast, relative area changes of these glaciers are strongly correlated with local factors, especially the area and the mean elevation of a glacier (R^2 = 0.640). Specifically, small glaciers tend to have large relative area loss, and glaciers at high elevations tend to recede slowly.

References

Aizen VB, Aizen EM and Melack JM (1995) Climate, snow cover, glaciers and runoff in the Tienshan, central Asia. *Water Resour. Bull.,* 31, 1113–1129

Aizen VB, Kuzmichenok VA, Surazakov AB and Aizen EM (2007) Glacier changes in the Tien Shan as determined from topographic and remotely sensed data. *Global Planet. Change,* 56, 328–340

Asahi K (2010) Equilibrium-line altitudes of the present and Last Glacial Maximum in the eastern Nepal Himalayas and their implications for SW monsoon climate. *Quatern. Int*., 212, 26–34

Benn DI and Lehmkuhl F (2000) Mass balance and equilibrium-line altitudes of glaciers in high-mountain environments. *Quatern. Int*., 65/66, 15–29

Bhambri R, Bolch T, Chaujar RK and Kulshreshtha SC (2011) Glacier changes in the Garhwal Himalaya, India, from 1968 to 2006 based on remote sensing. *J. Glaciol*., 57(203), 543–556

Bliss A, Hock R and Cogley JG (2013) A new inventory of mountain glaciers and ice caps for the Antarctic periphery. *Ann. Glaciol*., 54(63), 191–199

Bolch T (2007) Climate change and glacier retreat in northern Tien Shan (Kazakhstan/Kyrgyzstan) using remote sensing data. *Global Planet. Change*, 56, 1–12

Bolch T and 11 others (2012) The state and fate of Himalayan glaciers. *Science*, 336, 310–314

Chen JY (1989) The preliminary studies of several problems on lichenometry of glacial variation in the Holocene at the headwaters of the Urumqi river. *Sci. China Ser. B*, 1, 95–104

Chen Z, Luo GP, Xia J, Zhou KF, Lou SP and Ye MQ (2005) Ecological response to the climate change on the northern slope of the Tianshan Mountains in Xinjiang. *Sci. China Ser. D*, 48(6), 765–777

Cook AJ, Fox AJ, Vaughan DG and Ferrigno JG (2005) Retreating glacier fronts on the Antarctic Peninsula over the past half-century. *Science*, 308, 541–544

Evans IS (2006) Local aspect asymmetry of mountain glaciations: A global survey of consistency of favoured directions for glacier numbers and altitudes. *Geomorphology,* 73(1–2), 166–184

Frankl A, Zwertvagher A, Poesen J and Nyssen J (2013) Transferring Google Earth observations to GIS-software: example from gully erosion study. *Int. J. Digital Earth*, 6, 196–201

Gao MJ, Han TD, Ye BS and Jiao KQ (2013) Characteristics of melt water discharge in the Glacier No.1 basin, headwater of Urumqi River. *J. Hydrol*., 489, 180–188

Grove JM (2004) *Little Ice Ages, Ancient and Modern*. Routledge, London

Huybers K and Roe GH (2009) Spatial patterns of glaciers in response to spatial patterns in regional climate. *J. Climate*, 22, 4600–4620

Kamp U, Byrne M and Bolch T (2011) Glacier fluctuations between 1975 and 2008 in the greater Himalaya range of Zanskar, southern Ladakh. *J. Mt. Sci*., 8, 374–389

Kerr RA (2013) Melting glaciers, not just ice sheets, stoking sea-level rise. *Science*, 340,

Khromova TE, Dyurgerov MB and Barry RG (2003) Late-twentieth century changes in glacier extent in the Ak-shirak Range, Central Asia, determined from historical data and ASTER imagery. *Geophys. Res. Lett*., 30(16), 1863

Li KM, Li HL, Wang L and Gao WY (2011) On the relationship between local topography and small glacier change under climatic warming on Mt. Bogeda, eastern Tian Shan, *China. J. Earth Sci*., 22(4), 515–527

Li YK, Liu GN and Cui ZJ (2001) Glacial valley cross profile morphology, Tian Shan Mountains, China. Geomorphology, 38(1–2), 153–166

Li YK, Napieralski J and Harbor J (2008) A revised automated proximity and conformity analysis method to compare predicted and observed spatial boundaries of geologic phenomena. *Comput. Geosci*., 34, 1806–1814

Li YK, Liu GN, Kong P, Harbor J, Chen YX and Caffee MW (2011) Cosmogenic nuclide constraints on glacial chronology in the source area of the Urumqi River, Tian Shan, *China. J. Quaternary Sci*., 26(3), 297–304

Li YK, Liu GN, Chen YX, Li YN, Harbor J, Stroeven AP, Caffee M, Zhang M, Li CC and Cui ZJ (2014) Timing and extent of Quaternary glaciations in the Tianger Range, eastern Tian Shan, China, investigated using 10Be surface exposure dating. *Quatern. Sci. Rev*. 98, 7–23

Liu CH and Han TD (1992) Relation between recent glacier variations and climate in the Tien Shan Mountains, central Asia. *Ann. Glaciol*., 16, 11–16

Liu SY, Sun WX, Shen YP and Li G (2003) Glacier changes since the Little Ice Age maximum in the western Qilian Shan, northwest China, and consequences of glacier runoff for water supply. *J. Glaciol*., 49(164), 117–124

Maisch, M (1992) *Die Gletscher Graubündens: Rekonstruktionen und Auswertung der Gletscher und deren Veränderungen seit dem Hochstand von 1850 im Gebiet der östlichen Schweizer Alpen (Bündnerland und angrenzende Regionen)*. Zürich, Universität Zürich. Geographisches Institut. (Physische Geographie 33.)

Nainwal HC, Negi BDS, Chaudhary M, Sajwan KS and Gaurav A (2008) Temporal changes in rate of recession: evidence from Satopanth and Bhagirath Kharak glaciers, Uttarakhand, using Total Station Survey. *Current Sci*., 94(5), 653–660

Narama C, Kääb A, Duishonakunov M and Abdrakhmatov K (2010) Spatial variability of recent glacier area changes in the Tien Shan Mountains, Central Asia, using Corona (~1970), Landsat (~2000), and ALOS (~2007) satellite data. Global Planet. Change, 71(1–2), 42–54

Paul F, Kääb A, Maisch M, Kellenberger T and Haeberli W (2004) Rapid disintegration of Alpine glaciers observed with satellite data. *Geophys. Res. Lett*., 31, L21402

Pike RJ and Wilson SE (1971) Elevation-relief ratio, hypsometric integral and geomorphic area-altitude analysis. *Geol. Soc. Am*. Bull., 82(4), 1079–1084

Porter SC (1970) Quaternary glacial record in Swat Kohistan, west Pakistan. *Geol. Soc. Am*. Bull., 81(5), 1421–1446

Racoviteanu AE, Arnaud Y, Williams MW and Ordoñez J (2008) Decadal changes in glacier parameters in the Cordillera Blanca, Peru, derived from remote sensing. *J. Glaciol*., 54(186), 499–510

Savoskul OS (1997) Modern and Little Ice Age glaciers in 'humid' and 'arid' areas of the Tien Shan, Central Asia: two different patterns of fluctuation. *Ann. Glaciol*., 24, 142–147

Shi YF and Ren JW (1990) Glacier recession and lake shrinkage indicating a climatic warming and drying trend in Central Asia. *Ann. Glaciol*., 14, 261–265

Solomina ON (2000) Retreat of mountain glaciers of northern Eurasia since the Little Ice Age maximum. *Ann. Glaciol*., 31, 26–30

Solomina ON, Barry R and Bodnya M (2004) The retreat of Tien Shan glaciers (Kyrgyzstan) since the Little Ice Age estimated from aerial photographs, lichenometric and historical data. Geografiska Annaler. Series A, *Physical Geography*, 86(A2), 205– 215

Sorg A, Bolch T, Stoffel M, Solomina ON and Beniston M (2012) Climate change impacts on glaciers and runoff in Tien Shan (Central Asia). *Nature Climate Change*, 2, 1–7

Sun XJ, Shen SH, Leptoukh GG, Wang PX, Di LP and Lu MY (2012) Development of a Web-based visualization platform for climate research using Google Earth. *Comput. & Geosci.*, 47, 160–168

Wang ZC (2010) The changes of Lop Nur Lake and the disappearance of Loulan. *J. Arid Land*, 2(4), 295–303

Xu XK, Kleidon A, Miller L, Wang SQ, Wang LQ and Dong GC (2010) Late Quaternary glaciation in the Tianshan and implications for paleoclimatic change: a review. *BOREAS*, 39, 215–232

Yang B, Bräuning A, Dong ZB, Zhang ZY and Jiao KQ (2008) Late Holocene monsoonal temperate glacier fluctuations on the Tibetan Plateau. *Global Planet. Change*, 60, 126–140

Ye BS, Yang DQ, Jiao KQ, Han TD, Jin ZF, Yang HA and Li ZQ (2005) The Urumqi River source Glacier No.1, Tianshan, China: Changes over the past 45 years. *Geophys. Res. Lett.*, 32(21), L21504

Yi CL, Liu KX, Cui ZJ, Jiao KQ, Yao TD and He YQ (2004) AMS radiocarbon dating of late Quaternary glacial landforms, the source area of the Urumqi River, Tien Shan: a pilot study of 14C dating on inorganic carbon. *Quaternary Int.*, 121, 99–107

Yi CL, Chen HL, Yang JQ, Liu B, Fu P, Liu KX and Li SJ (2008) Review of Holocene glacial chronologies based on radiocarbon dating in Tibet and its surrounding mountains. *J. Quaternary Sci.*, 23(6–7), 533–543

Yu L and Gong P (2012) Google Earth as a virtual globe tool for Earth science applications at the global scale: progress and perspectives. *Int. J. Remote Sens.*, 33(12), 3966–3986

Appendix for Chapter 3

Table 3-1. Regression between ΔELA and six local factors (glacier area, slope, aspect, shape, hypsometry, and mean elevation)

Explanatory variable	Parameter estimate	p value	R^2
intercept	262.752	0.026	
ln (Area)	-2.542	0.485	
Mean elevation	-0.003	0.906	
Cosine of aspect	-60.057	0.000	
Slope	2.263	0.000	
Shape index	-87.052	0.001	
Hypsometric integral	-64.700	0.172	
The whole model		0.000	0.162

Table 3-2. Regression between the relative glacier area change and two statistically significant local factors (glacier area and mean elevation)

Explanatory variable	Parameter estimate	p value	R^2
Intercept	304.475	0.000	
ln (Area)	-11.286	0.000	
Mean elevation	-0.028	0.000	
The whole model		0.000	0.640

Table 3-3. Pearson correlation coefficients for topographic/geometric factors and glacier change indicators

	ln(Area) (m²)	Cosine of Aspect	Slope (˚)	Shape Index	Hypso-metric Integral	Mean Elevation (m)	Area Change (%)	ΔELA (m)
ln (Area) (m²)	1.000							
Cosine of Aspect	-0.096	1.000						
Slope (˚)	**-0.398**	0.027	1.000					
Shape Index	**-0.474**	**0.201**	-0.027	1.000				
Hypsometric Integral	**-0.253**	-0.106	**0.222**	**0.157**	1.000			
Mean Elevation (m)	**0.233**	**-0.604**	0.003	-0.140	**0.417**	1.000		
Area Change (%)	**-0.766**	**0.242**	**0.325**	**0.318**	0.124	**-0.405**	1.000	
ΔELA (m)	0.018	**-0.311**	**0.171**	**-0.231**	-0.021	**0.158**	0.018	1.000

Bold numbers indicate correlation significant at the 0.001 level (p < 0.001).
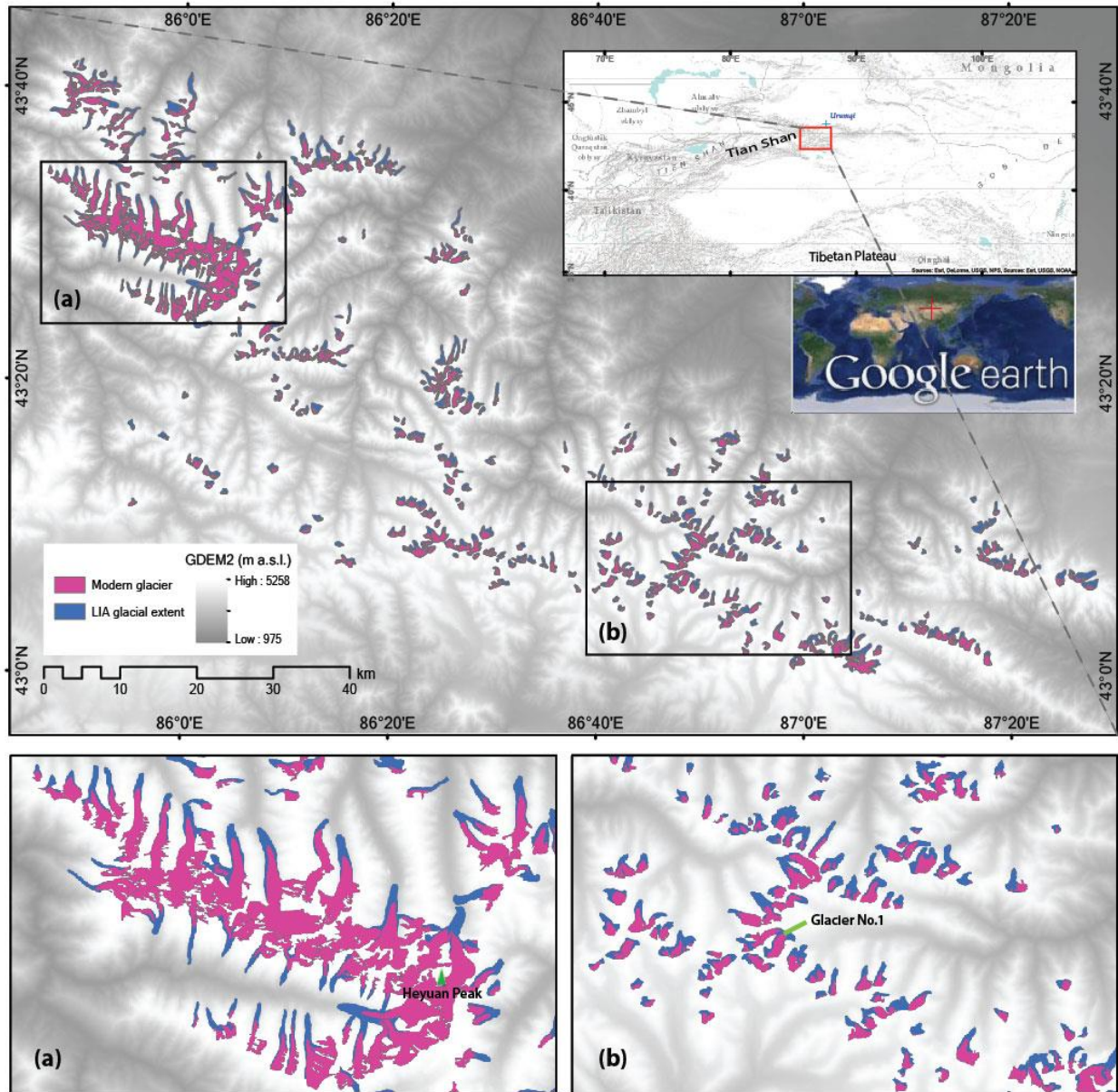
Figure 3-1. Map of the study area overlapped with GDEM V2. A total number of 487 modern glaciers (only the ones with corresponding LIA extents) is illustrated with pink and LIA extents in blue. The upper-right inset shows the terrain in Central Asia, the extent of Tian Shan, and the city of Urumqi (blue cross) close to our study area (red box). The Google Earth overview image provides the location of our study area in the world. Boxes (a) and (b) are enlarged to show detailed delineations of modern glaciers and LIA glacial extents around Mt. Heyuan Peak (a) and the Urumqi River headwaters (b).
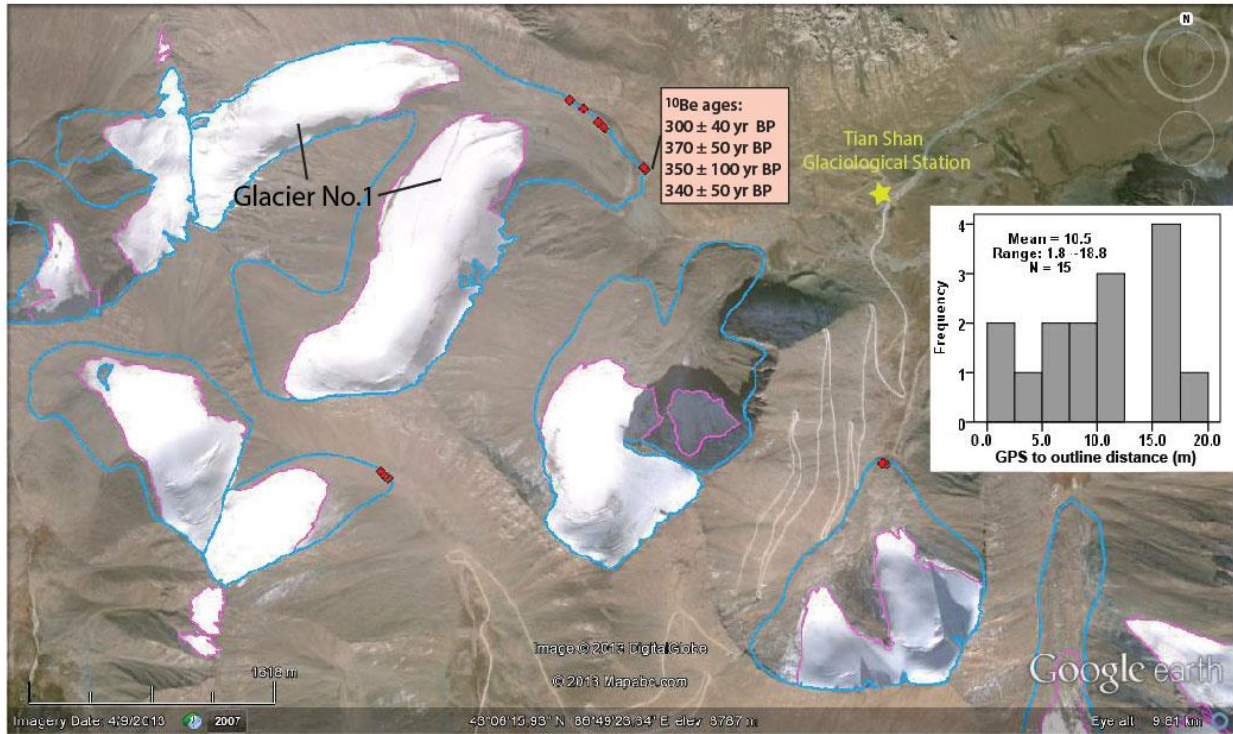
Figure 3-2. A bird's eye view of the Urumqi River headwaters in Google Earth, with delineated modern (pink) and LIA (blue) glacier outlines, field-measured 15 GPS coordinates (red dots), and four [10]Be dating results (Li and others, 2014) marked in the box. The frequency distribution of the shortest distances from 15 GPS coordinates to their corresponding LIA outlines is illustrated in the bar chart. The Tian Shan Glaciological Station is marked as a yellow star.
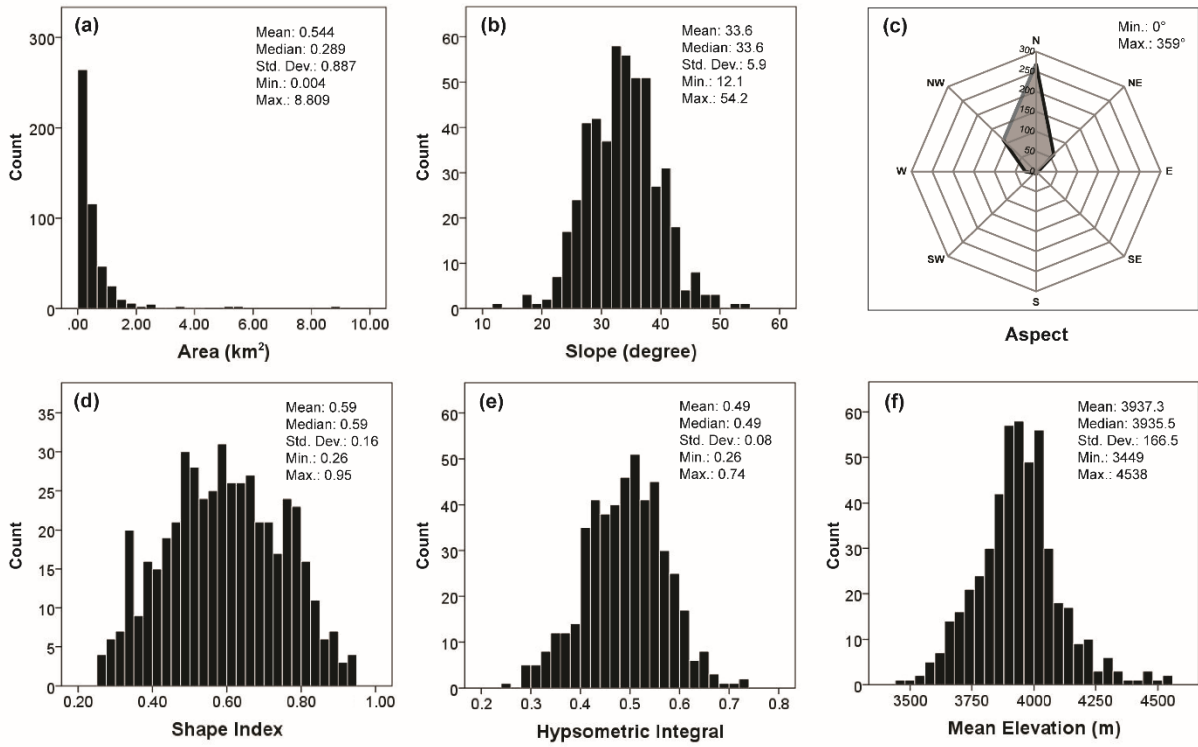
Figure 3-3. Frequency distribution of six local topographic/geometric parameters: (a) area, (b) slope, (c) aspect, (d) shape index, (e) hypsometric integral, and (f) mean elevation.
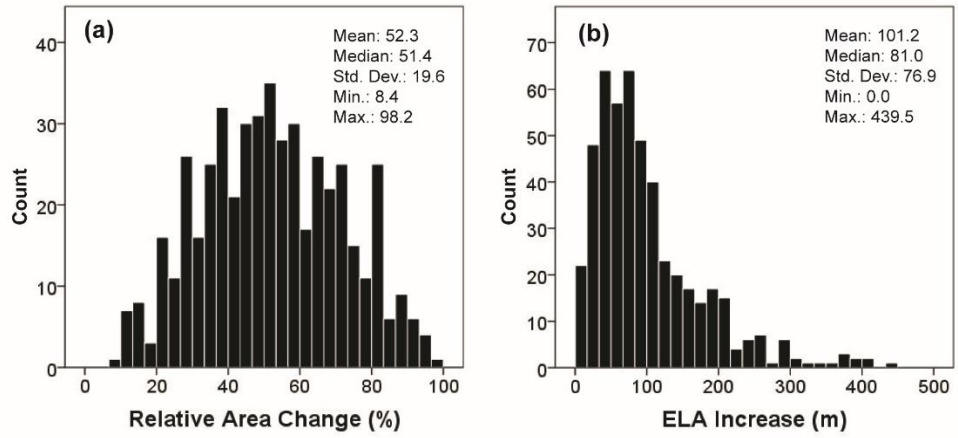
Figure 3-4. Frequency distribution of two glacier change indicators: (a) relative area change and (b) ΔELA.
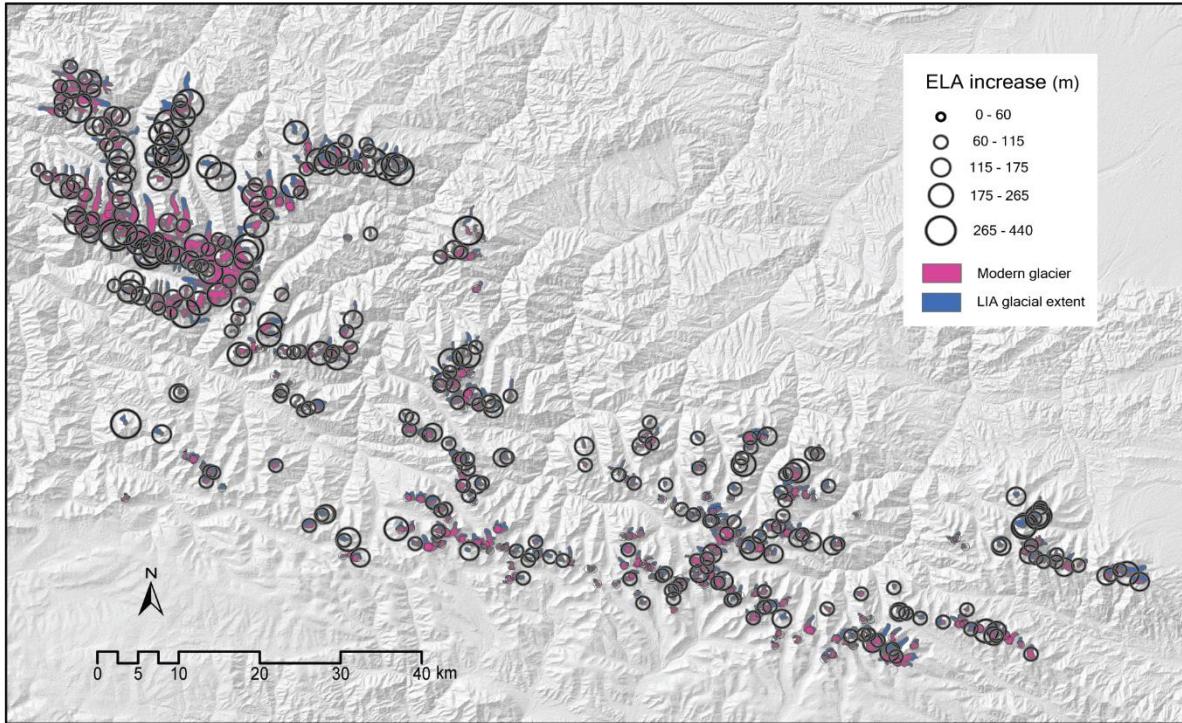
Figure 3-5. Spatial distribution of ΔELA in the Boro-Eren Range, Tian Shan: larger values occur in the west and on north-facing slopes, while smaller values occur in the central-eastern areas and on south-facing slopes.
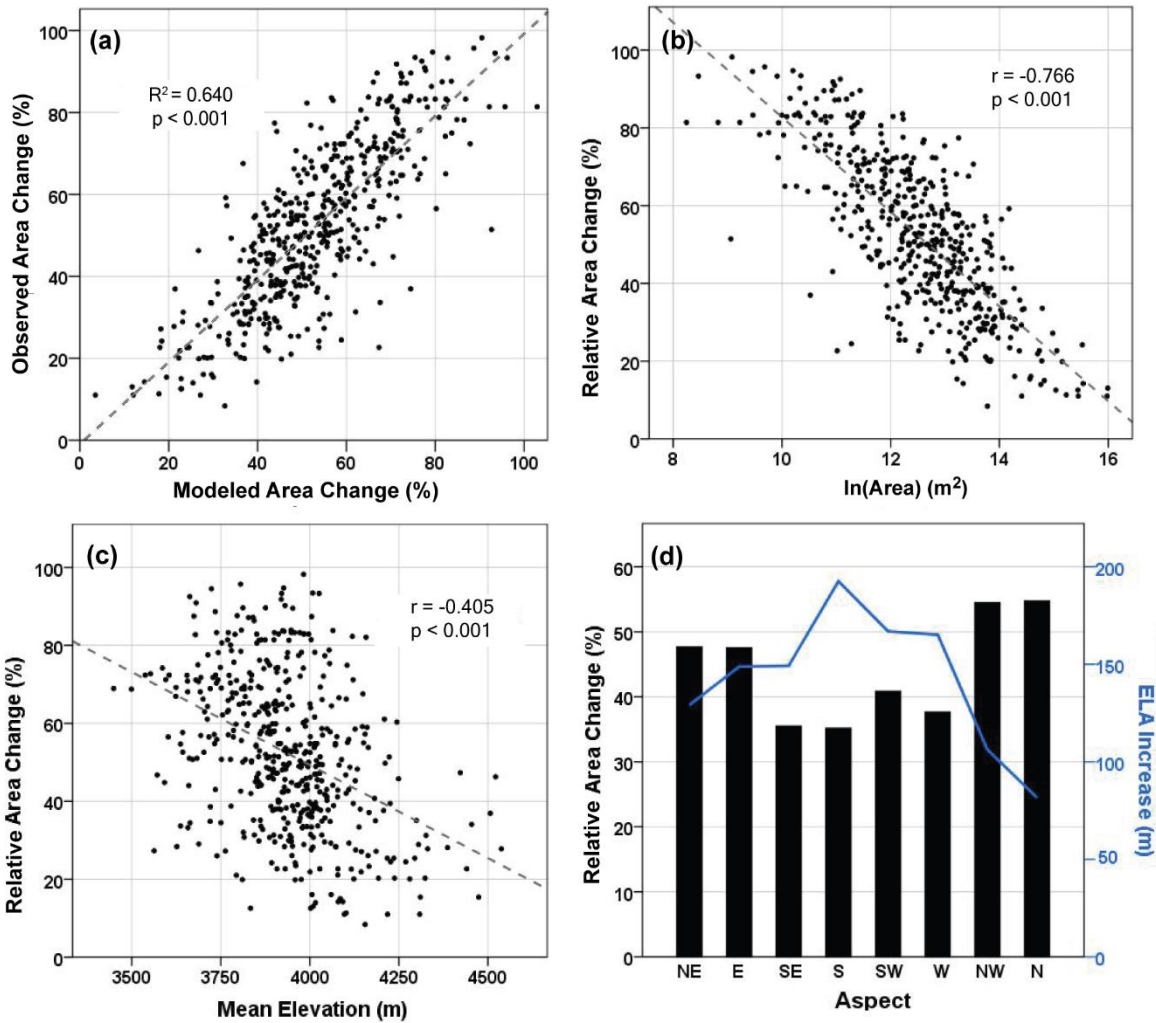
Figure 3-6. (a): Scatter plot of the observed relative area change (%) vs. the modeled area change (%) from equation (3). (b): Scatter plot of relative area change vs. ln (Area). (c): Scatter plot of relative area change vs. mean elevation. (d): Relative area change and ΔELA in eight different directions of the average aspect for each glacier. (Note: "relative area change" means the percent of change in glacier area compared to the maximum LIA extent.)

Chapter 4

Cosmogenic [10]Be Constraints on Little Ice Age Glacial Advances in the Eastern Tian Shan, China

This chapter is a manuscript in preparation for *Quaternary Science Review*. The use of "we" in this chapter refers to co-authors, Drs. Yingkui Li, Jon Harbor, Gengnian Liu, Chaolu Yi, Marc Caffee, and myself. As the first author, I conducted the field and laboratory work, led the data analysis, and wrote the manuscript.

Abstract

Glaciers provide critical freshwater supply in Central Asia, so understanding the dynamics of glaciers, especially during the last millennium, is of great importance. Little Ice Age (LIA) glacial advances, as represented by a set of fresh, sharp-crested, boulder covered and compact moraines a few hundred meters downstream from modern glaciers, have been widely recognized in the Central Asian highlands. However, few studies have constrained the formation ages of these moraines. We report 27 [10]Be exposure ages from presumed LIA moraines in five glacial valleys in the Urumqi River headwater area and the Haxilegen Pass area of the eastern Tian Shan, China. Our results suggest that the maximum LIA glacial extent was reached around 370±100 yr BP, an extremely cold and wet period as indicated by proxy data from ice cores, tree rings, and lake sediments in Central Asia. We also dated a later glacial advance to 210±50 yr BP. However, [10]Be exposure ages on presumed LIA moraines in front of small, thin glaciers are widely scattered and much older than the globally understood time of the LIA. Topographic maps indicate that these small, thin glaciers were more extensive in the early 1960s, and some of the [10]Be sample sites were covered by ice at that time. Boulders being transported by these small and thin glaciers may have significant inheritance and include material reworked from deposits originally formed prior to the LIA glacial advances, producing apparently old and widely scattered exposure ages. Other published ages indicate an earlier LIA glacial advance occurred around 730±300 yr BP in the easternmost Tian Shan, but in our study area the extensive advance at 370±100 yr BP presumably reworked or covered deposits from this event.

4.1. Introduction

The "Little Ice Age" (LIA) is a well-recognized cold period in the past millennium that occurred approximately between 1300 and 1850 AD (Grove, 2004; Mann et al., 2009). The timing and intensity of this cold event have been documented in historical records and natural proxies, such as tree rings, sediments, and ice cores, around the world (e.g. Chen et al., 2013; Chenet et al., 2010; Grove, 2004; Harrison et al., 2007; Luckman, 2000; Mann et al., 2008; Mann et al., 2009; Solomina et al., 2004; Xu and Yi, 2014; Yao et al., 1997). Abundant evidence has suggested that glaciers in many parts of the world expanded to a more extensive position during the LIA than they had at the beginning of the last millennium and since the twentieth century (e.g. Barclay et al., 2009; Benedict, 1968; Bräuning, 2006; Koch and Kilian, 2005; Mosley-Thompson et al., 1990; Schaefer et al., 2009; Xu and Yi, 2014). The timing and extent of LIA glacial advances were highly variable around the world, and LIA cooling was probably not a globally synchronous event (Bradley and Jones, 1993; Chenet et al., 2010; Kreutz et al., 1997; Luthi, 2014; Mann, 2002; Mann et al., 1999).

In introducing the term "Little Ice Age," Matthes (1939) observed that "…many of the small cirque glaciers on those ranges (mountain ranges in the western U.S.) are fronted by very fresh-looking terminal moraines arranged in compact concentric series or combined into one or two massive compound embankments…". Similar descriptions of LIA glacial landforms exist in other regions (e.g. Owen, 2009; Shi and Ren, 1990; Su and Shi, 2002; Xu and Yi, 2014). These moraines have been dated using radiocarbon, dendrochronology, and lichenometry based on proxy materials such as buried wood, trees, and lichens (e.g. Bräuning, 2006; Derbyshire et al., 1984; Jiao et al., 2005; Loso et al., 2014; Luckman, 2000; Solomina et al., 2004). However, it has been challenging to accurately constrain the timing of the LIA glacial advances because of

the lack of proxy materials for these methods in many locations, including the Central Asian highlands. Since the early 1990s, cosmogenic nuclide (CN) surface exposure dating has been widely used to constrain the timing of past glacial events (Gosse and Phillips, 2001; Ivy-Ochs and Kober, 2008; Li and Harbor, 2009). One advantage of this dating method is that the material that is needed for dating (boulders or sediments) is ubiquitous in glacial environments. The time range for CN surface exposure dating usually spans from 10^3 to 10^6 years; however, technical improvements have extended the range to date events on the 10^2 year timescale (Finkel et al., 2003; Kelly et al., 2008; Koppes et al., 2008; Li et al., 2014; Owen et al., 2005; Owen et al., 2010; Schaefer et al., 2009; Schimmelpfennig et al., 2014; Seong et al., 2009).

Constraining the timing and extent of past glacial events is critical for understanding past climate conditions and better assessing future glacial and environmental changes. Located at the confluence zone of the westerlies and the Siberian High, mountain glaciers in the Tian Shan are sensitive indicators of climate change (Aizen et al., 2001; Benn and Owen, 1998; Sorg et al., 2012). Glaciers provide a freshwater source for natural and human ecosystems in the arid and semi-arid area in Central Asia. Ongoing glacial retreat is causing water availability and food security issues in this rapidly developing region. Previous paleo-glacial reconstructions have been conducted to establish glacial chronologies in the Tian Shan over a range of timescales (e.g. Chen et al., 2015; Kong et al., 2009; Koppes et al., 2008; Li et al., 2011, 2014; Lifton et al., 2014; Narama et al., 2007; Zech, 2012; Zhao et al., 2006). However, only a few studies have constrained the formation ages of LIA moraines, using cosmogenic ^{10}Be exposure dating (Chen et al., 2015; Koppes et al., 2008; Li et al., 2014), lichenometry (Chen, 1989; Solomina et al., 2004), or radiocarbon dating of inorganic carbonates (Yi et al., 2004). More studies are needed to

74

constrain the timing and extent of LIA glacial advances to better understand climate conditions and changes during the last millennium in this critical region.

The purpose of this study is to constrain the formation ages of presumed LIA moraines from five glacial valleys in the Urumqi River source area and the Haxilegen Pass area of the eastern Tian Shan, China, using ^{10}Be surface exposure dating. Combined with other published LIA ages, we then examine the timing and extent of the LIA glacial extent across the eastern Tian Shan. We also compare our glacial chronology with proxy climate records derived from tree rings, sediment cores, ice cores, and other materials to examine the relationship between glacier changes and climate fluctuations during the LIA.

4.2. Study Sites and Previous Dating Work

The Tian Shan is one of the largest mountain ranges in Central Asia, formed by collision of the Indian and Eurasian continental plates about 40 to 50 million years ago (Kaban and Yuanda, 2014; Yin and Harrison, 2000). It includes a series of WSW-ENE trending ranges, stretching from the western boundary of Kyrgyzstan across the Xinjiang Uighur Autonomous Region in China and almost to Mongolia (Figure 4-1). Most peaks in these ranges reach about 4000 m above sea level (a.s.l.). The Tian Shan is bounded by the Taklimakan Desert to the south and the Gurbantonggut Desert to the north, producing a sharp contrast of environments between high mountains and intervening valleys/basins (Aizen et al., 1997). The continental climate of this area has high aridity and extremes of seasonal and diurnal temperatures (Aizen et al., 1997; Ye et al., 2005). The prevalent westerlies bring moisture from the Aral, Caspian, and Black Seas, as well as from the North Atlantic and Arctic Oceans, and they interplay with the mountain ranges (orographic effect), causing a sharp west-east decreasing gradient in precipitation (Aizen et al., 2006; Benn and Owen, 1998; Chen et al., 2008; Sorg et al., 2012). The Siberian High is

another important climate system that is associated with cold and dry winters (Gong and Ho, 2002; Owen and Dortch, 2014; Yang et al., 2009). Asian Monsoon systems do not typically penetrate into the Tian Shan area due to the orographic barriers of the Himalayas and the Tibetan Plateau (Chen et al., 2008). Large valley glaciers and ice caps occur mainly in the western ranges where there is more moisture; while the eastern Tian Shan (Chinese Tian Shan) contains relatively small glaciers.

We selected two areas in the eastern Tian Shan for this study: the headwaters of the Urumqi River and the Haxilegen Pass (Figure 4-2). These two areas are located west of Urumqi, the capital city of the Xinjiang Uyghur Autonomous Regions, China, and are about 200 km apart (Figure 4-1). Geomorphic evidence, such as erratics, striations, moraines, and U-shaped valleys, indicates that these areas have been glaciated in the past (Cui, 1981; Liu and Xiong, 1992; Li et al., 2001a, 2001b).

Headwaters of the Urumqi River

The headwater area of the Urumqi River (~43.10ºN, 86.83ºE) is located in the Tianger Range. The mean annual temperature is about −5.6 ºC, and the annual precipitation is about 430 mm (Liu and Xiong, 1992). This area is well-known in the field of glacial geomorphology due to its accessibility, well-preserved glacial landforms, and the presence of the Tian Shan Glaciological Station, established by the Chinese Academy of Sciences in 1959. Our samples were collected in front of two glaciers: Glacier No. 1 (UG1), and Glacier No. 3 (UG3) (Figure 4-2a). These two glaciers are located in the head of the Daxi Valley, an east-facing U-shaped valley on the northern slope of the mountain range that has double troughs (Cui, 1981; Li et al., 2001a). Meltwater from the glaciers in the head of the Daxi Valley flows into the Urumqi River and provides fresh water for the Urumqi city. UG1 is one of the most intensively studied glaciers

in Central Asia. Its current two branches were part of a single larger glacier, as shown on topographic maps from the early 1960s (Figure 4-2b; Li et al., 2008a). The total area of current two branches of UG1 is close to 3.0 km^2. The lower branch of UG1 ends at an elevation of 3750 m a.s.l. Fresh-looking moraines are located 700 m downstream from the lower branch terminus (Figures 4-3a and b).

Most available [10]Be ages in the Daxi Valley have provided evidence for glacial events during Marine Oxygen Isotope Stages (MIS) 2 (Kong et al., 2009; Li et al., 2011, 2014). The LIA event around 340±70 yr BP[1] has been constrained previously using [10]Be exposure dating from four boulders on top of the fresh-looking moraines in front of UG1 (Figure 4-2a; Li et al., 2014). Other dating methods have also been applied to constrain the formation age of this moraine set. Chen (1989) dated three moraine ridges in front of UG1 to 412±20 yr BP, 173±20 yr BP, and 79±20 yr BP using lichenometry. Yi et al. (2004) obtained ages of 400±120 yr BP and 430±120 yr BP using AMS ^{14}C dating of inorganic carbonate coatings on clasts within the moraines (recalculated in Xu and Yi, 2014).

UG3 is a small (area = 0.8 km^2) and thin glacier compared to UG1, and it resides on a sheltered steep slope, facing north (Figure 4-2a). The glacier front ends at 3660 m a.s.l., with presumed LIA moraines located 400 m downstream from the current terminus. The moraines in front of UG3 have gentle surfaces (Figures 4-3c and d), rather than crested moraine ridges. Considering the shape, size, and environmental conditions, these moraines might be continuously moved slowly downward after glacial retreat, forming a rock glacier (Liu et al., 1995). No prior dating work has been conducted on these moraines.

---

[1] BP: before present (1950 AD).

Haxilegen Pass

The Haxilegen Pass (~43.73ºN, 84.41ºE) is located in the Borohoro Range, with ridge elevations ranging from 3700 m to 4000 m a.s.l. The mean temperature is about −5.2 ºC on the southern slope, and −5.8 ºC on the northern slope, and the annual precipitation is about 500–600 mm (Liu and Xiong, 1992). No numerical dating of glacial landforms has been conducted in the Haxilegen Pass area.

We investigated the LIA moraines in front of three glaciers, coded as HDBA, HDBB, and HDBC in this study (Figure 4-2c). HDBA and HDBB are located on the northern slope of the ridge, while HDBC is located on the southern slope. The areas of HDBA and HDBB are over 2 km^2, similar to the size of UG1. The right margin of the HDBA fresh moraine merges with the HDBB fresh moraine, but these moraines are still distinguishable in Google Earth imagery and in the field (Figures 4-2c and 4-3e). The fresh moraine of HDBA ends at a higher elevation (3400 m a.s.l.) than that of HDBB (3380 m a.s.l.). Both moraines are rich in boulders, and the height of the fresh, outermost moraine was estimated to be about 10–15 m in the field. Such fresh-looking, non-vegetation-covered moraines overlap the grass-covered older landforms (Figures 4-3e and i). The distance from the young moraine to the glacier front is about 900 m. Two small tarns lie between the moraines and the glacier front (Figure 4-2c). Well-exposed large boulders (>1 m in diameter) and pebbles are scattered on the moraine surfaces (Figures 4-3f, j, and h). HDBC, located on the southern slope of the mountain ridge, is a small and thin glacier with an area of about 0.4 km^2 (Figure 4-3k), similar to that of UG3. The thin, fresh moraine lies on top of the older-looking moraines (Figure 4-3l). The HDBC fresh moraine is about 400 m away from the glacier front, with a tarn formed in front of the glacier.

4.3. Methods

4.3.1. Mapping and field sampling

Moraines that are fresh looking, sharp-crested, boulder-compact ridges located a few hundred meters away from a glacier terminus are usually assumed to be deposited during the LIA (Matthes, 1939; Owen, 2009; Shi and Ren, 1990). Studies have indicated that two or three lateral and/or terminal moraines were formed in the Central Asian highlands during different cold periods within the LIA (Liu et al., 2003; Shi and Ren, 1990; Su and Shi, 2002; Xu and Yi, 2014). The outermost moraine represents the maximum LIA glacial extent. Prior to the fieldwork, we identified and delineated these outermost moraines in Google Earth. We then checked these moraines in the field and also looked for twin or triplet moraine ridges that might be suitable for dating multiple LIA glacial advances.

We collected 1–4 cm thick rock chips (at least 1 kg) from the surfaces of quartz-rich boulders, using chisel and hammer, for ^{10}Be surface exposure dating. Pebble samples were also collected at some sites to evaluate moraine surface stability by comparing the ages of boulders and pebbles (Briner, 2009; Heyman et al., 2011a; Li et al., 2014). These samples were chosen from locations with minimized potential impact from shielding, movement, and overturning possibilities (Figure 4-3). Detailed sample information was recorded in the field, and descriptions are provided in Table 4-1. The topographic shielding factor for each sample was calculated using a Python tool and a Shuttle Radar Topography Mission (SRTM) digital elevation model (DEM), with 5º as both azimuth interval and elevation angle interval (Li, 2013). Four or five samples at each presumed LIA moraine were collected to constrain the exposure age. At the headwater area of the Urumqi River, we collected three samples from the lateral moraine at the UG1 site to complement previous dating (Chen, 1989; Yi et al., 2004; Li et al., 2014), and four samples from

79

the UG3 fresh moraine. At the Haxilegen Pass, we collected ten samples at HDBA, including

five samples from an internal moraine and five from an outer moraine. We also collected five

samples each from outermost moraines at HDBB and HDBC, respectively. In total, 27 samples

were collected from the presumed LIA moraines in these two study areas to constrain the timing

of the LIA glacial event using [10]Be surface exposure dating.

4.3.2. Laboratory methods

All samples were crushed and sieved to 250–500 μm in the College of Urban and

Environmental Sciences at Peking University. Physical and chemical preparations were

conducted in the cosmogenic nuclide sample preparation laboratory at University of Tennessee

using standard procedures modified from Kohl and Nishiizumi (1992). After quartz separation

and purification, about 1 g of each sample was extracted to check quartz purity using Olympus

X-ray Fluorescene (XRF) and X-ray Diffraction (XRD) Analyzers. The rest purified quartz

samples, ranging from 45.5 g to 102.3 g, was then dissolved with an addition of 0.2–0.4 mg [9]Be

carrier using hydrofluoric acid. Then through steps of chromatography columns and multiple

precipitations, beryllium was purified to make a BeO target. The [10]Be/[9]Be ratios were measured

using Accelerator Mass Spectrometry (AMS) at Purdue Rare Isotope Measurement Laboratory

(PRIME Lab) at Purdue University and corrected with procedural blanks ($0.7–5.8 \times 10^{-15}$). The

[10]Be/[9]Be ratios were converted to [10]Be concentrations for exposure age calculations (Table 4-1).

4.3.3. Exposure age calculation and determination

Cosmogenic [10]Be exposure ages were calculated using the CRONUS Earth 2.2 online

calculator (Balco et al., 2008) (http://hess.ess.washington.edu/math/) with an assumption of zero

erosion (Lal, 1991). We calculated [10]Be exposure ages derived from five different scaling

models. In the interpretation, we focus on ages derived from the Lal (1991)/Stone (2000) time-

dependent model (Table 4-2). We used the northeast North America production rate (NENA) as the production rate calibration dataset, which is 3.85±0.19 atoms g^{-1} yr^{-1}, because most estimates of ^{10}Be production rates published since Balco et al. (2009), with broad geographic coverage, generally agree within uncertainties with those values (e.g. Li et al., 2014; Lifton et al., 2014; Putnam et al., 2010). Rock density was assigned as 2.7 g cm^{-3}. Our ages were reported in the unit of yr BP, which were calculated by subtracting 60 years from the CRONUS calculated exposure ages. We also converted other exposure ages from previous publications to this unit to ensure consistent age format and age comparison in the study (Table 4-2).

We plotted the probability density distribution of all ^{10}Be exposure ages (with their uncertainties) for each moraine (Figures 4-4 and 4-5). These plots help identify age clusters and potential outliers. Ideally, boulders on top of a moraine should produce exposure ages reflecting the moraine formation time, but exposure ages on a moraine are usually scattered, reflecting uncertainties in sample preparation/measurement and/or complex geomorphic processes. Different strategies exist in interpreting scattered exposure ages, and different researchers may apply different methods to identify ourliers. We used the reduced chi-squared test (χ_R^2) to test if age scatter is due to measurement uncertainty (Balco, 2011; Balco and Schaefer, 2006; Chen et al., 2015; Li et al., 2014). If the χ_R^2 value is statistically significant (p < 0.05), the variation in ages can not be explained solely by measurement errors and the age scatter is likely caused by geomorphic processes. In this case, we refined the χ_R^2 value by gradually removing the ages outside the cluster until the test become not significant. If ages are excessively scattered and do not overlap within the error, no age can be used to represent the age for the moraine. If the χ_R^2 value is not statistically significant (p > 0.05), the variation in ages is caused mainly by

measurement errors (Chen et al., 2015) and, in this case, the weighted mean of the ages is assigned as the age of the moraine.

4.4. Results

4.4.1. Headwaters of the Urumqi River

Three samples (WY-12-21, 22, 23) from the UG1 lateral moraine produced exposure ages of 160±20, 230±40, and 490±150 yr BP. Four previously published [10]Be ages from the terminal moraine at this site have clustered ages with a weighted mean of 340±70 yr BP (Li et al., 2014). The whole group of [10]Be ages ranges from 160±20 to 490±150 yr BP, within the span of the LIA period (Table 4-2; Figure 4-4). The reduced chi-squared statistic on this group of seven samples is 10.8 ($p < 0.05$), indicating the scatter of these ages is not solely caused by measurement uncertainty. Two of the three samples from the lateral moraine are much younger than other ages. These boulders, located on a less stable lateral moraine, might have experienced some toppling or shielding from other boulders, causing apparently younger surface exposure ages. Another possibility is that these two young boulders around 190 yr BP were actually produced by a later glacial advance. After removing these two young ages, χ_R^2 is reduced to 1.05 ($p > 0.05$), allowing for the use of the weighted mean of the five remaining ages (370±110 yr BP) to represent the moraine age. Thus, we assigned the weighted mean age of 370±110 yr BP for the maximum LIA glacial advance in front of UG1 (Figure 4-4). This age is consistent with the oldest ages of the LIA glacial advances constrained by lichenometry (412±20 yr BP; Chen, 1989) and close to two AMS ^{14}C ages (400±120 yr BP and 430±120 yr BP) reported in Yi et al. (2004). Such consistent ages derived from multiple methods confirm that Glacier No. 1 advanced to about 700 m beyond the current terminal position around 370±110 yr BP.

The adjacent site, UG3, however, yielded four exposure ages ranging from 660±50 to 5230±290 yr BP. A large χ_R^2 of 1239.0 suggests that geomorphic processes played a critical role in the scatter of the ages (Figure 4-4). Thus, we cannot assign the age of the moraine to the LIA based on these old and widely scattered boulder ages.

4.4.2. Haxilegen Pass

Five samples (HDB-12-06 to 10) from the HDBA inner fresh moraine produced exposure ages ranging from 160±20 to 760±80 yr BP (Table 4-2). The probability density plot shows that three young ages are clustered, and two older ages, of 530±50 yr BP and 760±80 yr BP, do not overlap with this cluster (Figure 4-5). Removing these two older ages reduces the χ_R^2 value from 49.7 (p < 0.05) to 1.7 (p > 0.05). We use the weighted mean of three young exposure ages, 190±40 yr BP, as the minimum exposure age for the HDBA inner moraine. The pebble sample at this site, HDB-12-07, yielded an exposure age of 230±30 yr BP, consistent with the two boulder samples. The similarity between pebble and boulder exposure ages indicates that this moraine surface is relatively stable, so that pebbles and boulders might have experienced similar exposure histories (Briner, 2009; Heyman et al., 2011a). The two older ages (530±50 yr BP and 760±80 yr BP) may be incorporated from an earlier LIA glacial advance.

The exposure ages of five samples (HDB-12-10 to 15) from the HDBA outer moraine show an interesting pattern: four samples have ages within 1000 yr BP, but one sample, HDB-12-15, produced an age of 5930±330 yr BP, likely representing an outlier (Table 4-2; Figure 4-5). Removing this outlier, the other four exposure ages are still scattered ($\chi_R^2 = 19.6$, p < 0.05). The youngest boulder (170±40 yr BP) might have experienced incomplete exposure due to post-depositional processes, such as toppling and exhumation, or might indicate the presence of a young glacial event. The older age (690±60 yr BP) might correspond to an early LIA glacial

advance. The remaining two samples are clustered at 370±40 yr BP ($\chi_R^2 = 0.05$, p > 0.05). Considering the possibility that different LIA glacial advances might reach a similar extent and incorporate boulders from previous events, we argue that these two clustered ages may likely represent the age of this moraine, and the older ages may be incorporated from previous glacial events. We tentatively assign the weighted mean, 370±40 yr BP, as the formation age of the HDBA outer moraine.

Five boulder samples (HDB-12-16 to 20) taken from HDBB fresh moraine produced exposure ages ranging from 80±20 to 270 ± 60 yr BP (Table 4-2). The probability density plot shows that the youngest age is likely not part of the cluster of the other four ages (Figure 4-5). This youngest boulder might have experienced incomplete exposure. After removing this youngest age, the remaining four ages are highly clustered between 180±40 and 270±60 yr BP, with a χ_R^2 value of 0.7 (p > 0.05). The weighted mean of these four ages, 220±60 yr BP, was used to represent the age of the HDBB moraine, similar to the age of the HDBA inner moraine.

The five exposure ages from HDBC at the southern side of the Haxilegen Pass show an extremely scattered pattern, ranging from 1.3±0.1 to 9.3±0.5 kyr BP. The large value of χ_R^2 (471.1, p < 0.05) indicates that geomorphic processes have caused a wide range in exposure ages for individual samples. The widely scattered ages did not allow us to constrain the formation age for this moraine in front of HDBC.

4.5. Discussion

4.5.1.   Timing of LIA glacial advances in the Tian Shan

Four out of the six sampled moraines show the ages during the LIA (Figures 4-4 and 4-5). The UG1 and HDBA outermost moraines were dated to similar ages and indicate a maximum LIA glacial advance at 370±100 yr BP, a weighted mean of 370±110 yr BP at UG1 and 370±40

yr BP at outer HDBA. The HDBA inner moraine and HDBB yielded close ages around 210±50 yr BP, a weighted mean of 190±40 yr BP at inner HDBA and 220±60 yr BP at HDBB, indicating a late glacial advance during the LIA. Having these two distinct ages is consistent with previous descriptions of LIA moraines that include two or three sub-moraines in western China (Liu et al., 2003; Shi and Ren, 1990; Su and Shi, 2002; Xu and Yi, 2014).

In the easternmost Tian Shan, Chen et al. (2015) reported 11 [10]Be exposure ages from fresh-looking moraines in front of the glacier at the Turgan Valley in the Karlik Range (Figure 4-1). After removing outliers, their data indicate a moraine age of 730±300 yr BP (recalculated; Table 4-2), representing an earlier LIA advance. The existence of an early LIA glacial advance around 730 yr BP is also suggested by some of our ages, such as 760±80 yr BP at inner HDBA and 690±60 yr BP at outer HDBA, which were likely mixed with younger ages. In the western Tian Shan, Koppes et al. (2008) reported [10]Be exposure ages of 260±80 yr BP and 630±120 yr BP (recalculated in Li et al., 2014) on moraines from the Ala Archa Valley at the Kyrgyz Front Range (Figure 4-1). The older age is from an outer and lower moraine, while the younger age is from an inner and higher moraine. Although they are both LIA ages, the limited number of samples indicates that further work is required to constrain these moraines ages.

In summary, our ages along with other available data from the Tian Shan suggest that glaciers advanced at least three times during the LIA: the first advance occurred at 730±300 yr BP; the second advance was at 370±100 yr BP; and the most recent one was at 210±50 yr BP.

However, exposure ages from similar looking moraines in front of UG3 and HDBC are much older than the LIA and are widely scattered. To check the extents of these two glaciers in the past, we examined 1:50 000 topographic maps produced in China based on aerial photos in the early 1960s. The topographic maps indicate that these two glaciers were much more

extensive than their current positions and some of our sample sites were covered by ice in the early 1960s (Li et al., 2001a) (Figure 4-2b). It appears that the extents of these two glaciers during the LIA should at least reach our sample locations; thus, the moraines we sampled should be formed during the LIA. Therefore, we interpret that much older and widely scattered exposure ages from these moraines were likely caused by nuclide inheritance. Both UG3 and HDBC are small and thin glaciers. Glacial erosion under these small and thin glaciers has been likely limited and not powerful enough to produce fresh boulders from the ice-rock interface. Thus, the boulders and pebbles on top of moraines in front of these glaciers may be reworked materials that were formed during glacial advances or other processes, such as fluvial and slope processes prior to the LIA, with little subsequent disturbance during LIA advances. Therefore, the samples we collected may have considerable nuclide inheritance, yielding scattered and much older ages.

This interpretation is opposite to the argument of Heyman et al. (2011b) claiming that incomplete exposure is more important than prior exposure. Such a difference is because of different types of glaciers: small and thin glaciers, such as UG3 and HDBC, did not have enough power to produce fresh boulders, instead, they only disturbed previous deposits that may have experienced long-time exposure prior to the non-erosive ice coverage during the LIA; while a majority of boulders in Heyman et al. (2011b) came from moraines of large-sized valley or outlet glaciers that may have enough power to produce fresh boulders during glacial advances. In addition, ^{10}Be exposure ages compiled in Heyman et al. (2011b) are mainly >10 kyr BP, which is long enough to reflect the impact of post-glacial degradation on moraine ages (underestimating the true age). For young glacial events, such as the LIA, post-glacial degradation might not become significant enough to shift apparent exposure ages. For example, assuming that the effect of post-depositional shielding from cosmic rays (burial, erosion, or exhumation) is 10% on

exposure ages, such uncertainty only brings an order of tens of years shift in apparent exposure ages, which is not significant in constraining the timing of the young glacial events.

4.5.2. The extent of LIA glacial advances in the Tian Shan

The extent of LIA glacial advances can be measured by the distance from well-dated LIA moraines to the front of present-day glaciers. For the Urumqi River headwaters, the outermost LIA moraine is located about 700 m beyond the lower branch of the UG1 glacier snout (Figure 4-2). For the Haxilegen Pass, the [10]Be dated LIA moraines are within 900 m away from the glacier snout and comprise inner and outer moraine ridges located close to each other (Figure 4-2). In the easternmost Tian Shan, the fresh moraines dated to the LIA by Chen et al. (2015) are reported in distance up to 800 m away from the present glacier terminus. This level (700–900 m) of glacial retreat since the LIA maximum in the eastern Tian Shan is relatively less extensive compared to that in the western Tian Shan. For example, Solomina et al. (2004) examined retreats of 293 glaciers since the LIA in the Kyrgyz Tian Shan using 1980s aerial photographs and lichenometric dating and found a retreat distance of 989±540 m on average. Considering the continuous glacial retreat after the 1980s, the distance from the outermost LIA moraines to the front of present-day glaciers could be over 1 km. Differences in glacial retreat distance between the western and eastern Tian Shan are apparent, but more investigations are necessary to examine the spatial pattern of glacial retreat since the LIA across the entire Tian Shan.

Although [10]Be ages did not produce a conclusive age for the moraines at UG3 and HDBC, the glacial extent on the 1960s topographic maps suggests that 1) glaciers might have retained much of their LIA extent through the 1960s, or they might have retreated at the end of the LIA and then re-advanced to this extent by the 1960s; and 2) glaciers have retreated significantly within the most recent 50 years, which is consistent with remote sensing based

studies in the Tian Shan (e.g. Aizen et al., 2007; Bolch, 2007; Ding et al., 2006; Li et al., 2008b). If the maximum LIA extents at UG3 and HDBC were the same as the presumed LIA extent, these small and thin glaciers had expanded their ice coverage about 400 m further than their present terminus positions, about half of the distance downstream in the valley for LIA moraines in front of the relatively large and thick glaciers.

4.5.3. Climate imprint on LIA glacial advances

Climate conditions in Central Asia during the last millennium have been reconstructed from a range of proxy data (Figures 4-1 and 4-6). High-frequency climate records from tree rings, ice cores, and other proxies indicate that the coldest period in Central Asia occurred during the last half of the 17th century (~370 yr BP), and that was also a period of high precipitation (Figure 4-6; Yang et al., 2009). Ice core oxygen isotope records from the Dunde Ice Cap in the Qilian Mountains indicate several cold periods around 550 yr BP, 350 yr BP, and 150 yr BP, with the coldest period during 350 yr BP (Figure 4-6; Thompson et al., 1989; Yao et al., 1997). To the south of our study sites, aeolian sediment core analysis in the Tarim Basin indicates wet conditions during the period of 50–450 yr BP, and two distinct clay layers formed in a wet, depositional environment at ~320–390 yr BP (Figure 4-6; Liu et al., 2011).

Such a cold and wet climate around 350 yr BP in Central Asia could drive the maximum LIA glacial advance dated to 370±100 yr BP at our study area. The glacial advance dated to 210±50 yr BP also corresponds to a cold-wet period indicated in proxy records. For example, the carbonate content in a sediment core from Bosten Lake (Figure 4-1) reflects cold and humid conditions around 200 yr BP (Figure 4-6; Chen et al., 2006). An early LIA glacial advance at 730±300 yr BP does not coincide with distinct cold or wet periods in the proxy records, but does coincide with a slight temperature depression in the Northern Hemisphere and the development

of permafrost in the western Tian Shan (Figure 4-6; Esper et al., 2003; Marchenko and Gorbunov, 1997; Moberg et al., 2005).

Overall, the timing of the LIA glacial advances correlates well with temperature anomalies in the northern hemisphere as well as with proxies for regional environmental change in the past millennium (Figure 4-6). However, the maximum LIA glacial advance was reached asynchronously at different sectors of the eastern Tian Shan. Our results showed that the maximum LIA extent is similar (700–900 m) at the Urumqi River headwater, the Haxilegen Pass, and the Karlik Range, but the timing of reaching this extent was much earlier (730±300 yr BP) at the Karlik Range in the easternmost Tian Shan than the 370±100 yr BP at our two sites. Such variations potentially reflect regional climate influences and orographic effects. Large water bodies, such as the Caspian Sea, the Aral Sea, and Lake Issyk-Kul, serve as major moisture sources transported by the westerlies across the Tian Shan (Benn and Owen, 1998; Kreutz et al., 1997; Aizen et al. 2001). Glaciers are developed at high elevations in response of temporal shifts of the westerlies which cause a west-east decreasing gradient of precipitation in the Tian Shan (Sorg et al. 2012). Several studies (e.g. Boomer et al., 2009; Giralt et al., 2004; Karpychev, 2005; Sorrel et al., 2006) have reconstructed high lake levels at the moisture source area around 350 yr BP, in consistent with the cold and wet period suggested by climate proxy data in Central Asia. This is also the period we observe the maximum glacial advance at the Urumqi River headwaters and the Haxilegen Pass, but more restricted advances in the easternmost range. One explanation could be that the precipitation decrease from west to east due to the orographic effect, and thus less ice/snow accumulated to the easternmost range than to the west. Instead, the maximum LIA advance occurred at 730±300 yr BP in the easternmost range, possibly indicating more controls of low temperatures induced by the Siberian High, which may have counteracted the effect of

less precipitation to drive an extensive glacial advance in the early LIA (Chen et al., 2015). More work and data across the Tian Shan are necessary to better understand the spatial pattern of the climate systems and their temporal variations.

4.6. Conclusions

We used [10]Be surface exposure dating of 27 samples collected from fresh moraines at the Urumqi River headwater and the Haxilegen Pass in the eastern Tian Shan, China, to examine the timing and pattern of LIA glacial advances. Relatively large glaciers (>1 km^2) produced clustered ages around 370±100 yr BP, indicating that the moraines were formed during the LIA. This glacial advance was a response to the extreme cold and humid climate around 350 yr BP, as evidenced in other proxy data in Central Asia. We also constrained a slightly less extensive glacial advance occurred around 210±50 yr BP, corresponding to another cold and humid period in the 18th century.

Samples from fresh moraines of small and thin glaciers produced widely scattered ages much older than the LIA. These samples may be from pre-LIA advances with considerable nuclide inheritance. Small and thin glaciers are not erosive and may not produce a large amount of fresh boulders from bedrock with initial zero cosmogenic nuclide concentration. Such glaciers might only rework previous deposited materials that were already exposed prior to the LIA glacial advances, part of nuclide concentrations might be removed during glacial transport during the LIA. Therefore, samples collected from such moraines may produce widely scattered and much older ages due to varied nuclide inheritance.

Cosmogenic [10]Be ages for LIA glacial advances across the eastern Tian Shan indicate that the maximum extent about 700–900 m beyond the current glacier terminus occurred during 730±300 yr BP in the easternmost range, but 370±100 yr BP at our sites. It is possible that an

early LIA glacial advance occurred at our sites but was overridden by a later, but more extensive LIA advance. The more restricted advance of glaciers in the easternmost range in 370±100 yr BP likely reflects declined moisture availability from the westerlies. Additional chronological and proxy data are needed to better understand the spatio-temporal pattern of LIA glacial advances and its driving factors.

References

Aizen, E.M., Aizen, V.B., Melack, J.M., Nakamura, T., Ohta, T., 2001. Precipitation and atmospheric circulation patterns at mid-latitudes of Asia. Int. J. Climatol. 21, 535–556.

Aizen, V.B., Aizen, E.M., Joswiak, D.R., Fujita, K., Takeuchi, N., Nikitin, S.A., 2006. Climatic and atmospheric circulation pattern variability from ice-core isotope/geochemistry records (Altai, Tien Shan and Tibet). Ann. Glaciol. 43, 49–60.

Aizen, V.B., Aizen, E.M., Melack, J.M., Dozier, J., 1997. Climatic and hydrologic changes in the Tien Shan, Central Asia. J. Climatol. 10, 1393–1404.

Aizen, V.B., Kuzmichenok, V.A., Surazakov, A.B., Aizen, E.M., 2007. Glacier changes in the Tien Shan as determined from topographic and remotely sensed data. Glob. Planet. Change. 56, 328–340.

Balco, G., 2011. Contributions and unrealized potential contributions of cosmogenic-nuclide exposure dating to glacier chronology, 1990–2010. Quat. Sci. Rev. 30, 3–27.

Balco, G., Briner, J., Finkel, R.C., Rayburn, J.A., Ridge, J.C., Schaefer, J.M., 2009. Regional beryllium-10 production rate calibration for late-glacial northeastern North America. Quat. Geochronol. 4, 93–107.

Balco, G., Schaefer, J.M., 2006. Cosmogenic-nuclide and varve chronologies for the deglaciation of southern New England. Quat. Geochronol. 1, 15–28.

Balco, G., Stone, J.O., Lifton, N.A., Dunai, T.J., 2008. A complete and easily accessible means of calculating surface exposure ages or erosion rates from ^{10}Be and ^{26}Al measurements. Quat. Geochronol. 3, 174–195.

Barclay, D.J., Wiles, G.C., Calkin, P.E., 2009. Holocene glacier fluctuations in Alaska. Quat. Sci. Rev. 28, 2034–2048.

Barnard, P.L., Owen, L.A., Sharma, M.C., Finkel, R.C., 2004. Late Quaternary landscape evolution of a monsoon-influenced high Himalayan valley, Gori Ganga, Nanda Devi, NE Garhwal. Geomorphology 61, 91–110.

Benedict, J.B., 1968. Recent glacial history of an alpine area in the Colorado Front Range, USA. II: Dating the glacial deposits. J. Glaciol. 7, 77–87.

Benn, D.I., Owen, L.A., 1998. The role of the Indian summer monsoon and the mid-latitude westerlies in Himalayan glaciation: review and speculative discussion. J. Geol. Soc. 155, 353–363.

Bolch, T., 2007. Climate change and glacier retreat in northern Tien Shan (Kazakhstan/Kyrgyzstan) using remote sensing data. Glob. Planet. Change. 56, 1–12.

Boomer, I., Wunnemann, B., Mackay, A.W., Austin, P., Sorrel, P., Reinhardt, C., Keyser, D., Guichard, F., Fontugne, M., 2009. Advances in understanding the late Holocene history of the Aral Sea region. Quat. Int. 194, 79–90.

Bradley, R.S., Jones, P.D., 1993. 'Little Ice Age' summer temperature variations: their nature and relevance to recent global warming trends. Holocene 3, 367–376.

Bräuning, A., 2006. Tree-ring evidence of 'Little Ice Age' glacier advances in southern Tibet. Holocene 16, 369–380.

Briner, J.P., 2009. Moraine pebbles and boulders yield indistinguishable ^{10}Be ages: a case study from Colorado, USA. Quat. Geochronol. 4, 299–305.

Chen, F., Yuan, Y.J., Chen, F.H., Wei, W.S., Yu, S.L., Chen, X.J., Fan, Z.A., Zhang, R.B., Zhang, T.W., Shang, H.M., Qin, L., 2013. A 426-year drought history for Western Tian Shan, Central Asia,

inferred from tree rings and linkages to the North Atlantic and Indo–West Pacific Oceans. Holocene 23, 1095–1104.

Chen, F.H., Huang, X.Z., Zhang, J.W., Holmes, J.A., Chen, J.H., 2006. Humid Little Ice Age in and central Asia documented by Bosten Lake, Xinjiang, China. Sci. China Ser. D-Earth Sci. 49, 1280–1290.

Chen, F.H., Yu, Z.C., Yang, M.L., Ito, E., Wang, S.M., Madsen, D.B., Huang, X.Z., Zhao, Y., Sato, T., Birks, H.J.B., Boomer, I., Chen, J.H., An, C.B., Wunnemann, B., 2008. Holocene moisture evolution in arid central Asia and its out-of-phase relationship with Asian monsoon history. Quat. Sci. Rev. 27, 351–364.

Chen, J., 1989. Preliminary researches on lichenometric chronology of Holocene glacial fluctuations and on other topics in the headwater of Urumqi River, Tianshan Mountains. Sci. China Ser. B-Chemistry 32, 1487–1500.

Chen, Y., Li, Y., Wang, Y., Zhang, M., Cui, Z., Yi, C., Liu, G., 2015. Late Quaternary glacial history of the Karlik Range, easternmost Tian Shan, derived from [10]Be surface exposure and optically stimulated luminescence datings. Quat. Sci. Rev. 115, 17–27.

Chenet, M., Roussel, E., Jomelli, V., Grancher, D., 2010. Asynchronous Little Ice Age glacial maximum extent in southeast Iceland. Geomorphology 114, 253–260.

Cui, Z., 1981. Glacial erosion landforms and development of trough at the head of Urumqi River, Tian Shan. J. Glaciol. and Geocryology 3, 1–15.

Derbyshire, E., Li, J., Perrott, F., Xu, S., Waters, R., 1984. Quaternary glacial history of the Hunza Valley, Karakoram mountains, Pakistan. The International Karakoram Project 2, 456–495.

Desilets, D., Zreda, M., 2003. Spatial and temporal distribution of secondary cosmic-ray nucleon intensities and applications to in situ cosmogenic dating. Earth Planet. Sci. Lett. 206, 21–42.

Desilets, D., Zreda, M., Prabu, T., 2006. Extended scaling factors for in situ cosmogenic nuclides: new measurements at low latitude. Earth Planet. Sci. Lett. 246, 265–276.

Ding, Y., Liu, S., Li, J., Shangguan, D., 2006. The retreat of glaciers in response to recent climate warming in western China. Ann. Glaciol. 43, 97–105.

Dunai, T., 2001. Influence of secular variation of the geomagnetic field on production rates of in situ produced cosmogenic nuclides. Earth Planet. Sci. Lett. 193, 197–212.

Esper, J., Shiyatov, S.G., Mazepa, V.S., Wilson, R.J.S., Graybill, D.A., Funkhouser, G., 2003. Temperature-sensitive Tien Shan tree ring chronologies show multi-centennial growth trends. Clim. Dynam. 21, 699–706.

Fabel, D., Fink, D., Fredin, O., Harbor, J., Land, M., Stroeven, A., 2006. Exposure ages from relict lateral moraines overridden by the Fennoscandian ice-sheet. Quaternary Res. 65, 136-46.

Finkel, R.C., Owen, L.A., Barnard, P.L., Caffee, M.W., 2003. Beryllium-10 dating of Mount Everest moraines indicates a strong monsoon influence and glacial synchroneity throughout the Himalaya. Geology 31, 561–564.

Giralt, S., Julia, R., Klerkx, J., Riera, S., Leroy, S., Buchaca, T., Catalan, J., De Batist, M., Beck, C., Bobrov, V., Gavshin, V., Kalugin, I., Sukhorukov, F., Brennwald, M., Kipfer, R., Peeters, F., Lombardi, S., Matychenkov, V., Romanovsky, V., Podsetchine, V., Voltattorni, N., 2004. 1,000-year environmental history of Lake Issyk-Kul, in: Nihoul, J.C.J., Zavialov, P.O., Micklin, P.P. (Eds.), Dying and Dead Seas: Climatic Versus Anthropic Causes. Springer, Dordrecht, pp. 253–285.

Gong, D.Y., Ho, C.H., 2002. The Siberian High and climate change over middle to high latitude Asia. Theor. Appl. Climatol. 72, 1–9.

Gosse, J.C., Phillips, F.M., 2001. Terrestrial in situ cosmogenic nuclides: theory and application. Quat. Sci. Rev. 20, 1475–1560.

Grove, J.M., 2004. Little ice ages: ancient and modern (2 volumes). Routledge, London.

Harrison, S., Winchester, V., Glasser, N.F., 2007. The timing and nature of recession of outlet glaciers of Hielo Patagonico Norte, Chile, from their Neoglacial IV (Little Ice Age) maximum positions. Glob. Planet. Change 59, 67–78.

Heyman, J., Stroeven, A.P., Caffee, M.W., Hattestrand, C., Harbor, J.M., Li, Y., Alexanderson, H., Zhou, L., Hubbard, A., 2011a. Palaeoglaciology of Bayan Har Shan, NE Tibetan Plateau: exposure ages reveal a missing LGM expansion. Quat. Sci. Rev. 30, 1988–2001.

Heyman, J., Stroeven, A.P., Harbor, J.M., and Caffee, M.W., 2011b. Too young or too old: Evaluating cosmogenic exposure dating based on an analysis of compiled boulder exposure ages. Earth Planet. Sc. Lett. 302, 71–80.

Ivy-Ochs, S., Kober, F., 2008. Surface exposure dating with cosmogenic nuclides. Eiszeitalter und Gegenwart 57, 179–209.

Jiao, K.Q., Iwata, S., Yao, T.D., Jing, Z.F., Li, Z.Q., 2005. Variation of Zepu Glacier and environmental change in the eastern Nyainqentanglha range since 3.2 ka BP. J. Glaciol. and Geocryology 27, 74–79.

Kaban, M., Yuanda, T., 2014. Density Structure, Isostatic Balance and Tectonic Models of the Central Tien Shan. Surv. Geophys. 35, 1375–1391.

Karpychev, Y.A., 2005. Transgressive-regressive stages of the Caspian Sea for the last 20 ky inferred from radiocarbon dating of the coastal and bottom sediments. Oceanology 45, 420–430.

Kelly, M.A., Lowell, T.V., Hall, B.L., Schaefer, J.M., Finkel, R.C., Goehring, B.M., Alley, R.B., Denton, G.H., 2008. A 10Be chronology of lateglacial and Holocene mountain glaciation in the Scoresby Sund region, east Greenland: implications for seasonality during lateglacial time. Quat. Sci. Rev. 27, 2273–2282.

Koch, J., Kilian, R., 2005. 'Little Ice Age' glacier fluctuations, Gran Campo Nevado, southernmost Chile. Holocene 15, 20–28.

Kohl, C.P., Nishiizumi, K., 1992. Chemical isolation of quartz for measurement of insitu-produced cosmogenic nuclides. Geochim. Cosmochim. Acta .56, 3583–3587.

Kong, P., Fink, D., Na, C., Huang, F., 2009. Late Quaternary glaciation of the Tianshan, Central Asia, using cosmogenic ^{10}Be surface exposure dating. Quat. Res. 72, 229–233.

Koppes, M., Gillespie, A.R., Burke, R.M., Thompson, S.C., Stone, J., 2008. Late Quaternary glaciation in the Kyrgyz Tien Shan. Quat. Sci. Rev. 27, 846–866.

Kreutz, K., Mayewski, P., Meeker, L., Twickler, M., Whitlow, S., Pittalwala, I., 1997. Bipolar changes in atmospheric circulation during the Little Ice Age. Science 277, 1294–1296.

Lal, D., 1991. Cosmic ray labeling of erosion surfaces: in situ nuclide production rates and erosion models. Earth Planet. Sci. Lett. 104, 424–439.

Li, J., Zheng, B., Yang, X., 1986. Glacier in Tibet. Science Press, Beijing.

Li, Y.K., Liu, G.N., Cui, Z.J., 2001a. Glacial valley cross-profile morphology, Tian Shan Mountains, China. Geomorphology 38, 153–166.

Li, Y.K., Liu, G.N., Cui, Z.J., 2001b. Longitudinal variations in cross-section morphology along a glacial valley: a case-study from the Tien Shan, China. J. Glaciol. 47, 243–250.

Li, Y.K., 2013. Determining topographic shielding from digital elevation models for cosmogenic nuclide analysis: a GIS approach and field validation. J. Mt. Sci. 10, 355–362.

Li, Y.K., Harbor, J., 2009. Cosmogenic nuclides and geomorphology: Theory, limitations, and applications, in: Ferrari, D.M., Guiseppi, A.R. (Eds.), Geomorphology and Plate Tectonics. Nova Science Publishers, Inc. Hauppauge, New York, pp. 1–33.

Li, Y.K., Liu, G.N., Chen, Y.X., Li, Y.N., Harbor, J., Stroeven, A.P., Caffee, M., Zhang, M., Li, C.C., Cui, Z.J., 2014. Timing and extent of Quaternary glaciations in the Tianger Range, eastern Tian Shan, China, investigated using ^{10}Be surface exposure dating. Quat. Sci. Rev. 98, 7–23.

Li, Y.K., Liu, G.N., Kong, P., Harbor, J., Chen, Y.X., Caffee, M., 2011. Cosmogenic nuclide constraints on glacial chronology in the source area of the Urumqi River, Tian Shan, China. J. Quat. Sci. 26, 297–304.

Li, Y.K., Napieralski, J., Harbor, J., 2008. A revised automated proximity and conformity analysis method to compare predicted and observed spatial boundaries of geologic phenomena. Comput. & Geosci. 34, 1806–1814.

Li, Y.N., Li, Y.K., 2014. Topographic and geometric controls on glacier changes in the central Tien Shan, China, since the Little Ice Age. Ann. Glaciol. 55, 177–186.

Li, Z.Q., Shen, Y.P., Li, H.L., Dong, Z.W., Wang, L.W., 2008. Response of the melting Urumqi Glacier No. 1 in eastern Tianshan to climate change. Advances in Climate Change Research (Suppl.) 4, 67–72.

Lifton, N., Beel, C., Hättestrand, C., Kassab, C., Rogozhina, I., Heermance, R., Oskin, M., Burbank, D., Blomdin, R., Gribenski, N., Caffee, M., Goehring, B.M., Heyman, J., Ivanov, M., Li, Y., Li, Y., Petrakov, D., Usubaliev, R., Codilean, A.T., Chen, Y., 2014. Constraints on the late Quaternary glacial history of the Inylchek and Sary-Dzaz valleys from in situ cosmogenic ^{10}Be and ^{26}Al, eastern Kyrgyz Tian Shan. Quat. Sci. Rev. 101, 77–90.

Lifton, N.A., Bieber, J.W., Clem, J.M., Duldig, M.L., Evenson, P., Humble, J.E., Pyle, R., 2005. Addressing solar modulation and long-term uncertainties in scaling secondary cosmic rays for in situ cosmogenic nuclide applications. Earth Planet. Sci. Lett. 239, 140–161.

Liu, G.N., Xiong, H.G., 1992. The denudation rate of gelifraction and its influential factors in the periglacial environment of Tianshan Mountains (in China). J. Glaciol. and Geocryology 14, 333–341.

Liu, G.N., Xiong, H.G., Cui, Z.J., Song, C.Q., 1995. The morphological features and environmental condition of rockglaciers in Tianshan Mountains. Sci. Geograph. Sin. 15, 226–233 (in Chinese with English abstract).

Liu, S.Y., Sun, W.X., Shen, Y.P., Li, G., 2003. Glacier changes since the Little Ice Age maximum in the western Qilian Shan, northwest China, and consequences of glacier runoff for water supply. J. Glaciol. 49, 117–124.

Liu, W.G., Liu, Z.H., An, Z.S., Wang, X.L., Chang, H., 2011. Wet climate during the 'Little Ice Age' in the arid Tarim Basin, northwestern China. Holocene 21, 409–416.

Loso, M.G., Doak, D.F., Anderson, R.S., 2014. Lichenometric dating of Little Ice Age glacier moraines using explicit demographic models of lichen colonization, growth, and survival. Geogr. Ann. A: Physical Geography 96, 21–41.

Luckman, B.H., 2000. The Little Ice Age in the Canadian Rockies. Geomorphology 32, 357–384.

Luthi, M.P., 2014. Little Ice Age climate reconstruction from ensemble reanalysis of Alpine glacier fluctuations. Cryosphere 8, 639–650.

Mann, M.E., 2002. Little ice age. Encyclopedia of Global Environmental Change 1, 504–509.

Mann, M.E., Bradley, R.S., Hughes, M.K., 1999. Northern hemisphere temperatures during the past millennium: inferences, uncertainties, and limitations. Geophys. Res. Lett. 26, 759–762.

Mann, M.E., Zhang, Z., Hughes, M.K., Bradley, R.S., Miller, S.K., Rutherford, S., Ni, F., 2008. Proxy-based reconstructions of hemispheric and global surface temperature variations over the past two millennia. P. Natl. Acad. Sci. USA. 105, 13252–13257.

Mann, M.E., Zhang, Z.H., Rutherford, S., Bradley, R.S., Hughes, M.K., Shindell, D., Ammann, C., Faluvegi, G., Ni, F.B., 2009. Global Signatures and Dynamical Origins of the Little Ice Age and Medieval Climate Anomaly. Science 326, 1256–1260.

Marchenko, S.S., Gorbunov, A.P., 1997. Permafrost changes in the northern Tien Shan during the Holocene. Permafrost Periglac. 8, 427–435.

Matthes, F.E., 1939. Report of committee on glaciers, April 1939. Eos, Transactions American Geophysical Union 20, 518–523.

Moberg, A., Sonechkin, D.M., Holmgren, K., Datsenko, N.M., Karlen, W., 2005. Highly variable Northern Hemisphere temperatures reconstructed from low- and high-resolution proxy data. Nature 433, 613–617.

Mosley-Thompson, E., Thompson, L.G., Grootes, P.M., Gundestrup, N., 1990. Little ice age (neoglacial) paleoenvironmental conditions at siple station, Antarctica. Ann. Glaciol. 14, 199–204.

Narama, C., Kondo, R., Tsukamoto, S., Kajiura, T., Ormukov, C., Abdrakhmatov, K., 2007. OSL dating of glacial deposits during the last glacial in the Terskey-Alatoo Range, Kyrgyz Republic. Quat. Geochronol. 2, 249–254.

Ono, Y., Liu, D., Zhao, Y., 1997. Paleoenvironment of Tibetan Plateau viewed from glacial fluctuations in the north foot of the west Kunlun Mountains. Jpn. J. Geomorphol. 106, 184–198.

Owen, L.A., 2009. Latest Pleistocene and Holocene glacier fluctuations in the Himalaya and Tibet. Quat. Sci. Rev. 28, 2150–2164.

Owen, L.A., Dortch, J.M., 2014. Nature and timing of Quaternary glaciation in the Himalayan–Tibetan orogen. Quat. Sci. Rev. 88, 14–54.

Owen, L.A., Finkel, R.C., Barnard, P.L., Ma, H.Z., Asahi, K., Caffee, M.W., Derbyshire, E., 2005. Climatic and topographic controls on the style and timing of Late Quaternary glaciation throughout Tibet and the Himalaya defined by Be-10 cosmogenic radionuclide surface exposure dating. Quat. Sci. Rev. 24, 1391–1411.

Owen, L.A., Yi, C.L., Finkel, R.C., Davis, N.K., 2010. Quaternary glaciation of Gurla Mandhata (Naimon'anyi). Quat. Sci. Rev. 29, 1817–1830.

Putnam, A.E., Schaefer, J.M., Barrell, D.J.A., Vandergoes, M., Denton, G.H., Kaplan, M.R., Finkel, R.C., Schwartz, R., Goehring, B.M., Kelley, S.E., 2010. In situ cosmogenic Be-10 production-rate calibration from the Southern Alps, New Zealand. Quat. Geochronol. 5, 392–409.

Schaefer, J.M., Denton, G.H., Kaplan, M.R., Putnam, A., Finkel, R.C., Barrell, D.J.A., Andersen, B.G., Schwartz, R., Mackintosh, A., Chinn, T., Schluchter, C., 2009. High-Frequency Holocene Glacier Fluctuations in New Zealand Differ from the Northern Signature. Science 324, 622–625.

Schimmelpfennig, I., Schaefer, J.M., Akcar, N., Koffman, T., Ivy-Ochs, S., Schwartz, R., Finkel, R.C., Zimmerman, S., Schluechter, C., 2014. A chronology of Holocene and Little Ice Age glacier

culminations of the Steingletscher, Central Alps, Switzerland, based on high-sensitivity beryllium-10 moraine dating. Earth Planet. Sci. Lett. 393, 220–230.

Seong, Y.B., Owen, L.A., Yi, C.L., Finkel, R.C., Schoenbohm, L., 2009. Geomorphology of anomalously high glaciated mountains at the northwestern end of Tibet: Muztag Ata and Kongur Shan. Geomorphology 103, 227–250.

Shi, Y., Ren, J., 1990. Glacier recession and lake shrinkage indicating a climatic warming and drying trend in central Asia. Ann. Glaciol. 14, 261–265.

Solomina, O., Barry, R., Bodnya, M., 2004. The retreat of Tien Shan glaciers (Kyrgyzstan) since the Little Ice Age estimated from aerial photographs, lichenometric and historical data. Geogr. Ann. A: Physical Geography 86, 205–215.

Sorg, A., Bolch, T., Stoffel, M., Solomina, O., Beniston, M., 2012. Climate change impacts on glaciers and runoff in Tien Shan (Central Asia). Nat. Clim. Chang. 2, 725–731.

Sorrel, P., Popescu, S.M., Head, M.J., Suc, J.P., Klotz, S., Oberhansli, H., 2006. Hydrographic development of the Aral Sea during the last 2000 years based on a quantitative analysis of dinoflagellate cysts. Paleogeogr. Paleoclimatol. Paleoecol. 234, 304–327.

Stone, J.O., 2000. Air pressure and cosmogenic isotope production. J. Geophys. Res.-Sol. EA. 105, 23753–23759.

Su, Z., Shi, Y., 2002. Response of monsoonal temperate glaciers to global warming since the Little Ice Age. Quat. Int. 97–98, 123–131.

Thompson, L.G., Mosley-Thompson, E., Davis, M., Bolzan, J., Dai, J., Klein, L., Yao, T., Wu, X., Xie, Z., Gundestrup, N., 1989. Holocene—Late Pleistocene Climatic Ice Core Records from Qinghai-Tibetan Plateau. Science 246, 474–477.

Vitek, J.D., Giardino, J.R., 1987. Rock glaciers: A review of the knowledge base, in: Giardino, J.R., Shroder, J.F., Vitek, J.D. (Eds.), Rock Glaciers. Allen & Unwin, Inc. Boston, pp. 1–26.

Wang, Z., 1991. The glacier and environment in the middle sector of Tianshan and the eastern sector of Qilianshan since the little ice age. Acta Geograph. Sin. 46, 160–168 (in Chinese with English abstract).

Xu, X., Yi, C., 2014. Little Ice Age on the Tibetan Plateau and its bordering mountains: Evidence from moraine chronologies. Glob. Planet. Change 116, 41–53.

Yang, B., Wang, J.S., Brauning, A., Dong, Z.B., Esper, J., 2009. Late Holocene climatic and environmental changes in and central Asia. Quat. Int. 194, 68–78.

Yao, T., Shi, Y., Thompson, L.G., 1997. High resolution record of paleoclimate since the Little Ice Age from the Tibetan ice cores. Quat. Int. 37, 19–23.

Ye, B., Yang, D., Jiao, K., Han, T., Jin, Z., Yang, H., Li, Z., 2005. The Urumqi River source Glacier No. 1, Tianshan, China: Changes over the past 45 years. Geophys. Res. Lett. 32, L21504.

Yi, C., Liu, K., Cui, Z., Jiao, K., Yao, T., He, Y., 2004. AMS radiocarbon dating of late Quaternary glacial landforms, source of the Urumqi River, Tien Shan—a pilot study of 14C dating on inorganic carbon. Quat. Int. 121, 99–107.

Yi, C.L., Jiao, K.Q., Liu, K.X., He, Y.Q., Ye, Y.G., 2002. ESR dating of the sediments of the Last Glaciation at the source area of the Urumqi River, Tian Shan Mountains, China. Quat. Int. 97–98, 141–146.

Yin, A., Harrison, T.M., 2000. Geologic evolution of the Himalayan-Tibetan orogen. Ann. Rev. Earth Pl. Sci. 28, 211–280.

Zech, R., 2012. A late Pleistocene glacial chronology from the Kitschi-Kurumdu Valley, Tien Shan (Kyrgyzstan), based on Be-10 surface exposure dating. Quat. Res. 77, 281–288.

Zhao, J., Zhou, S., He, Y., Ye, Y., Liu, S., 2006. ESR dating of glacial tills and glaciations in the Urumqi River headwaters, Tianshan Mountains, China. Quat. Int. 144, 61–67.

Zhou, S., 2006. Quaternary glaciations in the Qilian Mountains. In: Shi, Y. (Ed.), The Quaternary glaciations and environmental variations in China. Hebei Science and Technology Publishing House, Shijiazhuang, pp. 359–373.

Appendix for Chapter 4

Table 4-1. Sample information and [10]Be concentration measurements used in this study

Sample ID	Site	Latitude (ºN)	Longitude (ºE)	Elevation (m a.s.l.)	Rock Type	Thickness (cm)	Topographic shielding factor	[10]Be concentration (atoms/g)
HDB-12-06	Haxilegen Pass (HDBA)	43.73852	84.40243	3484	quartzite	2	0.983	9435 ± 751
HDB-12-07	Haxilegen Pass (HDBA)	43.73849	84.40252	3485	quartzite	4	0.983	11955 ± 1145
HDB-12-08	Haxilegen Pass (HDBA)	43.73842	84.40280	3481	granite	2.5	0.979	35930 ± 3102
HDB-12-09	Haxilegen Pass (HDBA)	43.73804	84.40329	3483	granite	3	0.979	24928 ± 1712
HDB-12-10	Haxilegen Pass (HDBA)	43.73798	84.40335	3485	granite	2	0.979	10848 ± 1071
HDB-12-11	Haxilegen Pass (HDBA)	43.73871	84.40321	3477	granite	3	0.979	9502 ± 1616
HDB-12-12	Haxilegen Pass (HDBA)	43.73854	84.40307	3475	granite	2	0.979	18203 ± 1757
HDB-12-13	Haxilegen Pass (HDBA)	43.73866	84.40327	3473	pebbles	4	0.979	31738 ± 1925
HDB-12-14	Haxilegen Pass (HDBA)	43.73871	84.40321	3473	pebbles	4	0.979	17331 ± 1430
HDB-12-15	Haxilegen Pass (HDBA)	43.73871	84.40321	3477	quartzite	4	0.979	272712 ± 7051
HDB-12-16	Haxilegen Pass (HDBB)	43.73717	84.40733	3411	Gneiss	3	0.971	11313 ± 2434
HDB-12-17	Haxilegen Pass (HDBB)	43.73725	84.40686	3418	Gneiss	2	0.973	5460 ± 859
HDB-12-18	Haxilegen Pass (HDBB)	43.73717	84.40675	3417	Gneiss	4	0.973	10562 ± 1602
HDB-12-19	Haxilegen Pass (HDBB)	43.73717	84.40628	3420	Gneiss	4	0.973	13193 ± 2339
HDB-12-20	Haxilegen Pass (HDBB)	43.73702	84.40618	3424	Gneiss	4	0.973	9524 ± 1446

Table 4-1. Continued.

Sample ID	Site	Latitude (°N)	Longitude (°E)	Elevation (m a.s.l.)	Rock Type	Thickness (cm)	Topographic shielding factor	^{10}Be concentration (atoms/g)
HDB-12-21	Haxilegen Pass (HDBC)	43.72688	84.41199	3546	granite	4	0.987	57644 ± 3661
HDB-12-22	Haxilegen Pass (HDBC)	43.72692	84.41206	3546	granitic gneiss	3	0.987	447984 ± 13418
HDB-12-23	Haxilegen Pass (HDBC)	43.72652	84.41239	3542	granitic gneiss	3	0.986	347687 ± 10703
HDB-12-24	Haxilegen Pass (HDBC)	43.72637	84.41270	3544	granitic gneiss	4	0.987	202972 ± 13738
HDB-12-25	Haxilegen Pass (HDBC)	43.72626	84.41279	3540	granite	3	0.987	98864 ± 2990
WY-12-03	Glacier No. 3 (UG3)	43.09955	86.84198	3638	quartzite	4	0.917	30961 ± 1264
WY-12-04	Glacier No. 3 (UG3)	43.09918	86.84179	3639	quartzite	4	0.917	232496 ± 5855
WY-12-08	Glacier No. 3 (UG3)	43.09835	86.84121	3653	quartzite	3	0.914	245356 ± 5922
WY-12-09	Glacier No. 3 (UG3)	43.09849	86.84119	3656	quartz schist	2	0.914	131242 ± 6941
WY-12-21	Glacier No. 1 (UG1)	43.11760	86.82059	3785	quartzite	1	0.970	13915 ± 1693
WY-12-22	Glacier No. 1 (UG1)	43.11699	86.82162	3764	quartzite	1	0.945	26340 ± 7061
WY-12-23	Glacier No. 1 (UG1)	43.11673	86.82197	3758	quartzite	2	0.945	10027 ± 900

Note: The topographic shielding was calculated using a Python tool (Li, 2013) with 5° intervals in both azimuth and altitude angles; ^{10}Be concentration was converted from the AMS measured ^{10}Be/^{9}Be ratios from PRIME lab at Purdue University.

Table 4-2. ^{10}Be surface exposure ages calculated using different scaling schemes.

Data Source	Sample name	Moraine set, sample type	Constant Lal (1991)/Stone (2000) Exposure age (yr BP)	Desilets and Zreda (2003); Desilets et al. (2006) Exposure age (yr BP)	Dunai (2001) Exposure age (yr BP)	Lifton et al. (2005) Exposure age (yr BP)	Time-dependent Lal (1991)/Stone (2000) Exposure age (yr BP)
This study	HDB-12-06	HDBA, boulder	140 ± 20	140 ± 20	130 ± 20	140 ± 20	160 ± 20
	HDB-12-07	HDBA, pebbles	200 ± 30	200 ± 30	190 ± 30	200 ± 30	230 ± 30
	HDB-12-08	HDBA, boulder	710 ± 80	700 ± 80	690 ± 80	700 ± 70	760 ± 80
	HDB-12-09	HDBA, boulder	480 ± 50	480 ± 50	460 ± 40	470 ± 50	530 ± 50
	HDB-12-10	HDBA, boulder	170 ± 30	180 ± 30	160 ± 30	170 ± 30	200 ± 30
	HDB-12-11	HDBA, boulder	150 ± 40	150 ± 40	140 ± 40	140 ± 40	170 ± 40
	HDB-12-12	HDBA, boulder	330 ± 40	340 ± 40	320 ± 40	330 ± 40	370 ± 50
	HDB-12-13	HDBA, pebbles	630 ± 50	630 ± 50	620 ± 50	620 ± 50	690 ± 60
	HDB-12-14	HDBA, pebbles	320 ± 40	330 ± 40	310 ± 40	320 ± 40	360 ± 40
	HDB-12-15	HDBA, boulder	5900 ± 330	5400 ± 300	5630 ± 320	5300 ± 300	5930 ± 330
	HDB-12-16	HDBB, boulder	200 ± 60	200 ± 60	190 ± 60	190 ± 60	220 ± 60
	HDB-12-17	HDBB, boulder	60 ± 20	60 ± 20	60 ± 20	60 ± 20	80 ± 20
	HDB-12-18	HDBB, boulder	180 ± 40	190 ± 40	170 ± 40	180 ± 40	210 ± 40
	HDB-12-19	HDBB, boulder	240 ± 60	250 ± 60	230 ± 50	240 ± 60	270 ± 60
	HDB-12-20	HDBB, boulder	160 ± 30	160 ± 40	150 ± 30	150 ± 40	180 ± 40
	HDB-12-21	HDBC, boulder	1140 ± 100	1080 ± 90	1110 ± 90	1120 ± 90	1190 ± 100
	HDB-12-22	HDBC, boulder	9210 ± 530	8380 ± 480	8660 ± 500	8660 ± 480	9200 ± 530
	HDB-12-23	HDBC, boulder	7160 ± 410	6560 ± 380	6870 ± 400	6400 ± 370	7040 ± 410
	HDB-12-24	HDBC, boulder	4180 ± 350	3860 ± 330	4100 ± 350	4100 ± 320	4250 ± 360
	HDB-12-25	HDBC, boulder	1990 ± 120	1870 ± 110	2040 ± 120	1830 ± 110	2070 ± 120
	WY-12-03	UG3, boulder	610 ± 40	610 ± 40	590 ± 40	600 ± 40	660 ± 50
	WY-12-04	UG3, boulder	4970 ± 270	4590 ± 260	4860 ± 270	4510 ± 250	5030 ± 280
	WY-12-08	UG3, boulder	5180 ± 280	4770 ± 260	5030 ± 280	5040 ± 260	5230 ± 290
	WY-12-09	UG3, boulder	2710 ± 200	2570 ± 190	2800 ± 210	2520 ± 190	2820 ± 210
	WY-12-21	UG1, boulder	200 ± 30	200 ± 30	190 ± 30	190 ± 30	220 ± 40
	WY-12-22	UG1, boulder	440 ± 140	450 ± 140	430 ± 130	430 ± 140	490 ± 150
	WY-12-23	UG1, boulder	130 ± 20	140 ± 20	130 ± 20	130 ± 20	160 ± 20
Li et al. (2014)	1#-10-18	UG1, boulder	270 ± 40	270 ± 40	260 ± 40	270 ± 40	300 ± 40
	1#-10-19	UG1, boulder	330 ± 40	340 ± 40	320 ± 40	340 ± 40	370 ± 50
	1#-10-20	UG1, boulder	310 ± 40	320 ± 90	300 ± 90	320 ± 90	350 ± 50
	1#-10-21	UG1, boulder	300 ± 50	310 ± 50	290 ± 50	310 ± 50	340 ± 50

Table 4-2. Continued.

Data Source	Sample name	Moraine set, sample type	Constant Lal (1991)/Stone (2000) Exposure age (yr BP)	Desilets and Zreda (2003); Desilets et al. (2006) Exposure age (yr BP)	Dunai (2001) Exposure age (yr BP)	Lifton et al. (2005) Exposure age (yr BP)	Time-dependent Lal (1991)/Stone (2000) Exposure age (yr BP)
Chen et al. (2015)	YW-09-1-1	Karlik, boulder	740 ± 210	730 ± 210	720 ± 210	720 ± 200	790 ± 220
	YW-09-1-2	Karlik, boulder	630 ± 200	630 ± 200	620 ± 200	630 ± 200	680 ± 220
	YW-09-1-4	Karlik, boulder	1980 ± 320	1860 ± 300	1990 ± 320	1820 ± 290	2070 ± 330
	YW-09-1-5	Karlik, boulder	880 ± 300	870 ± 290	870 ± 290	850 ± 290	940 ± 310
	YW-09-2-1	Karlik, boulder	350 ± 150	360 ± 150	340 ± 140	360 ± 150	390 ± 160
	YW-09-2-2	Karlik, boulder	2400 ± 440	2280 ± 420	2490 ± 450	2230 ± 410	2520 ± 460
	YW-09-2-4	Karlik, boulder	830 ± 160	820 ± 160	820 ± 160	810 ± 160	890 ± 170
	YW-09-2-5	Karlik, boulder	620 ± 290	630 ± 290	620 ± 290	620 ± 290	680 ± 310
	YW-09-2-6	Karlik, boulder	11140 ± 700	9910 ± 620	10140 ± 600	9770 ± 610	11140 ± 700
	YW-09-4-2	Karlik, boulder	23540 ± 2200	20040 ± 1900	20040 ± 1900	19740 ± 1900	22840 ± 2200
	YW-09-4-3	Karlik, boulder	4620 ± 390	4290 ± 370	4560 ± 390	4210 ± 360	4710 ± 400

Note: we used the CRONUS-Earth 2.2 online calculator (Balco et al., 2008) to calculat all ages. We subtracted 60 years from the CRONUS ages and reported them in unit of yr BP (years before 1950). In the calculation, we assumed zero surface erosion, and used the Northeast North America (NENA) ^{10}Be production rate as the calibration dataset (Balco et al., 2009). 1#-10-18 to 21 are samples from the same site as UG1 and ages were calculated using the same method (Li et al., 2014). YW-09 samples are from the Turgan Valley in the Karlik Range (Chen et al., 2015), and their weighted mean age was recalculated using the same method as we used for our samples. The ages reported in this study are derived from the time-dependent Lal (1991)/Stone (2000) scaling scheme.
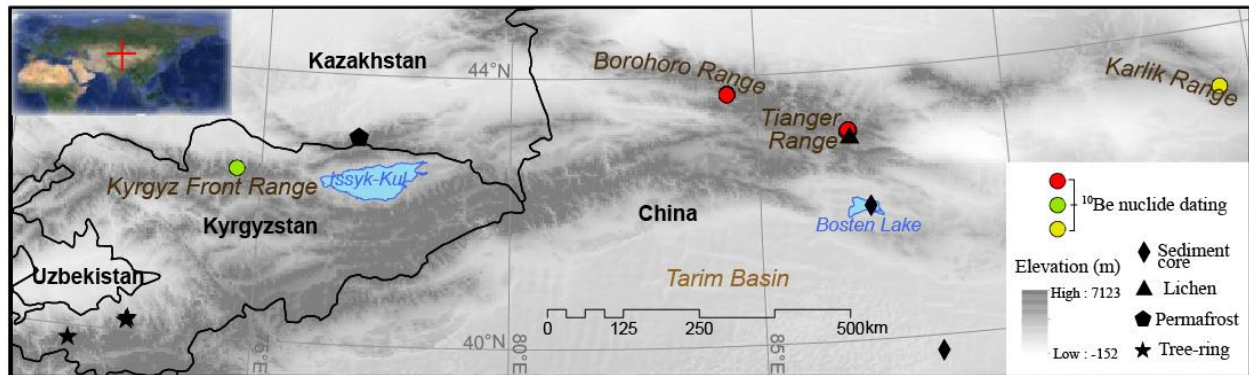
Figure 4-1. Overview of the Tian Shan with the study areas and other sites discussed in this paper. Red dots are our [10]Be CN sites; green dots are [10]Be CN ages in the Kyrgyz Front Range (Koppes et al., 2008); yellow dots are [10]Be CN ages in the Karlik Range (Chen et al. 2015). Other proxy data sites shown are: a lake sediment core from Bosten lake (Chen et al., 2006); an aeolian sediment section in the Tarim Basin (Liu et al., 2011); lichenometry dating at Glacier No. 1 (Chen, 1989); permafrost layers in the Zailiysky Alatau Range (Marchenko and Gorbunov, 1997); and dendrochrological studies in the western Kyrgyz Tian Shan (Esper et al., 2003).
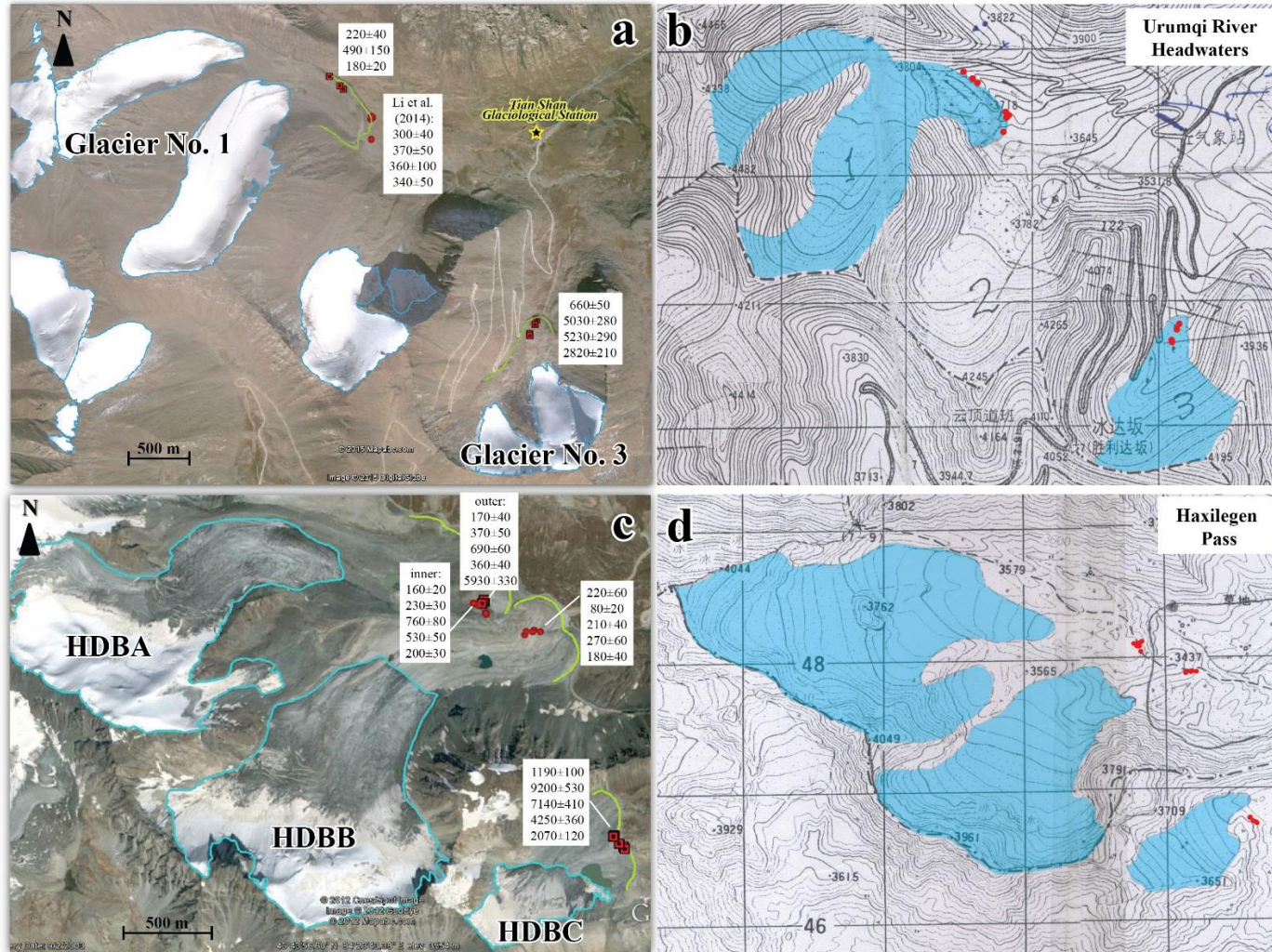
Figure 4-2. Google Earth and 1:50 000 topographic map views of two study sites: a) and b) are the Urumqi River headwater area; c) and d) are the Haxilegen Pass area. On a) and c), modern glacier boundaries (blue) and the presumed LIA moraines (green) were delineated based on the best available Google Earth images from 10/2/2010 and 9/2/2003, respectively, for the two regions. Available [10]Be exposure ages (in unit of yr BP) from our study and Li et al. (2014) were marked on the images and also listed in Table 4-2.The topographic maps how glacier status in the early 1960s, as represented by the blue polygons in b) and d). Red dots indicate sample locations.

104
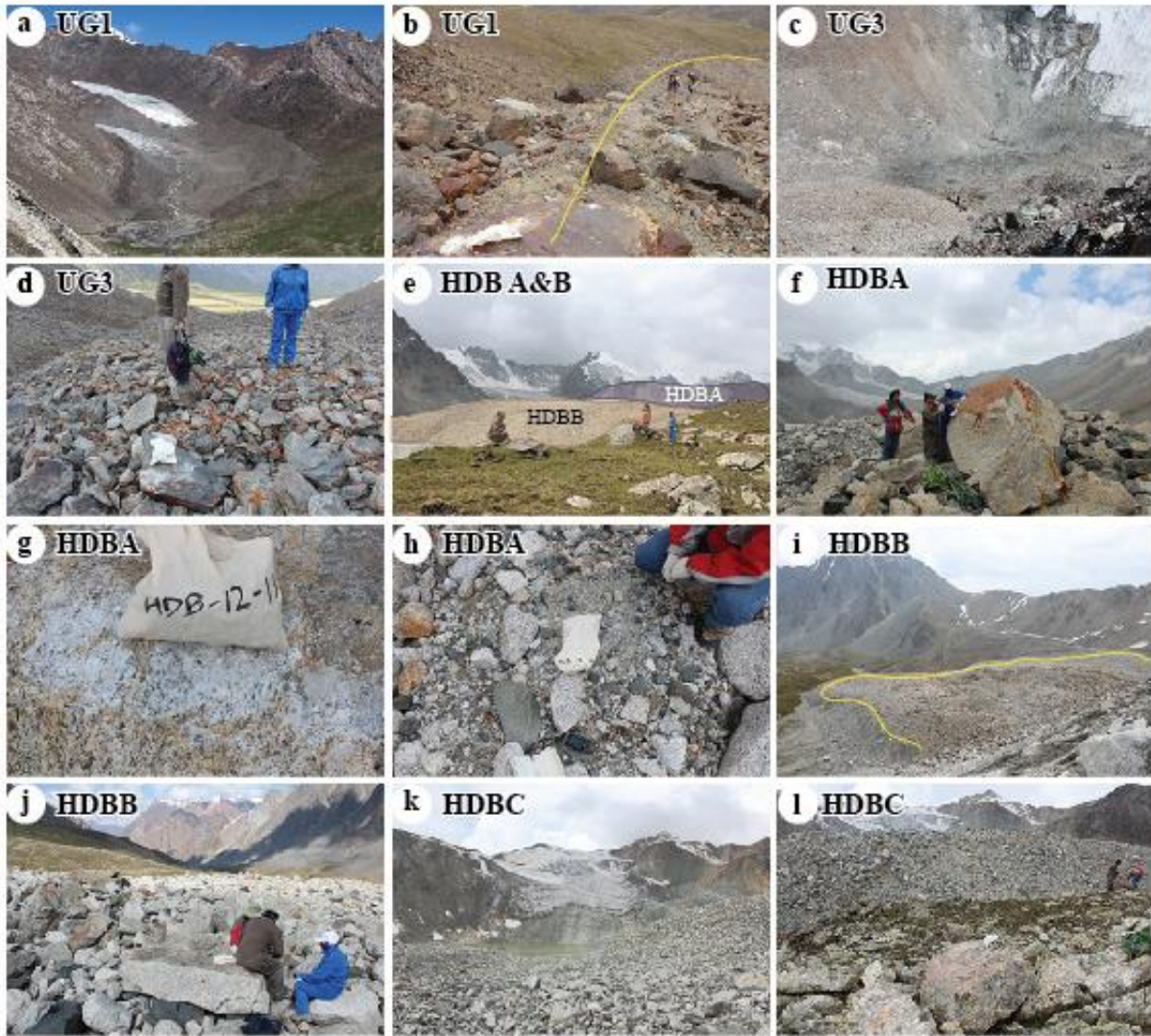
Figure 4-3. Selected photos of field sites. a) An overview of the morphology of the LIA moraine at UG1. b) Lateral LIA moraine at UG1 and adjacent older moraine beyond the LIA moraine. c) Thin front of UG3 and its surrounding steep slopes. d) Standing on the rock debris of UG3 and looking east (downstream). The orange color is lichen covers. e) A distant view of the moraines in front of the HDBA and HDBB at Haxilegen Pass. The darker colored, higher HDBA moraine partially overlaps the lighter colored, lower HDBB moraine. They both override more vegetated, boulder-scattered, older glacial landforms. f) Sampling a large boulder at HDBA. g) An example of granite samples (sample ID: HDB-12-11). h) Pebble sample of HDB-12-14 from HDBA. i) View of HDBB moraine extending to the highway. j) Sampling a well-exposed large boulder at HDBB. k) The small HDBC glacier on the southern side of the Haxilegen Pass. A tarn is formed in front of the glacier terminus. l) Steep gradient seen from lower older moraines at HDBC.
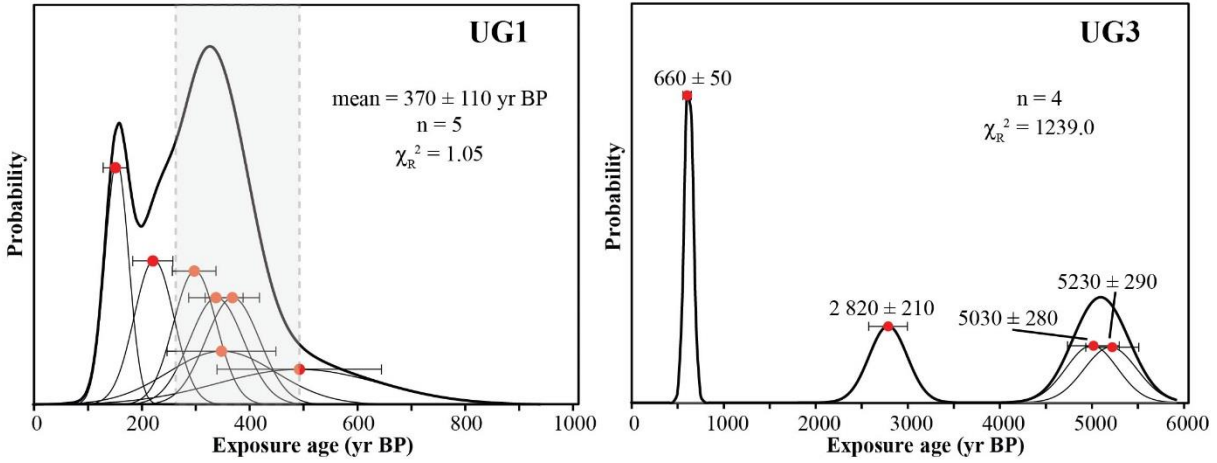
Figure 4-4. Probability density plot of ^{10}Be surface exposure ages for fresh moraine sets at UG1 and UG3 sites. Five samples highlighted at UG1 produced a small value of reduced chi-square statistic (χ_R^2), and the weighted mean (370±110 yr BP) was calculated; four samples at UG3 produced a large value of χ_R^2, and no age was assigned to this landform.
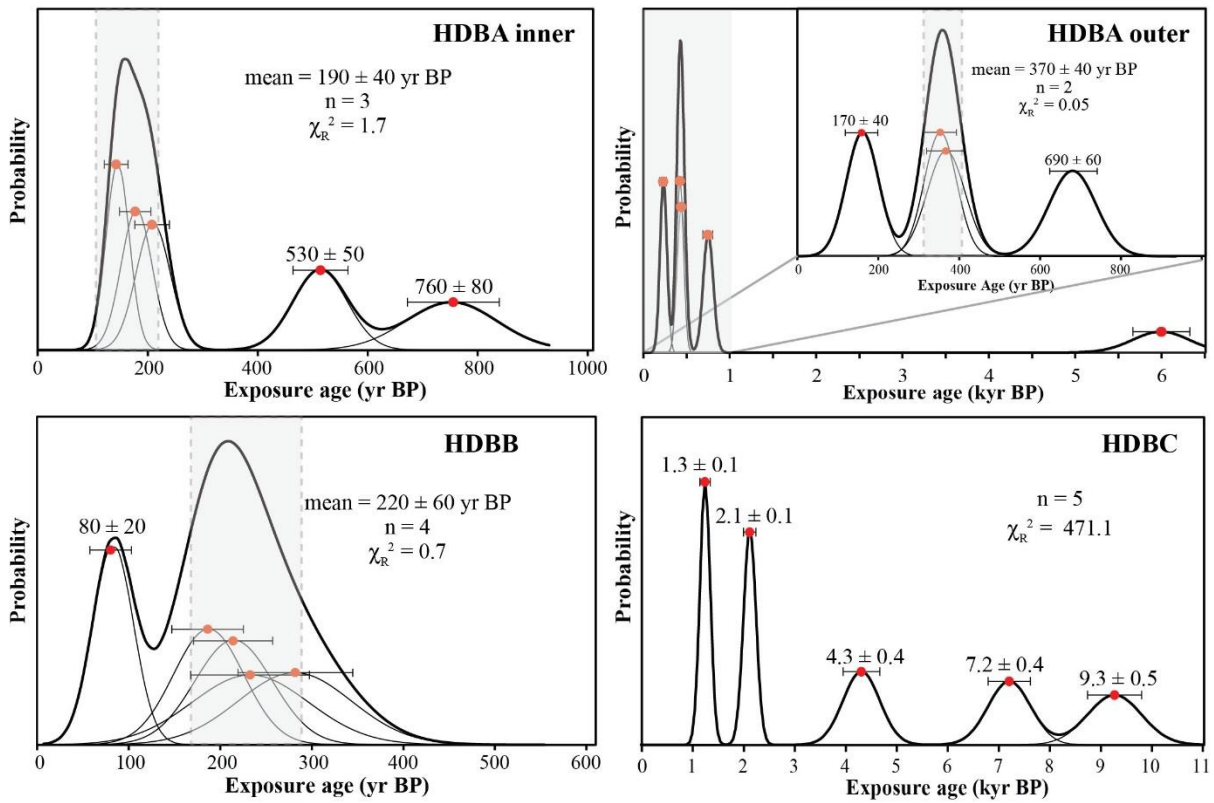
Figure 4-5. Probability density plot of ^{10}Be surface exposure ages for fresh moraine sets at the Haxilegen Pass sites. Each site has five samples. The assigned ages of the moraines are highlighted using dashed grey bars, with calculated weighted mean and χ_R^2. Five samples at HDBC produced widely scattered ages, and no age was assigned to this landform.
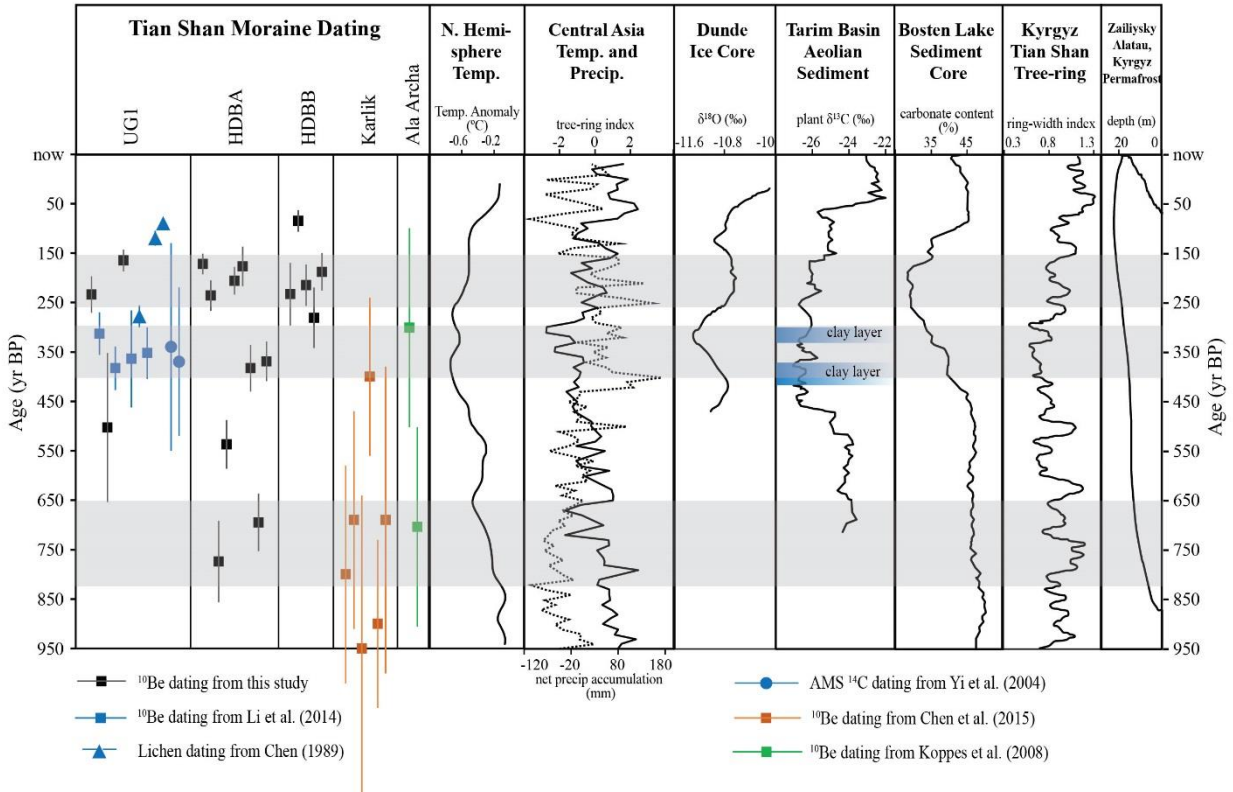
Figure 4-6. Comparison of dated moraine records in the Tian Shan and selected published climate records: N. hemisphere temperature (Moberg et al., 2005); Central Asia temperature and precipitation (Yang et al., 2009); Dunde ice core (Yao et al., 1997); Tarim Basin aeolian sediment (Liu et al., 2011); Bosten Lake sediment core (Chen et al., 2006); Kyrgyz Tian Shan tree rings (Esper et al., 2003); and Zailiysky, Alatau, Kyrgyz permafrost (Marchenko and Gorbunov, 1997).

Chapter 5

Summary and Future Work

5.1. Summary and Major Findings

This research investigated the extent and timing of Little Ice Age (LIA) glacial advances in the eastern Tian Shan, China. The methods involved in this study include glacier mapping, statistical analysis, field investigations, and cosmogenic surface exposure dating. Mapping the positions of LIA and modern glaciers provided a useful dataset for documenting the status of glaciers in this key region of Central Asia, as glaciers serve as critical freshwater supply in this arid and semi-arid area. Constraining the formation ages of the LIA moraines refines glacial chronology in the past millennium in Central Asia. Revealing the spatio-temporal pattern of the LIA glacial advances provides insights into the shifting dominance of different climate systems in the region, primarily the westerlies and the Siberian High, and the impacts of local topographic/geometric factors, such as slope, aspect, area, shape, hypsometry, and elevation, on glacial fluctuations. Such knowledge can help us better understand the response of glaciers to climate change during past centuries. It is of critical importance to predict future glacial and environmental changes that may impose significant impacts on water availability and security for this rapidly developing region. Major findings of my research are summarized here.

Direct mapping of glaciers and glacial landforms in Google Earth is of great value for documenting the presence and extents of glaciers in remote areas. In this research, I presented a map of contemporary glaciers and the LIA glacial extents for the eastern Tian Shan based on Google Earth high-resolution images. A total of 1173 glaciers and 747 corresponding LIA glacial extents were delineated for three sub-regions: the Boro-Eren Range, the Bogeda Range, and the Barkol-Karlik Range. This glacier map represents the boundaries of present glaciers from 2002 to 2013, mostly around 2010. The LIA moraines were identified in Google Earth based on the description in the literature, field observation, and available numerical dating results. The

average positional accuracy is about 10 m, based on the comparison between the delineated

boundaries and GPS ground tracks. This map indicates that the area occupied by glaciers in the

eastern Tian Shan has decreased from 796.5 km^2 during the LIA to 512.1 km^2 at present, a

change of 35.7%. The percentage of area loss is 42.3% in the Boro-Eren Range, 31.2% in the

Bogeda Range, and 20.4% in the Barkol-Karlik Range, respectively, showing a W-E decreasing

trend, which may be related to the precipitation pattern over the Tian Shan.

Using the glacier map for the Boro-Eren Range (487 glaciers), I examined local

topographic/geometric factors to determine the the most contributive factors to glacier changes

since the LIA. A set of parameters, including glacier area, slope, aspect, shape, hypsometry, and

mean elevation, were calculated as independent variables, while the percentage of glacier area

change and estimated change in ELA were used as dependent variables for a multivariate

stepwise regression analyses. Statistics of local factors showed that most glaciers are small

glaciers (area < 1 km^2) with north-facing aspects. The average slope is about 33.6°. Glaciers with

an elongated shape are only present around high peaks. Cirque and mountain-top glaciers are the

main type, located between 3800 and 4100 m a.s.l. Assuming a similar climate effect on glacier

changes in the relatively confined Boro-Eren sub-region, regression analysis revealed that the

area and the mean elevation of the glacier are the two major local factors to affect the relative

area changes. In contrast, none of these local factors are significant to the ELA changes. The

ELAs, reconstructed using the toe-to-summit altitude method (TSAM), showed an increase of

100 m from the LIA to present, similar to the change observed by other researchers in nearby

mountains. The spatial pattern of ELA changes in this sub-region indicated relatively large

changes in the west and northern slopes, suggesting that the ELA may be more sensitive to

climate factors, such as temperature and precipitation, rather than the local topographic/geometric settings.

I also applied cosmogenic ^{10}Be surface exposure dating to test if presumed LIA moraines were formed during the LIA. Based on ^{10}Be exposure ages from the Urumqi River headwaters and the Haxilegen Pass, as well as published ages in the literature, I concluded that three major glacial advances during the LIA: 730±300 yr BP, 370±100 yr BP, and 210±50 yr BP. The maximum LIA extent appears to have been reached asynchronously between our sites at the Boro-Eren Range and the site at the Karlik Range (easternmost Tian Shan). The outermost fresh moraines, located 700–900 m from the glacier terminus, were dated to 370±100 yr BP at both of two study areas. In contrast, a similar moraine was dated to 730±300 yr BP in the Karlik Range by Chen et al. (2015). At Haxilegen Pass, a set of inner moraine was dated to 210±50 yr BP, indicating a later glacial advance. These LIA glacial advances are correlated with periods that other proxy data suggest were relatively cold and wet. The asynchroneity of the maximum LIA glacial advance between the two study sites and the Karlik Range is likely due to the different controls of the westerlies and the Siberian High in the eastern Tian Shan. However, this observation is still preliminary. More studies are needed to fully understand the climate controls of the spatio-temporal pattern of glacier changes in this region.

In contrast to the LIA ages obtained in front of relatively large and thick glaciers, older boulders with widely scattered exposure ages were found in moraines in front of small and thin glaciers. Topographic maps indicated that these glaciers almost reached the presumed LIA extents in the early 1960s. It seems that these small and thin glaciers had advanced to the presumed LIA extent during the LIA, but they apparently did not deposit boulders with zero cosmogenic exposure age; instead, they presumably reworked deposits from events prior to the

LIA glacial advances, causing old and widely scattered exposure ages. This finding provides some insights into the potential impacts of glacial characteristics on [10]Be surface exposure dating, suggesting that nuclide inheritance may become an important issue to affect [10]Be exposure ages for moraines generated by relatively small and thin continental glaciers, especially when dating relatively young glacial events.

5.2. Plans for Future Work

I conducted the glacier mapping work in 2011–2013. It was laborious and time-consuming. However, through careful examination in Google Earth, I become familiar with the glacial features of the Tian Shan and different functions in Google Earth. As discussed in Chapter 2, the effectiveness of using Google Earth to map glaciers and glacial landforms has been demonstrated in terms of its wide coverage of high-resolution images, the archive of historical scenes with image date information, and an improved accuracy compared to other mapping methods. I plan to continue delineating glaciers across the Tian Shan. This work can be incorporated into undergraduate education. With basic knowledge of glaciers and training in using Google Earth, students will be able to participate in this mapping work. In addition, the comparison of delineations from different investigators, as well as more standard and automated methods are needed to improve the efficiency and objectivity of the delineation.

In this research, I successfully applied [10]Be cosmogenic exposure dating to constrain young glacial event such as the LIA, and also identified inheritance issues when dating moraines in front of small and thin glaciers. A hypothesis about the presence of relict surface were raised to explain the long-time pre-exposure of boulders at these sites. The inheritance problem might be common in dating young glacial landforms in front of small and thin glaciers because of lacking the production of newly exposed materials with zero initial nuclide concentration. It

would be interesting and necessary to apply comprehensive cosmogenic nuclide dating at more sites of small, thin glaciers to test if the argument of prior exposure being the more important geological process is true for glacial boulder groups younger than a thousand years. .

In future research, new sites and more glacial chronologies are needed to fill gaps in reconstructing past glaciations in the Tian Shan. This doctoral research was built upon a long-term international effort to study the paleo-glaciations in Central Asia. Several publications from this international group have focused on the long timescale to discuss the Quaternary glacial history in the Tian Shan, Tibetan Plateau, and nearby mountains (e.g. Li et al. 2014; Lifton et al. 2014; Fu et al. 2013; Heyman et al. 2011). Only a few studies have investigated the Holocene glacial events, such as the LIA, in the Tian Shan (Chen et al. 2015; Li et al. 2014; Li and Li 2014; Koppes et al. 2008). More studies are needed to examine the spatio-temporal pattern of the LIA glacial advances. For example, we observed the LIA moraines overlapping vegetated, old-looking moraines in the field (Figure 5-1). Knowing the formation age of this old moraine may help reveal other potential glacial advances during the Holocene.

This work and other studies have provided evidence that climate systems may control glacier changes differently across the Tian Shan. With more studies in the future, it will provide more data supports for the climate influence on glacier change during the LIA across the Tian Shan. Numerical modeling (e.g. Anderson and Mackintosh 2006; Bohner and Lehmkuhl 2005; Heyman et al. 2011; Hilton et al. 1994) of glacial fluctuations can also be used to quantify the roles of the changes in temperature and precipitation on glaciers. Using the modeling approach would also help predict the response of glaciers to future climate changes.

References

Anderson, B., and A. Mackintosh. 2006. Temperature change is the major driver of late-glacial and Holocene glacier fluctuations in New Zealand. *Geology* 34 (2):121–124.

Bohner, J., and F. Lehmkuhl. 2005. Environmental change modelling for Central and High Asia: Pleistocene, present and future scenarios. *Boreas* 34 (2):220–231.

Chen, Y., Y. Li, Y. Wang, M. Zhang, Z. Cui, C. Yi, and G. Liu. 2015. Late Quaternary glacial history of the Karlik Range, easternmost Tian Shan, derived from 10 Be surface exposure and optically stimulated luminescence datings. *Quaternary Science Reviews* 115:17–27.

Fu, P., J. M. Harbor, A. P. Stroeven, C. Hattestrand, J. Heyman, and L. Zhou. 2013. Glacial geomorphology and paleoglaciation patterns in Shaluli Shan, the southeastern Tibetan Plateau - Evidence for polythermal ice cap glaciation. *Geomorphology* 182:66–78.

Heyman, J., A. P. Stroeven, M. W. Caffee, C. Hattestrand, J. M. Harbor, Y. Li, H. Alexanderson, L. Zhou, and A. Hubbard. 2011. Palaeoglaciology of Bayan Har Shan, NE Tibetan Plateau: exposure ages reveal a missing LGM expansion. *Quaternary Science Reviews* 30 (15-16):1988–2001.

Hilton, N., D. Sugden, A. Payne, and C. Clapperton. 1994. Glacier modeling and the climate of Patagonia during the last glacial maximum. *Quaternary Research* 42 (1):1–19.

Koppes, M., A. R. Gillespie, R. M. Burke, S. C. Thompson, and J. Stone. 2008. Late Quaternary glaciation in the Kyrgyz Tien Shan. *Quaternary Science Reviews* 27 (7/8):846–866.

Li, Y. N., and Y. K. Li. 2014. Topographic and geometric controls on glacier changes in the central Tien Shan, China, since the Little Ice Age. *Annals of Glaciology* 55 (66):177–186.

Li, Y. K., G. N. Liu, Y. X. Chen, Y. N. Li, J. Harbor, A. P. Stroeven, M. Caffee, M. Zhang, C. C. Li, and Z. J. Cui. 2014. Timing and extent of Quaternary glaciations in the Tianger Range, eastern Tian Shan, China, investigated using Be-10 surface exposure dating. *Quaternary Science Reviews* 98:7–23.

Lifton, N., C. Beel, C. Hättestrand, C. Kassab, I. Rogozhina, R. Heermance, M. Oskin, D. Burbank, R. Blomdin, N. Gribenski, M. Caffee, B. M. Goehring, J. Heyman, M. Ivanov, Y. Li, Y. Li, D. Petrakov, R. Usubaliev, A. T. Codilean, and Y. Chen. 2014. Constraints on the late Quaternary glacial history of the Inylchek and Sary-Dzaz valleys from in situ cosmogenic 10Be and 26Al, eastern Kyrgyz Tian Shan. *Quaternary Science Reviews* 101:77–90.

Appendix for Chapter 5

Figure 5-1. Fresh LIA moraines adjacent to older moraines (foreground) at Haxilegen Pass.

Appendices

Appendix 1. Attribute information of 1173 glaciers mapped using Google Earth and DEM in the eastern Tian Shan

(Note: In column "Code", BE stands for Boro-Eren sub-region; BG stands for Bogeda sub-region; KL stands for Barkol-Karlik sub-region.)

Glacier ID	Code	Long (°E)	Lat (°N)	Google Earth Imagery Date	Glacial Feature	Area (km²)	Perimeter (km)
1	BE001	86.868	43.014	20101002	Clean_ice	0.042	0.837
2	BE002	86.985	43.013	20101002	Clean_ice	0.460	6.136
3	BE003	87.093	43.011	20100720/20090921	Clean_ice	3.205	12.844
4	BE004	87.305	43.016	20071029/2002	Clean_ice	0.690	4.107
5	BE005	87.081	43.020	20090921	Debris_covered	0.285	3.358
6	BE006	86.996	43.018	20100504/20101002	Debris_covered	0.521	4.805
7	BE007	86.437	43.467	20110912	Clean_ice	0.609	5.898
8	BE008	86.895	43.024	20101002	Clean_ice	0.186	2.538
9	BE009	87.047	43.022	20090921	Clean_ice	0.241	4.027
10	BE010	87.079	43.022	20090921	Debris_covered	0.557	7.679
11	BE011	87.091	43.021	20090921	Debris_covered	1.027	7.859
12	BE012	86.944	43.027	20101002	Clean_ice	0.048	1.572
13	BE013	86.940	43.028	20101002	Clean_ice	0.022	0.727
14	BE014	87.023	43.027	20090921	Clean_ice	0.222	3.255
15	BE015	86.907	43.028	20101002	Clean_ice	0.279	2.559
16	BE016	87.106	43.027	20090921	Clean_ice	0.431	3.672
17	BE017	87.118	43.028	20090921	Debris_covered	0.524	3.879
18	BE018	87.042	43.030	20090921	Clean_ice	0.105	1.651
19	BE019	87.279	43.029	20020916	Clean_ice	0.292	2.456
20	BE020	86.984	43.032	20101002	Clean_ice	0.078	2.041
21	BE021	87.025	43.033	20090921	Clean_ice	0.135	1.684
22	BE022	86.909	43.035	20101002	Clean_ice	0.040	0.840
23	BE023	87.078	43.035	20090921	Clean_ice	0.112	3.904
24	BE024	86.941	43.034	20101002	Clean_ice	0.305	4.136
25	BE025	87.066	43.034	20090921	Clean_ice	0.855	7.248
26	BE026	86.984	43.037	20101002	Clean_ice	0.136	2.495
27	BE027	87.014	43.033	20100504	Debris_covered	0.547	5.270
28	BE028	87.000	43.035	20100504	Clean_ice	0.698	5.478
29	BE029	87.057	43.031	20090921	Debris_covered	2.001	11.149
30	BE030	87.022	43.038	20100504/20090921	Clean_ice	0.136	2.300
31	BE031	87.243	43.039	20020916	Clean_ice	0.152	1.779
32	BE032	87.265	43.036	20020916	Clean_ice	0.953	4.372
33	BE033	87.049	43.041	20090921	Clean_ice	0.054	1.558
34	BE034	87.051	43.042	20090921	Clean_ice	0.023	1.101
35	BE035	87.098	43.043	20090921	Clean_ice	0.024	1.031
36	BE036	87.088	43.039	20090921	Debris_covered	0.628	5.405
37	BE037	87.095	43.042	20090921	Clean_ice	0.081	2.088
38	BE038	87.256	43.039	20020916	Clean_ice	0.914	4.322
39	BE039	87.043	43.043	20090921	Debris_covered	0.444	5.729
40	BE040	87.032	43.042	20090921	Clean_ice	0.347	4.356
41	BE041	86.912	43.043	20101002	Clean_ice	0.397	2.999
42	BE042	87.242	43.045	20020916	Clean_ice	0.156	2.044
43	BE043	87.236	43.042	20020916	Debris_covered	0.530	4.535
44	BE044	87.266	43.046	20020916	Clean_ice	0.142	1.444
45	BE045	87.206	43.047	20020916	Debris_covered	0.222	2.760
46	BE046	87.227	43.045	20020916	Clean_ice	0.455	3.015
47	BE047	86.928	43.050	20101002	Clean_ice	0.048	0.934
48	BE048	87.226	43.051	20020916	Clean_ice	0.092	1.245
49	BE049	86.987	43.051	20101002	Clean_ice	0.081	1.226

50	BE050	87.217	43.047	20020916	Clean_ice	0.651	3.722
51	BE051	86.960	43.048	20101002	Clean_ice	1.235	6.031
52	BE052	87.194	43.053	20020916	Debris_covered	0.451	2.943
53	BE053	87.160	43.055	20020916	Debris_covered	0.354	3.194
54	BE054	87.184	43.053	20020916	Clean_ice	0.524	4.041
55	BE055	86.918	43.058	20101002	Clean_ice	0.031	1.075
56	BE056	87.052	43.058	20090921	Clean_ice	0.026	0.770
57	BE057	86.890	43.057	20101002	Clean_ice	0.071	1.305
58	BE058	87.127	43.059	20090921	Clean_ice	0.027	0.881
59	BE059	86.985	43.060	20101002	Clean_ice	0.057	1.127
60	BE060	87.191	43.060	20020916	Clean_ice	0.185	2.173
61	BE061	87.041	43.058	20090921	Clean_ice	0.311	2.544
62	BE062	86.875	43.059	20101002	Clean_ice	0.772	5.489
63	BE063	86.987	43.063	20101002	Clean_ice	0.093	1.598
64	BE064	87.111	43.065	20090921	Clean_ice	0.070	1.998
65	BE065	87.104	43.065	20090921	Clean_ice	0.049	2.342
66	BE066	86.999	43.065	20100504	Clean_ice	0.032	1.032
67	BE067	87.096	43.066	20090921	Clean_ice	0.021	1.074
68	BE068	87.116	43.066	20090921	Clean_ice	0.074	1.134
69	BE069	87.093	43.067	20090921	Clean_ice	0.036	1.048
70	BE070	86.883	43.065	20101002	Clean_ice	0.392	2.802
71	BE071	87.198	43.069	20020916	Clean_ice	0.140	1.977
72	BE072	86.754	43.068	20101010	Clean_ice	0.372	3.171
73	BE073	86.988	43.069	20101002	Clean_ice	0.262	2.232
74	BE074	86.891	43.071	20101002	Clean_ice	0.446	2.704
75	BE075	86.900	43.072	20101002	Clean_ice	0.170	2.055
76	BE076	87.039	43.075	20090921	Clean_ice	0.075	1.220
77	BE077	86.992	43.075	20101002	Clean_ice	0.155	1.881
78	BE078	87.121	43.076	20090921	Clean_ice	0.025	1.201
79	BE079	87.117	43.075	20090921	Clean_ice	0.225	3.751
80	BE080	86.709	43.077	20101010	Clean_ice	0.165	2.309
81	BE081	86.841	43.080	20101002	Clean_ice	0.015	0.522
82	BE082	86.889	43.079	20101002	Clean_ice	0.208	3.289
83	BE083	86.845	43.081	20101002	Clean_ice	0.044	1.202
84	BE084	86.920	43.077	20101002	Clean_ice	0.599	3.512
85	BE085	86.753	43.081	20101010	Rock_glacier?	0.088	1.468
86	BE086	86.860	43.086	20101002	Clean_ice	0.084	2.199
87	BE087	86.698	43.086	20101010	Rock_glacier?	0.135	1.732
88	BE088	86.693	43.088	20101010	Clean_ice	0.011	0.393
89	BE089	87.038	43.087	20090921	Clean_ice	0.272	2.376
90	BE090	86.854	43.085	20101002	Debris_covered	0.228	2.824
91	BE091	87.093	43.090	20090921	Rock_glacier?	0.053	1.023
92	BE092	87.041	43.091	20090921	Rock_glacier?	0.022	0.749
93	BE093	86.863	43.089	20101002	Rock_glacier?	0.209	2.309
94	BE094	86.750	43.091	20101010	Clean_ice	0.050	1.125
95	BE095	86.623	43.090	20110912	Clean_ice	0.022	0.687
96	BE096	86.867	43.093	20101002	Clean_ice	0.038	0.990
97	BE097	86.878	43.088	20101002	Rock_glacier?	0.567	4.710
98	BE098	86.796	43.093	20101002	Rock_glacier?	0.065	1.937
99	BE099	86.891	43.090	20101002	Clean_ice	0.347	3.501
100	BE100	87.087	43.094	20090921	Clean_ice	0.064	1.579
101	BE101	86.841	43.092	20101002	Rock_glacier?	0.430	4.130
102	BE102	86.756	43.093	20100504/20101010	Clean_ice	0.198	2.097
103	BE103	86.800	43.097	20101002	Rock_glacier?	0.206	1.840
104	BE104	86.666	43.098	20100504	Debris_covered	0.198	2.390
105	BE105	86.763	43.097	20100504	Clean_ice	0.407	3.496

106	BE106	86.638	43.098	20101010	Debris_covered	0.208	2.153
107	BE107	86.829	43.102	20101002	Clean_ice	0.078	1.195
108	BE108	86.769	43.101	20100504/20101002	Clean_ice	0.307	2.397
109	BE109	86.463	43.102	20110912	Clean_ice	0.081	1.595
110	BE110	87.460	43.101	20071029	Clean_ice	0.438	4.125
111	BE111	86.823	43.100	20101002	Clean_ice	0.599	3.687
112	BE112	86.793	43.101	20101002	Clean_ice	0.504	3.877
113	BE113	86.662	43.103	20100504/20100811	Clean_ice	0.041	1.159
114	BE114	86.525	43.104	20110912	Clean_ice	0.028	0.845
115	BE115	86.761	43.105	20100811	Debris_covered	0.194	2.024
116	BE116	86.685	43.104	20100811	Clean_ice	0.231	2.156
117	BE117	86.504	43.102	20110912	Clean_ice	0.454	4.602
118	BE118	86.721	43.106	20100811	Clean_ice	0.095	1.380
119	BE119	86.737	43.108	20100811	Clean_ice	0.051	1.622
120	BE120	86.514	43.107	20110912	Debris_covered	0.260	2.485
121	BE121	86.778	43.108	20101002	Clean_ice	0.120	1.572
122	BE122	86.762	43.110	20101002	Clean_ice	0.018	0.695
123	BE123	87.417	43.108	20071029	Debris_covered	0.146	2.452
124	BE124	86.741	43.111	20100811	Clean_ice	0.048	0.943
125	BE125	86.785	43.109	20101002	Debris_covered	0.133	2.034
126	BE126	86.719	43.111	20100811	Clean_ice	0.033	0.679
127	BE127	87.423	43.108	20071029	Clean_ice	0.337	3.258
128	BE128	86.691	43.108	20100811	Clean_ice	0.554	3.166
129	BE129	87.445	43.110	20071029	Clean_ice	0.568	5.356
130	BE130	86.730	43.108	20100811	Debris_covered	0.443	4.583
131	BE131	87.410	43.108	20071029	Clean_ice	0.446	3.157
132	BE132	86.764	43.112	20100811	Clean_ice	0.097	2.598
133	BE133	86.682	43.115	20100811	Clean_ice	0.054	0.928
134	BE134	86.502	43.115	20110912	Clean_ice	0.013	0.588
135	BE135	86.809	43.110	20101002	Clean_ice	1.000	5.676
136	BE136	86.631	43.115	20110912	Debris_covered	0.098	1.515
137	BE137	87.430	43.114	20071029	Clean_ice	0.265	2.827
138	BE138	86.793	43.113	20101002	Clean_ice	0.376	4.348
139	BE139	86.625	43.116	20100811	Clean_ice	0.114	1.588
140	BE140	86.794	43.119	20101002	Clean_ice	0.008	0.682
141	BE141	86.803	43.116	20101002	Clean_ice	0.569	4.178
142	BE142	86.712	43.117	20100811	Clean_ice	0.219	2.095
143	BE143	86.720	43.117	20100811	Clean_ice	0.359	3.391
144	BE144	86.745	43.121	20100811	Clean_ice	0.041	0.886
145	BE145	86.508	43.118	20110912	Clean_ice	0.337	3.175
146	BE146	87.369	43.120	20071029	Debris_covered	0.239	2.801
147	BE147	86.678	43.120	20100811	Clean_ice	0.453	3.046
148	BE148	86.744	43.124	20100811	Clean_ice	0.036	0.989
149	BE149	87.351	43.119	2002	Debris_covered	0.942	7.194
150	BE150	87.394	43.124	20071029	Clean_ice	0.027	0.728
151	BE151	86.517	43.126	20100811	Clean_ice	0.031	0.851
152	BE152	86.709	43.123	20100811	Clean_ice	0.271	2.635
153	BE153	86.532	43.125	20110912	Debris_covered	0.175	2.449
154	BE154	87.195	43.126	2002	Clean_ice	0.121	1.755
155	BE155	86.584	43.126	20110912	Debris_covered	0.205	3.064
156	BE156	87.314	43.126	20020916	Clean_ice	0.419	4.825
157	BE157	87.329	43.124	20020916	Debris_covered	0.821	6.406
158	BE158	86.278	43.127	20100811	Clean_ice	0.009	0.374
159	BE159	86.745	43.128	20100811	Clean_ice	0.097	1.679
160	BE160	87.365	43.128	2007	Clean_ice	0.018	0.769
161	BE161	87.363	43.127	2007	Clean_ice	0.059	1.480

162	BE162	86.788	43.126	20101002		Clean_ice	0.934	4.280
163	BE163	87.304	43.128	2002		Debris_covered	0.253	3.107
164	BE164	86.573	43.129	20110912		Clean_ice	0.128	1.985
165	BE165	86.564	43.129	20110912		Clean_ice	0.078	1.562
166	BE166	86.508	43.130	20110912		Clean_ice	0.015	0.708
167	BE167	86.270	43.126	20100811		Clean_ice	0.484	3.097
168	BE168	86.699	43.124	20100811		Clean_ice	0.911	5.576
169	BE169	86.832	43.129	20101002		Clean_ice	0.299	3.473
170	BE170	87.396	43.130	2007		Clean_ice	0.094	1.630
171	BE171	86.312	43.131	20100811		Clean_ice	0.008	0.504
172	BE172	86.355	43.129	20100811		Clean_ice	0.128	1.592
173	BE173	86.245	43.129	20100811		Clean_ice	0.100	1.469
174	BE174	86.538	43.131	20110912		Clean_ice	0.097	1.503
175	BE175	86.598	43.125	20110912		Debris_covered	0.611	4.906
176	BE176	86.795	43.130	20101002		Clean_ice	0.212	2.199
177	BE177	86.804	43.129	20101002		Debris_covered	0.814	7.005
178	BE178	86.900	43.133	20101002		Clean_ice	0.016	0.553
179	BE179	86.710	43.133	20100811		Clean_ice	0.018	0.578
180	BE180	86.687	43.132	20100811		Clean_ice	0.085	1.461
181	BE181	86.494	43.133	20110912		Clean_ice	0.004	0.227
182	BE182	87.295	43.132	20020916		Debris_covered	0.389	3.611
183	BE183	87.336	43.131	20020916		Clean_ice	0.292	3.828
184	BE184	86.748	43.134	20100811		Clean_ice	0.056	1.262
185	BE185	86.905	43.134	20101002		Clean_ice	0.139	2.152
186	BE186	86.786	43.134	20101002		Clean_ice	0.106	1.565
187	BE187	86.256	43.130	20100811		Clean_ice	0.508	4.773
188	BE188	86.811	43.133	20101002		Clean_ice	0.363	3.039
189	BE189	86.548	43.132	20110912		Debris_covered	0.394	5.124
190	BE190	86.711	43.135	20100811		Clean_ice	0.040	0.783
191	BE191	86.870	43.136	20101002		Clean_ice	0.007	0.325
192	BE192	86.447	43.135	20110912		Clean_ice	0.021	0.738
193	BE193	87.346	43.136	2002		Clean_ice	0.008	0.397
194	BE194	86.515	43.136	20110912		Debris_covered	0.153	2.853
195	BE195	86.443	43.136	20100811		Clean_ice	0.045	1.227
196	BE196	86.896	43.135	20101002		Clean_ice	0.230	2.597
197	BE197	86.380	43.133	20100811		Clean_ice	0.393	3.507
198	BE198	86.473	43.136	20100811		Debris_covered	0.235	2.795
199	BE199	86.749	43.139	20100811		Clean_ice	0.019	0.937
200	BE200	86.822	43.136	20101002		Clean_ice	0.410	3.839
201	BE201	86.464	43.139	20110912		Clean_ice	0.102	1.250
202	BE202	86.684	43.138	20100811		Clean_ice	0.588	3.022
203	BE203	87.192	43.141	20020916		Clean_ice	0.014	0.592
204	BE204	86.490	43.139	20110912		Debris_covered	0.177	1.913
205	BE205	87.251	43.142	20020916		Clean_ice	0.014	0.572
206	BE206	86.872	43.140	20101002		Clean_ice	0.157	2.505
207	BE207	86.866	43.140	20101002		Debris_covered	0.151	2.539
208	BE208	87.284	43.137	20020916		Clean_ice	0.602	7.579
209	BE209	86.994	43.143	20100811		Clean_ice	0.023	0.802
210	BE210	86.500	43.139	20110912		Debris_covered	0.420	4.538
211	BE211	86.812	43.141	20101002		Clean_ice	0.414	2.848
212	BE212	87.247	43.143	20020916		Debris_covered	0.055	1.373
213	BE213	86.381	43.140	20100811		Clean_ice	1.576	8.362
214	BE214	86.361	43.143	20100811		Clean_ice	0.140	1.445
215	BE215	86.401	43.143	20100811		Clean_ice	0.340	2.389
216	BE216	86.962	43.147	20101002		Clean_ice	0.009	0.351
217	BE217	87.296	43.143	20020916		Clean_ice	0.540	4.498

218	BE218	86.883	43.141	20101002	Clean_ice	0.820	4.839
219	BE219	86.393	43.145	20100811	Clean_ice	0.131	1.389
220	BE220	87.002	43.145	20100811	Clean_ice	0.368	4.275
221	BE221	86.853	43.146	20101002	Debris_covered	0.207	2.001
222	BE222	86.480	43.148	20110912	Clean_ice	0.008	0.541
223	BE223	86.544	43.146	20110912	Clean_ice	0.249	2.792
224	BE224	86.253	43.147	20100811	Clean_ice	0.020	0.728
225	BE225	86.258	43.147	20100811	Clean_ice	0.006	0.360
226	BE226	86.259	43.148	20100811	Clean_ice	0.005	0.334
227	BE227	86.514	43.149	20100811	Clean_ice	0.018	0.786
228	BE228	87.177	43.148	20020916	Clean_ice	0.164	2.380
229	BE229	86.968	43.148	20101002	Clean_ice	0.159	2.615
230	BE230	86.806	43.150	20101002	Clean_ice	0.013	0.943
231	BE231	86.812	43.149	20101002	Clean_ice	0.078	2.425
232	BE232	86.421	43.159	20100811	Clean_ice	0.662	3.771
233	BE233	86.983	43.151	20101002	Clean_ice	0.082	1.545
234	BE234	86.455	43.146	20100811	Clean_ice	0.969	5.923
235	BE235	86.986	43.152	20101002	Clean_ice	0.015	0.700
236	BE236	87.318	43.152	20020916	Clean_ice	0.010	0.527
237	BE237	86.394	43.150	20100811	Clean_ice	0.336	3.945
238	BE238	86.677	43.152	20100811	Clean_ice	0.115	1.393
239	BE239	87.307	43.147	20020916	Debris_covered	0.730	8.059
240	BE240	86.882	43.153	20101002	Debris_covered	0.080	1.244
241	BE241	87.183	43.151	20020916	Clean_ice	0.186	2.365
242	BE242	86.434	43.148	20110912	Debris_covered	0.861	6.254
243	BE243	87.313	43.152	20020916	Clean_ice	0.107	2.753
244	BE244	86.483	43.154	20100811	Clean_ice	0.013	0.500
245	BE245	86.940	43.153	20101002	Debris_covered/Rock_glacier?	0.248	3.667
246	BE246	86.827	43.149	20101002	Clean_ice	1.274	7.176
247	BE247	86.472	43.147	20100811	Clean_ice	1.028	6.379
248	BE248	86.801	43.155	20101002	Clean_ice	0.093	1.951
249	BE249	87.191	43.156	20020916	Clean_ice	0.065	1.257
250	BE250	86.891	43.157	20101002	Clean_ice	0.012	0.460
251	BE251	86.689	43.154	20100811	Debris_covered	0.710	7.777
252	BE252	86.949	43.155	20101002	Rock_glacier?	0.343	3.222
253	BE253	86.854	43.157	20101002	Debris_covered	0.074	1.398
254	BE254	86.849	43.157	20101002	Debris_covered	0.284	3.478
255	BE255	86.893	43.159	20101002	Clean_ice	0.033	0.985
256	BE256	86.703	43.156	20100811	Debris_covered	0.366	3.101
257	BE257	87.283	43.159	20020916	Clean_ice	0.094	1.466
258	BE258	86.396	43.158	20100811	Clean_ice	0.343	2.762
259	BE259	86.220	43.158	20100811	Clean_ice	0.139	2.028
260	BE260	86.675	43.161	20100811	Clean_ice	0.032	1.004
261	BE261	86.333	43.160	20100811	Clean_ice	0.056	1.084
262	BE262	86.833	43.156	20101002	Clean_ice	1.451	8.206
263	BE263	86.926	43.158	20101002	Clean_ice	1.045	5.995
264	BE264	86.342	43.160	20100811	Clean_ice	0.490	3.706
265	BE265	87.284	43.165	20020916	Clean_ice	0.093	1.976
266	BE266	86.843	43.165	20101002	Clean_ice	0.042	1.211
267	BE267	86.409	43.157	20100811	Clean_ice	1.077	5.321
268	BE268	86.902	43.163	20101002	Clean_ice	0.587	4.285
269	BE269	86.958	43.164	20101002	Clean_ice	0.179	3.031
270	BE270	86.354	43.162	20100811	Clean_ice	0.382	3.044
271	BE271	86.490	43.161	20100811	Clean_ice	0.959	5.708
272	BE272	86.433	43.165	20100811	Clean_ice	0.151	1.945
273	BE273	87.288	43.167	20020916	Clean_ice	0.055	1.161

274	BE274	86.385	43.165	20100811	Clean_ice	0.063	1.042
275	BE275	86.200	43.164	20100811	Clean_ice	0.456	3.753
276	BE276	86.852	43.170	20101002	Clean_ice	0.010	0.556
277	BE277	86.326	43.168	20100811	Clean_ice	0.022	0.632
278	BE278	86.915	43.166	20101002	Clean_ice	0.490	4.334
279	BE279	86.908	43.169	20101002	Clean_ice	0.145	1.690
280	BE280	86.676	43.167	20100811	Clean_ice	0.335	3.381
281	BE281	86.808	43.171	20101002	Debris_covered	0.024	1.054
282	BE282	87.293	43.170	20020916	Debris_covered	0.080	1.310
283	BE283	86.829	43.169	20101002	Debris_covered/Rock_glacier?	0.137	2.377
284	BE284	86.810	43.172	20101002	Debris_covered	0.079	1.475
285	BE285	86.841	43.167	20101002	Debris_covered/Rock_glacier?	0.419	4.577
286	BE286	86.510	43.171	20100811	Clean_ice	0.110	1.531
287	BE287	87.305	43.175	20020916	Clean_ice	0.004	0.328
288	BE288	86.410	43.171	20100811	Clean_ice	0.228	1.946
289	BE289	87.306	43.176	20020916	Clean_ice	0.010	0.407
290	BE290	87.301	43.174	20020916	Clean_ice	0.089	1.793
291	BE291	87.308	43.177	20020916	Clean_ice	0.007	0.437
292	BE292	86.819	43.172	20101002	Debris_covered/Rock_glacier?	0.312	4.209
293	BE293	86.920	43.177	20101002	Clean_ice	0.054	1.142
294	BE294	86.776	43.177	20101002	Debris_covered	0.120	1.448
295	BE295	87.030	43.178	20071018	Clean_ice	0.061	0.992
296	BE296	86.223	43.176	20100811	Clean_ice	0.013	0.530
297	BE297	85.873	43.173	20110703	Clean_ice	0.036	1.129
298	BE298	86.219	43.176	20100811	Clean_ice	0.074	1.282
299	BE299	86.783	43.178	20101002	Debris_covered	0.143	1.533
300	BE300	86.225	43.177	20100811	Clean_ice	0.028	0.730
301	BE301	86.842	43.180	20101002	Debris_covered	0.057	1.141
302	BE302	86.926	43.181	20101002	Clean_ice	0.070	1.664
303	BE303	86.788	43.182	20101002	Debris_covered	0.033	0.710
304	BE304	86.751	43.181	20100811	Clean_ice	0.160	2.773
305	BE305	86.795	43.180	20101002	Debris_covered	0.227	3.634
306	BE306	86.921	43.183	20101002	Clean_ice	0.019	0.603
307	BE307	86.923	43.184	20101002	Clean_ice	0.025	0.786
308	BE308	86.820	43.183	20101002	Debris_covered/Rock_glacier?	0.109	1.643
309	BE309	87.028	43.184	20071018	Clean_ice	0.059	1.384
310	BE310	86.406	43.184	20100811	Clean_ice	0.031	0.705
311	BE311	86.763	43.184	20100811	Debris_covered	0.109	2.768
312	BE312	86.812	43.182	20101002	Rock_glacier?	0.433	2.920
313	BE313	86.399	43.182	20100811	Clean_ice	0.343	2.563
314	BE314	86.804	43.185	20101002	Clean_ice	0.079	1.572
315	BE315	86.737	43.186	20100811	Clean_ice	0.019	0.768
316	BE316	87.031	43.185	20071018	Clean_ice	0.115	2.466
317	BE317	86.454	43.185	20110912	Clean_ice	0.059	1.124
318	BE318	86.390	43.183	20100811	Clean_ice	0.230	2.112
319	BE319	86.740	43.187	20100811	Clean_ice	0.027	1.010
320	BE320	86.210	43.185	20100811	Clean_ice	0.038	0.852
321	BE321	87.310	43.186	20020916	Rock_glacier?	0.232	2.452
322	BE322	86.742	43.189	20100811	Clean_ice	0.016	0.632
323	BE323	86.760	43.187	20100811	Clean_ice	0.091	2.592
324	BE324	86.455	43.188	20110912	Clean_ice	0.029	1.131
325	BE325	86.763	43.190	20100811	Clean_ice	0.029	1.041
326	BE326	86.745	43.191	20100811	Clean_ice	0.031	0.997
327	BE327	86.754	43.189	20100811	Debris_covered	0.348	2.843
328	BE328	86.764	43.193	20100811	Clean_ice	0.071	1.425
329	BE329	86.922	43.195	20100811	Clean_ice	0.065	1.363

330	BE330	86.449	43.192	20110912	Clean_ice	0.219	2.311
331	BE331	86.383	43.191	20100811	Clean_ice	0.564	5.397
332	BE332	86.736	43.196	20100811	Clean_ice	0.147	1.789
333	BE333	86.839	43.197	20100811	Clean_ice	0.158	2.320
334	BE334	86.972	43.199	20100811	Clean_ice	0.016	0.686
335	BE335	86.807	43.198	20100811	Clean_ice	0.049	1.084
336	BE336	87.274	43.199	20090913	Clean_ice	0.016	0.821
337	BE337	86.368	43.195	20100811	Clean_ice	0.595	4.260
338	BE338	86.352	43.196	20100811	Clean_ice	0.522	4.176
339	BE339	85.919	43.193	20110703	Clean_ice	0.314	3.766
340	BE340	86.442	43.199	20110912	Clean_ice	0.029	0.747
341	BE341	86.929	43.198	20100811	Clean_ice	0.659	4.661
342	BE342	86.795	43.201	20100811	Clean_ice	0.012	0.550
343	BE343	86.966	43.198	20100811	Clean_ice	0.205	2.937
344	BE344	85.930	43.196	20110703	Clean_ice	0.093	1.547
345	BE345	86.801	43.199	20100811	Clean_ice	0.273	3.010
346	BE346	86.943	43.203	20100811	Clean_ice	0.008	0.553
347	BE347	86.916	43.204	20100811	Clean_ice	0.063	1.699
348	BE348	86.081	43.203	20100811	Clean_ice	0.004	0.278
349	BE349	86.079	43.203	20100811	Clean_ice	0.038	1.079
350	BE350	86.846	43.207	20100811	Clean_ice	0.058	2.256
351	BE351	86.954	43.202	20100811	Clean_ice	0.562	5.526
352	BE352	86.977	43.208	20100811	Clean_ice	0.023	0.887
353	BE353	86.940	43.205	20100811	Clean_ice	0.734	4.785
354	BE354	86.067	43.205	20100811	Clean_ice	0.044	1.937
355	BE355	86.928	43.209	20100811	Clean_ice	0.295	3.207
356	BE356	86.986	43.211	20100811	Clean_ice	0.146	4.433
357	BE357	86.466	43.211	20110912	Clean_ice	0.020	1.042
358	BE358	86.740	43.212	20100811	Clean_ice	0.034	1.125
359	BE359	86.453	43.212	20110912	Debris_covered	0.042	1.199
360	BE360	86.430	43.210	20100811	Clean_ice	0.581	4.125
361	BE361	86.791	43.214	20100811	Clean_ice	0.048	1.271
362	BE362	86.460	43.213	20100811	Clean_ice	0.150	3.248
363	BE363	86.698	43.216	20100811	Clean_ice	0.018	1.074
364	BE364	86.692	43.215	20100811	Debris_covered	0.335	4.619
365	BE365	86.043	43.213	20100811	Clean_ice	0.269	2.156
366	BE366	86.666	43.219	20100811	Clean_ice	0.040	1.512
367	BE367	86.055	43.216	20100811	Clean_ice	0.057	1.292
368	BE368	86.680	43.221	20100811	Debris_covered	0.332	3.276
369	BE369	86.816	43.224	20100811	Clean_ice	0.035	0.887
370	BE370	86.925	43.225	20100811	Clean_ice	0.097	1.782
371	BE371	86.432	43.222	20110912	Clean_ice	0.446	3.060
372	BE372	86.671	43.227	20100811	Debris_covered/Rock_glacier?	0.209	2.409
373	BE373	86.054	43.223	20100811	Debris_covered	0.100	1.650
374	BE374	86.445	43.228	20110912	Clean_ice	0.016	0.907
375	BE375	86.662	43.228	20100811	Debris_covered	0.083	1.310
376	BE376	86.140	43.226	20100811	Clean_ice	0.135	2.005
377	BE377	86.048	43.224	20100811	Clean_ice	0.169	1.745
378	BE378	86.940	43.230	20100811	Debris_covered	0.371	6.376
379	BE379	86.439	43.229	20100811	Debris_covered	0.212	2.536
380	BE380	86.791	43.232	20100811	Clean_ice	0.416	6.820
381	BE381	86.942	43.236	20100811	Clean_ice	0.002	0.181
382	BE382	86.165	43.232	20100811	Clean_ice	0.084	1.798
383	BE383	86.943	43.236	20100811	Clean_ice	0.009	0.449
384	BE384	86.950	43.235	20100811	Clean_ice	0.034	1.226
385	BE385	86.020	43.231	20100811	Clean_ice	0.061	1.257

386	BE386	86.854	43.235	20100811	Debris_covered	0.114	2.197
387	BE387	86.859	43.236	20100811	Clean_ice	0.035	0.929
388	BE388	86.039	43.229	20100811	Clean_ice	0.363	2.710
389	BE389	86.157	43.233	20100811	Clean_ice	0.068	1.553
390	BE390	86.937	43.228	20100811	Debris_covered	1.114	6.132
391	BE391	86.955	43.236	20100811	Clean_ice	0.158	2.020
392	BE392	86.416	43.236	20100811	Clean_ice	0.033	1.039
393	BE393	86.618	43.235	20110912	Clean_ice	0.191	2.420
394	BE394	86.148	43.232	20100811	Clean_ice	0.412	4.382
395	BE395	86.797	43.238	20100811	Clean_ice	0.135	1.711
396	BE396	86.435	43.240	20100811	Debris_covered/Rock_glacier?	0.040	1.461
397	BE397	86.439	43.241	20100811	Debris_covered/Rock_glacier?	0.100	1.629
398	BE398	86.860	43.242	20100811	Debris_covered	0.267	4.213
399	BE399	86.493	43.243	20110912	Debris_covered	0.060	1.157
400	BE400	86.499	43.243	20110912	Debris_covered	0.171	2.331
401	BE401	86.863	43.246	20071018	Clean_ice	0.073	1.330
402	BE402	86.024	43.238	20100811	Clean_ice	0.757	5.176
403	BE403	86.428	43.241	20110912	Debris_covered/Rock_glacier?	0.574	3.683
404	BE404	86.400	43.245	2010	Clean_ice	0.016	0.807
405	BE405	86.404	43.246	2010	Clean_ice	0.014	0.516
406	BE406	86.446	43.245	20100811/2010	Clean_ice	0.184	2.360
407	BE407	86.617	43.247	2010	Clean_ice	0.016	0.869
408	BE408	86.406	43.246	2010	Clean_ice	0.020	0.730
409	BE409	86.704	43.247	2010	Clean_ice	0.044	1.110
410	BE410	86.010	43.242	20110625	Clean_ice	0.236	2.313
411	BE411	86.034	43.244	20110625	Clean_ice	0.153	1.915
412	BE412	86.964	43.248	20071018	Clean_ice	0.079	1.543
413	BE413	86.409	43.249	2010	Clean_ice	0.049	1.824
414	BE414	86.971	43.249	20071018	Clean_ice	0.222	2.374
415	BE415	86.418	43.247	2010	Debris_covered	0.231	2.781
416	BE416	86.412	43.252	2010	Clean_ice	0.100	1.402
417	BE417	86.796	43.253	20071018	Clean_ice	0.085	1.304
418	BE418	86.483	43.252	2010	Clean_ice	0.306	3.064
419	BE419	86.724	43.255	2010	Debris_covered	0.099	1.905
420	BE420	86.870	43.256	20071018	Clean_ice	0.210	2.322
421	BE421	86.617	43.257	20110912	Debris_covered/Rock_glacier?	0.066	1.257
422	BE422	85.999	43.251	20110625	Clean_ice	0.291	4.158
423	BE423	86.731	43.256	2010	Debris_covered	0.191	3.128
424	BE424	86.700	43.256	2010	Clean_ice	0.346	4.859
425	BE425	86.411	43.259	2010	Clean_ice	0.214	3.490
426	BE426	86.791	43.262	20071018	Clean_ice	0.116	1.659
427	BE427	86.861	43.263	20071018	Clean_ice	0.046	0.991
428	BE428	86.791	43.266	20071018	Clean_ice	0.110	1.560
429	BE429	85.987	43.263	20110625	Clean_ice	0.059	1.805
430	BE430	86.728	43.267	2010	Debris_covered	0.095	1.754
431	BE431	86.895	43.269	20071018	Rock_glacier?	0.020	0.607
432	BE432	86.869	43.267	20071018	Clean_ice	0.893	5.187
433	BE433	86.887	43.268	20071018	Rock_glacier?	0.350	3.164
434	BE434	86.709	43.268	2010	Debris_covered	0.324	4.841
435	BE435	86.879	43.270	20071018	Rock_glacier?	0.181	2.456
436	BE436	86.700	43.271	2010	Clean_ice	0.035	0.756
437	BE437	86.720	43.263	2010	Debris_covered	0.812	6.230
438	BE438	85.974	43.267	20110625	Debris_covered	0.056	1.468
439	BE439	86.386	43.271	2010	Clean_ice	0.061	1.206
440	BE440	86.381	43.269	2010	Clean_ice	0.466	4.066
441	BE441	86.368	43.271	2010	Debris_covered	0.283	3.367

442	BE442	86.702	43.274	2010	Debris_covered	0.075	1.384
443	BE443	86.893	43.275	20071018	Clean_ice	0.108	1.744
444	BE444	86.308	43.276	2010	Clean_ice	0.036	1.147
445	BE445	86.351	43.274	2010	Debris_covered	0.801	7.489
446	BE446	86.702	43.282	2010	Clean_ice	0.139	1.589
447	BE447	85.920	43.278	20110703	Clean_ice	0.072	2.225
448	BE448	86.715	43.284	2010	Debris_covered	0.090	1.588
449	BE449	86.360	43.283	2010	Debris_covered	0.053	1.256
450	BE450	86.243	43.285	2010	Debris_covered	0.090	1.897
451	BE451	86.354	43.288	2010	Debris_covered	0.096	1.912
452	BE452	86.698	43.291	2010	Clean_ice	0.216	2.353
453	BE453	86.335	43.291	2010	Clean_ice	0.012	0.522
454	BE454	86.346	43.290	2010	Clean_ice	0.088	1.482
455	BE455	86.057	43.294	20110625	Clean_ice	0.048	1.240
456	BE456	86.223	43.296	2010	Clean_ice	0.055	1.509
457	BE457	86.432	43.299	20110912	Clean_ice	0.067	1.138
458	BE458	86.187	43.297	2010	Debris_covered	0.243	3.454
459	BE459	86.197	43.298	2010	Debris_covered	0.140	2.341
460	BE460	86.478	43.300	2010	Rock_glacier?	0.098	1.735
461	BE461	86.499	43.302	2010	Clean_ice	0.091	2.373
462	BE462	86.212	43.300	2010	Debris_covered	0.300	3.303
463	BE463	86.170	43.303	2010	Clean_ice	0.031	0.774
464	BE464	86.475	43.306	2010	Rock_glacier?	0.076	1.549
465	BE465	86.471	43.307	2010	Clean_ice	0.059	1.118
466	BE466	86.178	43.304	2010	Debris_covered	0.192	2.885
467	BE467	86.228	43.308	2010	Clean_ice	0.067	2.070
468	BE468	86.456	43.305	20110912	Debris_covered	0.943	6.862
469	BE469	86.148	43.312	2010	Clean_ice	0.037	1.028
470	BE470	86.446	43.314	2010	Clean_ice	0.201	2.076
471	BE471	86.154	43.313	2010	Clean_ice	0.191	2.976
472	BE472	85.999	43.314	20110625	Clean_ice	0.029	1.339
473	BE473	86.003	43.315	20110625	Clean_ice	0.105	3.487
474	BE474	86.424	43.313	2010	Clean_ice	0.929	12.218
475	BE475	86.504	43.316	20110912	Debris_covered	0.367	6.655
476	BE476	86.156	43.318	2010	Clean_ice	0.222	2.417
477	BE477	85.975	43.318	20110625	Clean_ice	0.054	1.615
478	BE478	86.440	43.316	20110912	Debris_covered	1.324	7.476
479	BE479	86.475	43.325	2010	Clean_ice	0.020	0.854
480	BE480	86.397	43.326	2010	Clean_ice	0.257	2.383
481	BE481	86.474	43.330	2010	Clean_ice	0.009	0.420
482	BE482	86.427	43.329	2010	Clean_ice	0.135	2.400
483	BE483	86.169	43.327	2010	Debris_covered	0.119	2.126
484	BE484	86.417	43.325	2010	Debris_covered	0.645	5.281
485	BE485	86.159	43.330	2010	Clean_ice	0.056	1.125
486	BE486	86.387	43.333	2010	Clean_ice	0.078	1.097
487	BE487	86.405	43.328	2010	Debris_covered	0.572	5.730
488	BE488	86.475	43.334	2010	Clean_ice	0.022	0.588
489	BE489	86.412	43.334	2010	Clean_ice	0.630	7.205
490	BE490	86.147	43.335	2010	Clean_ice	0.216	2.622
491	BE491	86.443	43.339	2010	Debris_covered	0.139	1.981
492	BE492	86.402	43.345	2010	Clean_ice	0.014	0.514
493	BE493	86.411	43.343	2010	Debris_covered	0.404	4.129
494	BE494	86.431	43.340	2010	Debris_covered	1.261	9.207
495	BE495	86.415	43.349	2010	Clean_ice	0.129	1.391
496	BE496	86.423	43.345	2010	Debris_covered	0.466	4.460
497	BE497	86.667	43.354	2010	Clean_ice	0.037	1.455

498	BE498	86.334	43.355	2010	Clean_ice	0.025	0.950
499	BE499	86.671	43.356	2010	Clean_ice	0.067	1.187
500	BE500	86.204	43.358	2010	Clean_ice	0.019	0.914
501	BE501	86.184	43.357	2010	Clean_ice	0.059	1.177
502	BE502	86.416	43.357	2010	Clean_ice	0.202	3.809
503	BE503	86.240	43.357	2010	Clean_ice	0.362	4.440
504	BE504	86.079	43.358	2010	Clean_ice	0.011	0.828
505	BE505	86.081	43.358	2010	Clean_ice	0.023	0.908
506	BE506	86.089	43.359	2010	Clean_ice	0.157	2.695
507	BE507	86.150	43.360	2010	Clean_ice	0.095	2.141
508	BE508	86.157	43.360	2010	Clean_ice	0.047	1.157
509	BE509	86.205	43.363	2010	Clean_ice	0.031	0.961
510	BE510	86.213	43.362	2010	Clean_ice	0.153	2.499
511	BE511	86.105	43.363	2010	Clean_ice	0.038	1.254
512	BE512	86.398	43.366	2010	Clean_ice	0.046	1.101
513	BE513	86.192	43.360	2010	Clean_ice	0.465	4.535
514	BE514	86.174	43.361	2010	Clean_ice	0.249	3.209
515	BE515	86.125	43.365	2010	Clean_ice	0.036	1.090
516	BE516	86.132	43.364	2010	Clean_ice	0.116	2.962
517	BE517	86.096	43.363	2010	Clean_ice	0.471	3.531
518	BE518	86.441	43.363	2010	Clean_ice	0.148	2.763
519	BE519	86.159	43.363	2010	Clean_ice	0.248	2.252
520	BE520	86.227	43.365	2010	Clean_ice	0.063	1.961
521	BE521	86.207	43.366	2010	Clean_ice	0.126	2.480
522	BE522	86.430	43.361	2010	Clean_ice	0.544	5.909
523	BE523	86.131	43.366	2010	Clean_ice	0.115	1.617
524	BE524	86.183	43.363	2010	Clean_ice	0.252	2.830
525	BE525	86.202	43.362	2010	Clean_ice	0.547	6.143
526	BE526	86.123	43.367	2010	Clean_ice	0.068	1.980
527	BE527	86.225	43.362	2010	Clean_ice	1.105	8.404
528	BE528	86.255	43.368	2010	Clean_ice	0.581	6.163
529	BE529	86.273	43.371	2010	Clean_ice	0.085	1.421
530	BE530	86.212	43.370	2010	Clean_ice	0.095	1.307
531	BE531	86.233	43.366	2010	Clean_ice	0.825	7.932
532	BE532	86.451	43.370	2010	Clean_ice	0.084	1.988
533	BE533	86.269	43.370	2010	Clean_ice	0.076	2.026
534	BE534	86.238	43.372	2010	Clean_ice	0.078	1.367
535	BE535	86.101	43.369	2010	Clean_ice	0.569	4.507
536	BE536	86.398	43.374	2010	Clean_ice	0.045	1.172
537	BE537	86.205	43.375	2010	Clean_ice	0.019	0.685
538	BE538	86.058	43.374	2010	Clean_ice	0.010	0.484
539	BE539	86.119	43.372	2010	Clean_ice	0.283	2.550
540	BE540	86.114	43.369	2010	Clean_ice	0.779	5.911
541	BE541	86.244	43.373	2010	Clean_ice	0.534	5.683
542	BE542	86.206	43.379	2010	Clean_ice	0.084	1.439
543	BE543	86.209	43.382	2010	Clean_ice	0.150	1.966
544	BE544	86.119	43.383	2010	Clean_ice	0.056	1.168
545	BE545	86.135	43.382	2010	Rock_glacier?	0.298	2.746
546	BE546	86.066	43.382	2010	Clean_ice	0.501	3.390
547	BE547	86.079	43.386	2010	Clean_ice	0.101	1.498
548	BE548	86.212	43.387	2010	Clean_ice	0.070	1.608
549	BE549	86.251	43.385	2010	Clean_ice	0.524	4.234
550	BE550	85.995	43.387	2010	Clean_ice	0.094	1.508
551	BE551	86.153	43.391	2010	Clean_ice	0.049	0.872
552	BE552	86.077	43.394	2010	Clean_ice	0.089	1.524
553	BE553	86.095	43.396	2010	Clean_ice	0.032	0.850

554	BE554	86.070	43.392	2010	Clean_ice	0.231	4.315
555	BE555	86.079	43.397	2010	Clean_ice	0.068	1.589
556	BE556	86.099	43.397	2010	Clean_ice	0.076	2.040
557	BE557	86.132	43.392	2010	Clean_ice	1.275	6.428
558	BE558	86.115	43.394	2010	Clean_ice	0.704	6.133
559	BE559	86.254	43.403	2010	Clean_ice	0.045	1.310
560	BE560	86.104	43.400	2010	Clean_ice	0.258	3.567
561	BE561	86.088	43.401	2010	Clean_ice	0.276	3.652
562	BE562	86.265	43.404	2010	Clean_ice	0.058	2.518
563	BE563	86.098	43.403	2010	Clean_ice	0.309	3.156
564	BE564	86.255	43.407	2010	Clean_ice	0.014	1.126
565	BE565	86.134	43.407	2010	Clean_ice	0.053	1.015
566	BE566	86.027	43.408	2010	Clean_ice	0.095	1.689
567	BE567	86.680	43.411	2010	Clean_ice	0.132	1.635
568	BE568	86.132	43.410	2010	Clean_ice	0.034	0.768
569	BE569	86.007	43.407	2010	Clean_ice	0.680	8.437
570	BE570	86.275	43.417	2010	Clean_ice	0.023	0.720
571	BE571	86.145	43.418	2010	Clean_ice	0.025	0.717
572	BE572	86.141	43.417	2010	Clean_ice	0.088	1.188
573	BE573	86.711	43.420	2010	Clean_ice	0.069	1.187
574	BE574	85.942	43.416	20110703	Clean_ice	0.052	1.109
575	BE575	86.705	43.421	2010	Clean_ice	0.031	0.720
576	BE576	86.096	43.419	2010	Clean_ice	0.620	7.612
577	BE577	86.005	43.420	2010	Clean_ice	0.183	5.430
578	BE578	86.141	43.422	2010	Clean_ice	0.261	2.226
579	BE579	86.073	43.419	2010	Clean_ice	0.463	3.341
580	BE580	86.084	43.421	2010	Clean_ice	0.384	3.919
581	BE581	86.144	43.426	2010	Clean_ice	0.079	1.478
582	BE582	86.003	43.427	2010	Clean_ice	0.063	1.315
583	BE583	86.526	43.429	2010	Clean_ice	0.268	2.654
584	BE584	85.989	43.414	2010	Debris_covered	2.616	11.272
585	BE585	85.953	43.428	20110625	Clean_ice	0.077	1.549
586	BE586	85.994	43.424	2010	Clean_ice	1.001	8.366
587	BE587	86.143	43.430	2010	Clean_ice	0.066	1.077
588	BE588	86.154	43.429	2010	Clean_ice	0.250	2.826
589	BE589	85.961	43.420	20110625	Debris_covered	0.892	7.245
590	BE590	86.018	43.418	20110625	Debris_covered	1.476	12.508
591	BE591	86.109	43.430	2010	Clean_ice	0.267	3.067
592	BE592	85.914	43.433	20110703	Debris_covered	0.533	5.168
593	BE593	85.949	43.431	20110703	Clean_ice	0.122	3.659
594	BE594	86.009	43.431	2010	Clean_ice	0.323	3.460
595	BE595	86.534	43.435	2010	Clean_ice	0.357	3.649
596	BE596	85.970	43.421	20110625	Debris_covered	0.948	9.923
597	BE597	85.924	43.432	20110703	Clean_ice	0.416	4.656
598	BE598	86.032	43.423	20110625	Debris_covered	1.814	14.037
599	BE599	85.943	43.428	20110625	Debris_covered	0.819	11.796
600	BE600	86.452	43.438	2010	Clean_ice	0.578	4.827
601	BE601	86.059	43.428	20110625	Debris_covered	5.127	27.347
602	BE602	85.929	43.439	20110703	Clean_ice	0.102	2.285
603	BE603	85.899	43.439	20110703	Debris_covered/Rock_glacier?	0.196	3.440
604	BE604	85.890	43.440	20110703	Clean_ice	0.051	1.300
605	BE605	86.107	43.440	2010	Clean_ice	0.350	3.102
606	BE606	85.925	43.441	20110703	Debris_covered	0.088	1.474
607	BE607	86.439	43.444	2010	Clean_ice	0.361	3.618
608	BE608	86.104	43.445	2010	Clean_ice	0.418	3.317
609	BE609	86.044	43.454	2010	Clean_ice	0.079	1.565

610	BE610	86.117	43.456	2010	Clean_ice	0.178	2.550
611	BE611	86.030	43.458	20110625	Debris_covered	0.127	4.824
612	BE612	86.041	43.459	20110625	Debris_covered	0.737	8.061
613	BE613	86.021	43.460	20110625	Debris_covered	0.222	4.194
614	BE614	86.104	43.460	20110625	Debris_covered	0.796	7.563
615	BE615	87.295	43.018	2002/20071029	Clean_ice	0.806	4.822
616	BE616	86.059	43.451	20110625	Debris_covered	8.714	34.458
617	BE617	86.395	43.472	2010	Clean_ice	0.059	1.478
618	BE618	86.396	43.474	2010	Clean_ice	0.126	2.273
619	BE619	86.004	43.475	20060526	Clean_ice	0.079	1.862
620	BE620	85.951	43.474	20060526	Clean_ice	0.212	2.426
621	BE621	86.013	43.468	20060526	Clean_ice	1.444	14.359
622	BE622	86.444	43.475	20050821	Debris_covered	1.174	10.629
623	BE623	85.953	43.477	20060526	Clean_ice	0.191	3.432
624	BE624	85.993	43.472	20060526	Clean_ice	0.924	10.174
625	BE625	86.100	43.478	2010	Clean_ice	0.272	2.844
626	BE626	86.405	43.476	20050821	Debris_covered	0.638	7.949
627	BE627	86.102	43.482	2010	Clean_ice	0.061	1.068
628	BE628	86.427	43.479	20050821	Debris_covered	1.051	13.410
629	BE629	86.417	43.482	20050821	Debris_covered	0.369	4.648
630	BE630	85.963	43.478	20060526	Debris_covered	0.551	6.768
631	BE631	85.979	43.476	20060526	Debris_covered	2.104	14.920
632	BE632	86.099	43.485	2010	Clean_ice	0.142	1.626
633	BE633	86.089	43.470	2010	Clean_ice	3.448	12.255
634	BE634	85.952	43.480	20060526	Debris_covered	0.763	7.223
635	BE635	85.942	43.485	20060526	Clean_ice	0.161	2.842
636	BE636	86.072	43.477	2010	Clean_ice	2.502	11.251
637	BE637	85.910	43.487	20060526	Clean_ice	0.165	3.893
638	BE638	86.067	43.489	2010	Clean_ice	0.139	1.984
639	BE639	86.468	43.495	2010	Clean_ice	0.031	1.202
640	BE640	85.934	43.487	20060526	Debris_covered	0.967	7.241
641	BE642	86.281	43.491	2010	Clean_ice	0.106	2.090
642	BE643	86.461	43.495	2010	Clean_ice	0.092	1.934
643	BE644	86.255	43.495	2010	Clean_ice	0.159	1.949
644	BE645	85.910	43.491	20060526	Clean_ice	0.186	4.719
645	BE646	86.057	43.492	2010	Clean_ice	0.632	4.855
646	BE647	86.013	43.485	2010	Clean_ice	3.396	16.171
647	BE648	86.109	43.494	2010	Clean_ice	0.133	2.279
648	BE649	85.902	43.493	20060526	Debris_covered	0.151	3.815
649	BE650	86.472	43.497	2010	Clean_ice	0.168	2.086
650	BE651	85.884	43.493	20060526	Clean_ice	0.250	3.467
651	BE652	85.931	43.492	20060526	Clean_ice	0.648	4.696
652	BE653	86.452	43.498	2010	Clean_ice	0.158	1.951
653	BE654	86.289	43.500	2010	Clean_ice	0.088	1.550
654	BE655	85.915	43.493	20060526	Debris_covered	1.026	10.573
655	BE656	86.042	43.483	2010	Clean_ice	5.090	21.777
656	BE657	85.983	43.500	20060526	Clean_ice	0.231	3.037
657	BE658	85.836	43.498	20060526	Clean_ice	0.650	6.735
658	BE659	85.854	43.497	20060526	Debris_covered	0.842	8.315
659	BE660	86.059	43.502	2010	Clean_ice	0.571	4.844
660	BE661	86.430	43.507	20050821	Clean_ice	0.060	2.310
661	BE662	86.449	43.506	20050821	Clean_ice	0.147	2.204
662	BE663	86.120	43.505	2010	Clean_ice	0.086	1.314
663	BE664	85.896	43.498	20060526	Debris_covered	0.788	12.304
664	BE665	86.438	43.505	20050821	Clean_ice	0.428	5.881
665	BE666	86.139	43.507	2010	Clean_ice	0.346	5.085

666	BE667	86.423	43.511	20050821	Clean_ice	0.044	1.082
667	BE668	85.863	43.504	20060526	Debris_covered	1.027	12.106
668	BE669	86.114	43.507	2010	Debris_covered	1.020	6.020
669	BE671	85.841	43.509	20060526	Debris_covered	1.733	11.144
670	BE672	86.061	43.517	2010	Clean_ice	0.038	0.914
671	BE674	85.839	43.518	20060526	Debris_covered	0.622	9.191
672	BE675	85.916	43.519	20060526	Debris_covered	0.282	4.082
673	BE676	86.118	43.522	2010	Clean_ice	0.703	5.694
674	BE677	85.968	43.524	20060526	Clean_ice	0.169	3.526
675	BE678	85.983	43.524	20060526	Clean_ice	0.207	2.865
676	BE679	86.159	43.525	2010	Clean_ice	0.363	2.880
677	BE680	86.003	43.508	20060526	Debris_covered	3.808	20.205
678	BE681	85.846	43.525	20060526	Clean_ice	0.184	2.165
679	BE682	86.155	43.530	2010	Clean_ice	0.053	0.915
680	BE683	86.101	43.529	2010	Clean_ice	0.125	1.548
681	BE684	85.969	43.529	20060526	Clean_ice	0.298	4.084
682	BE685	86.130	43.525	2010	Debris_covered	1.086	9.092
683	BE686	85.836	43.530	20060526	Clean_ice	0.104	2.284
684	BE687	85.962	43.505	20060526	Debris_covered	8.809	32.173
685	BE688	85.979	43.532	20060526	Clean_ice	0.116	1.844
686	BE689	85.918	43.515	20060526	Debris_covered	5.528	26.161
687	BE690	85.882	43.537	20060526	Clean_ice	0.103	1.900
688	BE691	85.968	43.537	20060526	Clean_ice	0.422	3.853
689	BE692	85.905	43.536	20060526	Clean_ice	0.617	6.184
690	BE693	85.986	43.522	20060526	Clean_ice	2.574	15.349
691	BE694	86.196	43.537	2010	Clean_ice	0.682	4.955
692	BE695	86.149	43.537	2010	Clean_ice	0.930	5.663
693	BE696	86.165	43.534	2010	Clean_ice	1.498	7.205
694	BE697	86.207	43.545	2010	Clean_ice	0.117	1.812
695	BE698	86.056	43.546	2010	Clean_ice	0.048	1.199
696	BE699	86.109	43.533	2010	Debris_covered	2.423	12.411
697	BE700	86.110	43.544	2010	Clean_ice	0.593	5.133
698	BE701	85.905	43.547	2010	Clean_ice	0.029	0.963
699	BE702	85.889	43.521	20060526	Debris_covered	5.600	27.222
700	BE703	86.114	43.548	2010	Clean_ice	0.295	3.314
701	BE704	85.966	43.548	2010	Clean_ice	0.297	2.457
702	BE705	85.812	43.549	2006	Clean_ice	0.029	1.390
703	BE706	86.172	43.554	2010	Clean_ice	0.171	2.888
704	BE707	86.050	43.553	2010	Clean_ice	0.141	3.060
705	BE708	86.122	43.555	2010	Clean_ice	0.052	1.444
706	BE709	86.197	43.556	2010	Clean_ice	0.097	1.375
707	BE710	85.967	43.555	2010	Clean_ice	0.084	1.314
708	BE711	85.810	43.553	2006	Clean_ice	0.031	0.891
709	BE712	85.905	43.554	2006	Clean_ice	0.186	2.051
710	BE713	85.865	43.529	20060526	Debris_covered	4.104	22.901
711	BE714	85.817	43.551	2006	Clean_ice	0.395	4.532
712	BE715	86.182	43.552	2010	Debris_covered	1.592	10.131
713	BE716	86.111	43.558	2010	Debris_covered	0.844	5.923
714	BE717	86.133	43.547	2010	Debris_covered	1.830	9.978
715	BE718	85.967	43.561	2006	Clean_ice	0.399	2.804
716	BE719	85.830	43.548	2006	Clean_ice	1.805	13.951
717	BE720	86.060	43.563	2010	Debris_covered	0.475	4.831
718	BE721	86.194	43.565	2010	Clean_ice	0.078	1.682
719	BE722	85.852	43.543	20060526	Clean_ice	2.746	20.234
720	BE723	85.907	43.564	20060526	Clean_ice	0.261	3.234
721	BE724	85.839	43.555	20060526	Clean_ice	0.796	7.736

722	BE725	85.792	43.560	20060526	Debris_covered/Rock_glacier?	0.495	5.158
723	BE726	85.977	43.566	2006	Clean_ice	0.162	2.197
724	BE727	85.918	43.567	20060526	Debris_covered	0.234	4.302
725	BE728	85.806	43.562	20060526	Debris_covered/Rock_glacier?	1.019	5.200
726	BE729	86.043	43.571	20090925	Clean_ice	0.201	2.598
727	BE730	85.958	43.572	20060526	Clean_ice	0.134	1.779
728	BE731	86.331	43.573	20050821	Clean_ice	0.204	2.025
729	BE732	85.780	43.569	20060526	Rock_glacier?	0.198	2.043
730	BE733	86.044	43.575	20090925	Clean_ice	0.205	2.769
731	BE734	85.903	43.573	20060526	Clean_ice	0.662	3.818
732	BE735	86.313	43.578	20050821	Debris_covered	0.571	8.282
733	BE736	86.111	43.576	20090925	Clean_ice	0.228	2.517
734	BE737	85.967	43.575	20060526	Clean_ice	0.871	8.377
735	BE738	86.113	43.580	20090925	Clean_ice	0.033	1.251
736	BE739	86.330	43.580	20050821	Clean_ice	0.285	2.679
737	BE740	86.249	43.579	20090914	Clean_ice	0.952	8.128
738	BE741	86.265	43.578	20090914	Clean_ice	0.385	4.370
739	BE742	86.323	43.580	20090914	Clean_ice	0.249	4.997
740	BE743	86.190	43.577	20090914	Clean_ice	1.278	8.223
741	BE744	86.287	43.585	2010	Clean_ice	0.056	1.238
742	BE745	86.208	43.584	20090914	Clean_ice	0.056	1.289
743	BE746	85.985	43.578	2006	Clean_ice	0.526	4.413
744	BE747	85.970	43.583	2006	Clean_ice	0.048	1.067
745	BE748	86.220	43.581	20090914	Clean_ice	1.248	9.993
746	BE749	86.282	43.580	20090914	Clean_ice	0.534	4.589
747	BE750	85.981	43.583	2006	Clean_ice	0.366	3.460
748	BE751	86.295	43.585	2010	Debris_covered	0.608	7.630
749	BE752	86.225	43.588	20090914	Clean_ice	0.183	3.177
750	BE753	85.902	43.584	2006	Clean_ice	0.290	4.060
751	BE754	86.117	43.589	20090925	Debris_covered	0.082	2.377
752	BE755	85.909	43.588	2012	Clean_ice	0.117	1.917
753	BE756	85.963	43.588	2006	Clean_ice	0.350	3.645
754	BE757	85.896	43.591	2006	Clean_ice	0.067	1.417
755	BE758	86.293	43.593	20090914	Debris_covered	0.101	2.221
756	BE759	86.228	43.593	20090914	Clean_ice	0.061	1.427
757	BE760	86.047	43.588	20090925	Debris_covered	0.275	5.617
758	BE761	85.977	43.592	2006	Debris_covered	0.518	4.297
759	BE762	86.241	43.591	20090914	Debris_covered	1.037	8.902
760	BE763	85.895	43.594	2006	Clean_ice	0.013	0.479
761	BE764	86.286	43.595	20090914	Clean_ice	0.200	3.392
762	BE765	86.051	43.596	20090925	Clean_ice	0.055	1.352
763	BE766	85.887	43.597	2006	Clean_ice	0.134	2.631
764	BE767	85.959	43.598	2006	Clean_ice	0.692	3.685
765	BE768	86.281	43.603	20090914	Clean_ice	0.081	2.189
766	BE769	86.166	43.604	20120403	Clean_ice	0.029	1.337
767	BE770	85.976	43.601	2006	Clean_ice	0.337	3.060
768	BE771	86.179	43.603	20090914	Clean_ice	0.250	2.761
769	BE772	85.886	43.603	2006	Clean_ice	0.018	0.673
770	BE773	85.879	43.600	2006	Clean_ice	0.697	5.851
771	BE774	86.250	43.607	20090914	Debris_covered	0.165	2.020
772	BE775	86.170	43.606	20120403	Clean_ice	0.091	1.611
773	BE776	85.904	43.599	2006	Debris_covered	0.998	10.054
774	BE777	86.195	43.598	20090914	Debris_covered	1.321	9.758
775	BE778	86.172	43.608	20120403	Clean_ice	0.088	1.422
776	BE779	86.060	43.609	20120403	Clean_ice	0.033	0.846
777	BE780	85.886	43.608	2012	Clean_ice	0.090	1.334

778	BE781	85.995	43.613	2010	Clean_ice	0.035	0.890
779	BE782	85.898	43.612	2012	Clean_ice	0.459	4.176
780	BE783	86.172	43.617	20090914	Debris_covered	0.313	3.722
781	BE784	85.987	43.614	2010	Clean_ice	0.301	2.837
782	BE785	86.065	43.614	20120403	Clean_ice	0.264	2.489
783	BE786	85.958	43.621	2012	Clean_ice	0.073	1.366
784	BE787	85.865	43.620	2012	Clean_ice	0.095	1.603
785	BE788	85.876	43.621	2012	Clean_ice	0.311	3.872
786	BE789	85.967	43.614	2010	Debris_covered	1.023	5.969
787	BE790	85.867	43.623	2012	Debris_covered	0.166	2.612
788	BE791	85.870	43.625	2012	Debris_covered	0.055	1.591
789	BE792	85.979	43.625	2010	Debris_covered	0.295	3.326
790	BE793	85.980	43.632	2010	Clean_ice	0.218	2.288
791	BE794	86.000	43.633	2010	Debris_covered	0.167	2.717
792	BE795	85.897	43.626	2012	Debris_covered/Rock_glacier?	1.086	7.750
793	BE796	85.876	43.634	2012	Debris_covered	0.146	2.569
794	BE797	85.858	43.635	2012	Debris_covered	0.588	7.371
795	BE798	85.888	43.632	2012	Debris_covered/Rock_glacier?	0.968	9.991
796	BE799	85.805	43.637	2012	Debris_covered	1.104	7.463
797	BE800	85.843	43.638	2012	Clean_ice	0.657	6.493
798	BE801	85.988	43.639	2010	Clean_ice	1.436	9.368
799	BE802	85.828	43.641	2012	Clean_ice	0.340	3.714
800	BE803	85.853	43.642	2012	Debris_covered	0.583	4.779
801	BE804	85.836	43.645	2012	Debris_covered	0.570	4.628
802	BE805	85.996	43.651	2010	Clean_ice	0.089	1.261
803	BE806	85.851	43.646	2012	Debris_covered	2.646	14.465
804	BE807	86.009	43.648	2010	Debris_covered	0.743	5.209
805	BE808	85.798	43.651	2012	Debris_covered	0.852	7.026
806	BE809	85.818	43.650	2012	Debris_covered	1.541	11.595
807	BE810	85.873	43.665	2012	Debris_covered	1.644	15.011
808	BE811	85.850	43.667	2012	Debris_covered	1.054	7.203
809	BE812	85.900	43.674	2012	Clean_ice	0.180	1.729
810	BE813	85.794	43.672	2012	Clean_ice	0.487	3.907
811	BE814	85.847	43.674	2012	Clean_ice	0.322	3.204
812	BE815	85.829	43.670	2012	Debris_covered	2.143	15.119
813	BE816	85.812	43.667	2012	Debris_covered	1.588	15.469
814	BE817	85.843	43.680	2012	Debris_covered	0.101	1.916
815	BE818	85.866	43.681	2012	Clean_ice	0.164	2.467
816	BE819	85.827	43.688	2012	Clean_ice	0.217	2.400
817	BE820	85.818	43.691	2012	Clean_ice	0.136	2.117
818	BE821	85.814	43.699	2012	Debris_covered	0.587	5.502
819	BG001	89.528	43.352	20020926	Debris_covered	0.265	4.172
820	BG002	89.518	43.354	20020926	Clean_ice	0.293	4.555
821	BG003	89.538	43.356	20020926	Clean_ice	0.091	2.099
822	BG004	89.502	43.358	20020926	Clean_ice	0.235	2.797
823	BG005	89.551	43.360	20020926	Clean_ice	0.799	5.872
824	BG006	89.551	43.368	20020926	Clean_ice	0.085	1.981
825	BG007	89.559	43.369	20020926	Clean_ice	0.017	0.857
826	BG008	89.556	43.369	20020926	Clean_ice	0.034	0.924
827	BG009	89.543	43.369	20020926	Clean_ice	0.102	2.440
828	BG010	89.561	43.375	20020926	Clean_ice	0.077	1.291
829	BG011	89.570	43.373	20020926	Clean_ice	0.377	3.787
830	BG012	89.581	43.374	20020926	Clean_ice	0.362	4.595
831	BG013	89.707	43.377	20021029	Clean_ice	0.207	2.185
832	BG014	89.593	43.383	20020926	Clean_ice	0.693	5.377
833	BG015	89.700	43.382	20021029	Clean_ice	0.375	3.554

834	BG016	89.650	43.384	20021029	Clean_ice	1.467	9.171
835	BG017	89.611	43.381	20020926	Clean_ice	1.424	8.018
836	BG018	89.672	43.384	20021029	Clean_ice	1.263	7.340
837	BG019	89.629	43.384	20020926	Clean_ice	1.122	6.328
838	BG020	89.597	43.435	20020926	Clean_ice	0.142	1.597
839	BG021	89.570	43.435	20020926	Clean_ice	0.551	7.579
840	BG022	89.391	43.446	2002	Clean_ice	0.061	1.075
841	BG023	89.360	43.446	2002	Clean_ice	0.069	1.464
842	BG024	89.425	43.448	20020926	Clean_ice	0.390	2.713
843	BG025	89.602	43.442	20020926	Clean_ice	0.381	3.219
844	BG026	89.452	43.450	20020926	Clean_ice	0.599	5.168
845	BG027	89.505	43.452	20020926	Debris_covered	0.528	3.965
846	BG028	89.492	43.455	20020926	Clean_ice	0.188	2.290
847	BG029	89.472	43.453	20020926	Clean_ice	0.635	6.902
848	BG030	89.363	43.458	2002	Rock_glacier?	0.520	3.742
849	BG031	89.484	43.457	20020926	Clean_ice	0.443	4.618
850	BG032	89.435	43.455	20020926	Clean_ice	1.392	8.692
851	BG033	89.344	43.465	2002	Clean_ice	0.314	3.175
852	BG034	89.408	43.457	20020926	Clean_ice	2.469	12.320
853	BG035	89.348	43.469	2002	Clean_ice	0.080	1.163
854	BG036	89.397	43.466	20020926	Clean_ice	0.418	3.702
855	BG037	89.388	43.464	2002	Clean_ice	0.634	4.843
856	BG038	89.382	43.467	2002	Clean_ice	0.743	4.785
857	BG039	89.427	43.468	20020926	Clean_ice	0.738	5.502
858	BG040	89.364	43.467	2002	Clean_ice	2.452	10.423
859	BG041	89.440	43.478	20020926	Clean_ice	0.034	0.831
860	BG042	89.389	43.491	2002	Clean_ice	0.083	1.412
861	BG043	89.373	43.492	2002	Rock_glacier?	0.205	2.225
862	BG044	89.381	43.495	2002	Clean_ice	0.050	1.121
863	BG045	89.061	43.564	20060423/2006	Clean_ice	1.093	5.939
864	BG046	88.881	43.582	20100910	Clean_ice	0.032	0.843
865	BG047	88.885	43.583	20100910	Clean_ice	0.035	0.976
866	BG048	88.927	43.595	20100910/20101002	Clean_ice	0.056	1.236
867	BG049	88.914	43.600	20101002	Clean_ice	0.152	3.218
868	BG050	88.905	43.602	20101002	Clean_ice	0.113	2.158
869	BG051	88.898	43.605	20101002	Clean_ice	0.060	2.022
870	BG052	88.863	43.605	20101002	Clean_ice	0.296	4.122
871	BG053	88.872	43.609	20101002	Clean_ice	0.311	2.770
872	BG054	89.000	43.608	20101002	Clean_ice	0.241	3.530
873	BG055	88.850	43.611	20101002	Clean_ice	0.146	1.695
874	BG056	88.817	43.613	20101002	Clean_ice	0.207	1.899
875	BG057	89.028	43.610	2010	Clean_ice	0.151	1.976
876	BG058	89.033	43.612	2010	Clean_ice	0.039	0.922
877	BG059	88.827	43.613	20101002	Clean_ice	0.231	2.154
878	BG060	88.840	43.612	20101002	Clean_ice	1.034	6.796
879	BG061	88.763	43.621	20101002	Clean_ice	0.143	1.933
880	BG062	88.825	43.619	20101002	Clean_ice	0.631	5.557
881	BG063	88.810	43.623	20101002	Clean_ice	0.573	4.156
882	BG064	88.768	43.628	20101002	Clean_ice	0.010	0.425
883	BG065	88.774	43.629	20101002	Clean_ice	0.075	1.373
884	BG066	88.788	43.636	20101002	Clean_ice	0.033	0.719
885	BG067	88.794	43.637	20101002	Clean_ice	0.097	2.138
886	BG068	88.800	43.638	20101002	Clean_ice	0.151	3.055
887	BG069	88.777	43.642	20101002	Clean_ice	0.208	1.849
888	BG070	88.807	43.647	20101002	Clean_ice	0.028	1.171
889	BG071	88.781	43.645	20101002	Clean_ice	0.202	2.354

890	BG072	88.870	43.672	20101002	Rock_glacier?	0.129	2.353
891	BG073	88.924	43.674	20101002	Rock_glacier?	0.009	0.477
892	BG074	88.918	43.675	20101002	Rock_glacier?	0.119	2.012
893	BG075	88.885	43.678	20101002	Rock_glacier?	0.109	1.487
894	BG076	88.911	43.677	20101002	Rock_glacier?	0.070	1.856
895	BG077	88.905	43.679	20101002	Rock_glacier?	0.085	1.795
896	BG078	88.890	43.681	20101002	Rock_glacier?	0.014	0.736
897	BG079	88.898	43.683	20101002	Rock_glacier?	0.118	2.667
898	BG080	88.877	43.681	20101002	Rock_glacier?	0.493	4.726
899	BG081	88.684	43.700	20101002	Clean_ice	0.098	3.051
900	BG082	88.752	43.701	20101002	Clean_ice	0.167	2.721
901	BG083	88.760	43.702	20101002	Clean_ice	0.294	3.244
902	BG084	88.720	43.705	20101002	Debris_covered	0.096	1.373
903	BG085	88.763	43.708	20101002	Clean_ice	0.325	3.606
904	BG086	88.717	43.710	20101002	Clean_ice	0.317	2.750
905	BG087	88.759	43.714	20101002	Clean_ice	0.044	0.909
906	BG088	88.692	43.709	20101002	Clean_ice	1.643	8.810
907	BG089	88.712	43.712	20101002	Debris_covered	0.582	5.663
908	BG090	88.737	43.714	20101002	Clean_ice	0.317	4.699
909	BG091	88.782	43.713	20101002	Clean_ice	0.230	3.007
910	BG092	88.750	43.713	20101002	Debris_covered	0.780	4.522
911	BG093	88.798	43.718	20101002	Debris_covered	0.115	2.921
912	BG094	88.225	43.730	20101024	Clean_ice	0.057	1.003
913	BG095	88.641	43.724	20101002	Clean_ice	0.265	2.293
914	BG096	88.694	43.723	20101002	Clean_ice	0.480	5.209
915	BG097	88.651	43.727	20101002	Clean_ice	0.237	2.994
916	BG098	88.705	43.725	20101002	Clean_ice	0.404	3.505
917	BG099	88.230	43.734	20101002	Clean_ice	0.274	2.892
918	BG100	88.237	43.735	20101002	Clean_ice	0.092	2.603
919	BG101	88.646	43.732	20101002	Debris_covered	0.195	1.955
920	BG102	88.332	43.735	20101002	Clean_ice	0.300	5.081
921	BG103	88.390	43.737	20101002	Clean_ice	0.255	3.761
922	BG104	88.639	43.736	20101002	Clean_ice	0.026	0.650
923	BG105	88.310	43.736	20101002	Debris_covered	0.746	9.100
924	BG106	88.467	43.739	20101002	Clean_ice	0.502	3.859
925	BG107	88.461	43.744	20101002	Clean_ice	0.263	2.384
926	BG108	88.612	43.741	20071026/20090412/20101002	Clean_ice	0.249	3.058
927	BG109	88.343	43.744	2010/20031010	Clean_ice	0.811	4.518
928	BG110	88.537	43.742	20071026/20101002	Clean_ice	0.910	4.394
929	BG111	88.319	43.745	2010	Clean_ice	1.007	8.865
930	BG112	88.393	43.748	20031010	Clean_ice	0.302	2.787
931	BG113	88.457	43.747	20071026	Debris_covered	0.422	4.047
932	BG114	88.097	43.755	20100907	Debris_covered	0.138	2.230
933	BG115	88.640	43.746	20090412	Clean_ice	0.678	3.416
934	BG116	88.550	43.747	20071026	Clean_ice	1.050	6.143
935	BG117	88.239	43.753	20090402	Clean_ice	0.248	3.240
936	BG118	88.531	43.750	20071026	Clean_ice	0.445	3.276
937	BG119	88.722	43.747	20090412	Rock_glacier?	0.260	2.947
938	BG120	88.336	43.754	2010	Clean_ice	0.113	1.616
939	BG121	88.406	43.752	20031010	Clean_ice	0.497	4.233
940	BG122	88.326	43.756	2010	Clean_ice	0.435	3.133
941	BG123	88.537	43.755	20071026	Clean_ice	0.231	2.072
942	BG124	88.614	43.751	20071026/20090412	Clean_ice	0.842	4.576
943	BG125	88.448	43.755	20071026	Clean_ice	0.218	2.448
944	BG126	88.345	43.757	20031010	Clean_ice	0.461	3.300

945	BG127	88.137	43.759	20100907	Debris_covered/Rock_glacier?	0.302	3.024
946	BG128	88.239	43.761	2009	Clean_ice	0.147	2.092
947	BG129	88.146	43.762	20100907	Debris_covered/Rock_glacier?	0.066	1.113
948	BG130	88.393	43.756	20031010	Clean_ice	1.059	5.984
949	BG131	88.643	43.755	20090412	Clean_ice	0.629	3.572
950	BG132	88.203	43.760	20101024	Clean_ice	1.034	6.093
951	BG133	88.158	43.762	20101024	Debris_covered/Rock_glacier?	0.614	4.206
952	BG134	88.167	43.762	20101024	Rock_glacier?	0.262	2.885
953	BG135	88.547	43.758	20071026	Clean_ice	0.802	6.945
954	BG136	88.189	43.766	20101024	Clean_ice	0.132	2.462
955	BG137	88.538	43.763	20071026	Clean_ice	0.069	1.115
956	BG138	88.604	43.759	20071026	Clean_ice	0.749	3.549
957	BG139	88.458	43.762	20071026	Clean_ice	0.791	5.756
958	BG140	88.691	43.762	20090412	Clean_ice	0.341	2.500
959	BG141	88.649	43.766	20090412	Debris_covered	0.152	2.301
960	BG142	88.628	43.767	20090412	Clean_ice	0.108	1.582
961	BG143	88.201	43.767	20101024	Clean_ice	0.691	4.951
962	BG144	88.247	43.772	2003	Clean_ice	0.141	1.798
963	BG145	88.209	43.771	20101024	Clean_ice	0.307	3.914
964	BG146	88.634	43.767	20090412	Clean_ice	0.082	2.029
965	BG147	88.638	43.769	20090412	Clean_ice	0.058	1.103
966	BG148	88.658	43.764	20090412	Clean_ice	0.504	3.613
967	BG149	88.445	43.768	20071026	Clean_ice	2.073	10.754
968	BG150	88.395	43.769	20031010	Clean_ice	0.800	5.973
969	BG151	88.264	43.773	2003	Clean_ice	0.295	3.254
970	BG152	88.211	43.776	20101024	Debris_covered	0.268	3.877
971	BG153	88.612	43.772	20090412	Clean_ice	0.193	1.848
972	BG154	88.540	43.771	20071026	Clean_ice	0.341	2.555
973	BG155	88.255	43.777	2003	Clean_ice	0.385	3.767
974	BG156	88.550	43.772	20071026	Clean_ice	0.918	4.204
975	BG157	88.259	43.781	2003	Clean_ice	0.144	2.110
976	BG158	88.666	43.778	20090412	Clean_ice	0.064	1.399
977	BG159	88.218	43.781	20101024	Clean_ice	0.536	4.951
978	BG160	88.230	43.774	20031024/2003/20101024	Clean_ice	2.691	11.920
979	BG161	88.545	43.779	20071026	Clean_ice	0.266	2.199
980	BG162	88.317	43.777	2003	Clean_ice	1.115	7.616
981	BG163	88.537	43.782	20071026	Clean_ice	0.292	2.236
982	BG164	88.614	43.780	20090412	Clean_ice	0.337	4.252
983	BG165	88.305	43.784	2003	Clean_ice	0.413	4.260
984	BG166	88.415	43.775	2003	Debris_covered	4.933	24.629
985	BG167	88.295	43.787	2003	Debris_covered	0.503	6.761
986	BG168	88.540	43.786	20071026	Clean_ice	0.215	2.013
987	BG169	88.327	43.785	2003	Clean_ice	1.214	7.802
988	BG170	88.485	43.785	20071026	Clean_ice	0.550	3.917
989	BG171	88.246	43.786	2003	Clean_ice	0.840	5.011
990	BG172	88.266	43.793	2003	Clean_ice	0.168	1.788
991	BG173	88.546	43.790	20071026	Clean_ice	0.175	1.963
992	BG174	88.385	43.782	2003	Debris_covered	2.327	11.423
993	BG175	88.315	43.794	2003	Clean_ice	0.665	3.743
994	BG176	88.472	43.788	20071026	Clean_ice	1.175	6.038
995	BG177	88.459	43.790	20071026	Clean_ice	0.878	5.184
996	BG178	88.352	43.779	2003	Debris_covered	7.117	29.816
997	BG179	88.259	43.793	2003	Clean_ice	1.006	6.993
998	BG180	88.406	43.795	2003	Clean_ice	1.342	11.193
999	BG181	88.231	43.802	20031024	Debris_covered	0.164	1.680
1000	BG182	88.543	43.799	20071026	Debris_covered	0.220	2.307

1001	BG183	88.238	43.803	2003	Clean_ice	0.106	1.625
1002	BG184	88.448	43.793	20071026	Debris_covered	7.582	29.708
1003	BG185	88.353	43.803	2003	Clean_ice	2.050	9.596
1004	BG186	88.293	43.800	2003	Clean_ice	2.414	11.284
1005	BG187	88.584	43.803	20071026	Clean_ice	0.366	2.581
1006	BG188	88.241	43.807	2003	Clean_ice	0.269	2.355
1007	BG189	88.251	43.809	2003	Clean_ice	0.099	1.287
1008	BG190	88.256	43.809	2003	Clean_ice	0.225	1.825
1009	BG191	88.562	43.803	20071026	Clean_ice	0.953	4.106
1010	BG192	88.608	43.808	20071026	Clean_ice	0.186	1.842
1011	BG193	88.441	43.812	20071026	Clean_ice	0.200	2.230
1012	BG194	88.246	43.817	2003	Clean_ice	0.102	1.670
1013	BG195	88.538	43.807	20071026	Clean_ice	2.123	7.298
1014	BG196	88.629	43.813	20090412	Clean_ice	0.551	3.159
1015	BG197	88.235	43.824	2003	Clean_ice	0.107	1.505
1016	BG198	88.381	43.810	2003	Clean_ice	3.832	19.341
1017	BG199	88.408	43.811	2003	Clean_ice	3.173	14.776
1018	BG200	88.310	43.811	2003	Clean_ice	7.863	30.059
1019	BG201	88.530	43.820	20071026	Rock_glacier?	0.477	4.686
1020	BG202	88.440	43.819	2003/20071026	Rock_glacier?	2.780	12.657
1021	BG203	88.484	43.823	20071026	Clean_ice	1.143	5.940
1022	BG204	88.225	43.830	20031024	Clean_ice	0.155	2.670
1023	BG205	88.363	43.822	2003	Clean_ice	5.963	22.065
1024	BG206	88.275	43.833	2003	Clean_ice	0.519	4.119
1025	BG207	88.492	43.837	20071026	Clean_ice	0.355	2.717
1026	BG208	88.327	43.832	2003	Clean_ice	2.736	11.676
1027	BG209	88.477	43.836	20071026	Clean_ice	0.978	4.492
1028	BG210	88.355	43.838	2003	Clean_ice	1.084	5.793
1029	BG211	88.379	43.845	2003	Clean_ice	0.087	1.271
1030	BG212	88.390	43.849	2003	Rock_glacier?	0.214	2.749
1031	BG213	88.320	43.849	2003	Clean_ice	0.566	3.765
1032	BG214	88.380	43.851	2003	Clean_ice	0.306	3.254
1033	BG215	88.303	43.851	2003	Debris_covered	0.533	3.159
1034	BG216	88.491	43.850	20071026	Debris_covered/Rock_glacier?	0.366	4.292
1035	BG217	88.337	43.844	2003	Clean_ice	2.237	9.526
1036	BG218	88.386	43.854	2003	Clean_ice	0.156	1.840
1037	BG219	88.351	43.853	2003	Clean_ice	0.285	3.671
1038	BG220	88.388	43.860	2003	Clean_ice	0.068	1.100
1039	BG221	88.398	43.864	2003	Clean_ice	0.160	1.775
1040	BG222	88.295	43.869	2003	Clean_ice	0.067	1.185
1041	BG223	88.512	43.861	20071026	Clean_ice	1.586	6.686
1042	BG224	88.338	43.872	2003	Clean_ice	0.081	1.212
1043	BG225	88.570	43.872	20040908	Clean_ice	0.065	1.240
1044	BG226	88.303	43.874	2006	Clean_ice	0.281	2.211
1045	BG227	88.289	43.882	2006	Clean_ice	0.181	3.453
1046	KL001	94.542	42.976	20110303	Debris_covered	0.083	1.437
1047	KL002	94.599	42.975	20110303	Debris_covered	0.315	3.375
1048	KL003	94.589	42.980	20110303	Clean_ice	0.110	1.899
1049	KL004	94.648	42.981	20110303	Clean_ice	0.040	1.416
1050	KL005	94.641	42.980	20110303	Clean_ice	0.233	3.900
1051	KL006	94.587	42.983	20110303	Debris_covered	0.060	1.824
1052	KL007	94.542	42.982	20110303	Clean_ice	0.245	3.483
1053	KL008	94.620	42.986	20110303	Clean_ice	0.192	1.878
1054	KL009	94.636	42.988	20110303	Clean_ice	0.024	0.666
1055	KL010	94.637	42.989	20110303	Clean_ice	0.011	0.420
1056	KL011	94.620	42.990	20110303	Clean_ice	0.068	1.378

1057	KL012	94.603	42.986	20110303	Clean_ice	1.438	11.557
1058	KL013	94.630	42.989	20110303	Clean_ice	0.599	3.573
1059	KL014	94.549	42.988	20110303	Clean_ice	1.183	9.005
1060	KL015	94.532	42.990	20110303	Clean_ice	0.896	6.308
1061	KL016	94.524	42.995	20110303	Clean_ice	0.127	2.025
1062	KL017	94.587	42.991	20110303	Clean_ice	0.904	4.856
1063	KL018	94.481	42.996	20110303	Clean_ice	0.143	1.828
1064	KL019	94.576	42.994	20110303	Clean_ice	0.837	5.979
1065	KL020	94.411	43.000	20030912	Clean_ice	0.238	2.780
1066	KL021	94.525	43.001	20110303	Clean_ice	0.185	2.888
1067	KL022	94.502	43.002	20110303	Clean_ice	0.083	1.978
1068	KL023	94.451	42.997	20030920	Clean_ice	0.710	7.078
1069	KL024	94.562	42.996	20110303	Clean_ice	0.855	6.650
1070	KL025	94.442	43.005	20030912	Clean_ice	0.070	1.529
1071	KL026	94.468	43.006	20131213	Clean_ice	0.283	2.365
1072	KL027	94.421	43.003	20030912	Clean_ice	0.630	5.159
1073	KL028	94.428	43.008	20030912	Clean_ice	0.158	2.070
1074	KL029	94.442	43.009	20030912	Clean_ice	0.056	1.784
1075	KL030	94.552	43.005	20110303	Clean_ice	0.993	6.551
1076	KL031	94.502	43.010	20110303	Clean_ice	0.402	4.488
1077	KL032	94.534	43.005	20110303	Clean_ice	1.820	7.877
1078	KL033	94.434	43.007	20030912	Clean_ice	0.785	5.494
1079	KL034	94.464	43.012	20030920	Clean_ice	1.315	5.273
1080	KL035	94.486	43.012	20030920	Clean_ice	0.878	5.415
1081	KL036	94.450	43.010	20030920	Clean_ice	0.855	5.749
1082	KL037	94.502	43.016	20110303	Debris_covered	0.151	3.210
1083	KL038	94.564	43.018	20110303	Clean_ice	0.329	2.989
1084	KL039	94.353	43.019	20030912	Clean_ice	0.085	1.930
1085	KL040	94.459	43.022	20030920	Clean_ice	0.110	2.388
1086	KL041	94.511	43.020	20030920	Clean_ice	1.419	6.600
1087	KL042	94.464	43.025	20030920	Clean_ice	0.054	1.565
1088	KL043	94.469	43.023	20030920	Clean_ice	0.281	2.681
1089	KL044	94.400	43.025	20030912	Clean_ice	0.352	3.549
1090	KL045	94.390	43.030	20030912	Clean_ice	0.111	1.509
1091	KL046	94.561	43.025	20061013	Clean_ice	0.723	5.954
1092	KL047	94.444	43.031	20030920	Clean_ice	0.156	2.407
1093	KL048	94.527	43.025	20030920	Clean_ice	1.194	9.386
1094	KL049	94.453	43.033	20030920	Clean_ice	0.148	1.555
1095	KL050	94.399	43.032	20030912	Clean_ice	0.343	3.897
1096	KL051	94.545	43.022	20030920/20110303	Clean_ice	1.891	12.876
1097	KL052	94.462	43.031	20030920	Clean_ice	0.891	5.291
1098	KL053	94.472	43.035	20030920	Clean_ice	0.971	4.814
1099	KL054	94.500	43.039	20030920	Clean_ice	0.183	2.663
1100	KL055	94.353	43.040	20030912	Clean_ice	0.050	1.020
1101	KL056	94.380	43.039	20030912	Clean_ice	0.095	1.989
1102	KL057	94.399	43.039	20030912	Clean_ice	0.478	5.256
1103	KL058	94.364	43.033	20030912	Clean_ice	2.398	11.508
1104	KL059	94.488	43.029	20030920	Clean_ice	4.438	19.957
1105	KL060	94.448	43.038	20030920	Clean_ice	1.173	5.537
1106	KL061	94.426	43.043	20030912	Clean_ice	0.062	1.231
1107	KL062	94.503	43.043	20030920	Clean_ice	0.079	2.443
1108	KL063	94.516	43.038	20030920	Clean_ice	1.806	7.326
1109	KL064	94.354	43.046	20030912	Clean_ice	0.189	2.201
1110	KL065	94.507	43.048	20030920	Clean_ice	0.043	2.265
1111	KL066	94.397	43.043	20030912	Clean_ice	1.838	10.987
1112	KL067	94.437	43.050	20030912	Clean_ice	0.154	1.801

1113	KL068	94.370	43.047	20030912	Clean_ice	0.847	6.382
1114	KL069	94.357	43.050	20030912	Clean_ice	0.549	3.924
1115	KL070	94.408	43.050	20030912	Clean_ice	0.743	3.845
1116	KL071	94.516	43.053	20030920	Clean_ice	0.658	3.727
1117	KL072	94.464	43.048	20030920	Clean_ice	1.981	11.860
1118	KL073	94.359	43.056	20030912	Clean_ice	1.266	7.227
1119	KL074	94.327	43.054	20030912	Clean_ice	2.028	8.526
1120	KL075	94.419	43.061	20030912	Clean_ice	0.143	1.943
1121	KL076	94.447	43.062	20030920	Clean_ice	0.034	1.039
1122	KL077	94.439	43.061	20030912	Clean_ice	0.559	4.447
1123	KL078	94.341	43.061	20030912	Clean_ice	1.107	8.831
1124	KL079	94.452	43.058	20030920	Clean_ice	1.652	8.865
1125	KL080	94.408	43.061	20030912	Clean_ice	0.795	4.894
1126	KL081	94.353	43.066	20030912	Clean_ice	0.370	3.559
1127	KL082	94.426	43.058	20030912	Clean_ice	2.157	8.945
1128	KL083	94.382	43.064	20030912	Clean_ice	1.574	8.629
1129	KL084	94.389	43.057	20030912	Clean_ice	3.367	19.322
1130	KL085	94.449	43.073	20030920	Clean_ice	0.966	4.550
1131	KL086	94.391	43.078	20030912	Clean_ice	0.311	4.924
1132	KL087	94.316	43.067	20121207/20030912/2012	Clean_ice	6.551	25.073
1133	KL088	94.439	43.081	20030912	Clean_ice	0.575	3.448
1134	KL089	94.371	43.076	20030912/20121207	Clean_ice	4.546	20.163
1135	KL090	94.309	43.078	20121207	Clean_ice	3.036	14.727
1136	KL091	94.298	43.090	20121207	Clean_ice	4.123	16.036
1137	KL092	94.277	43.094	20121207	Clean_ice	1.962	8.496
1138	KL093	94.383	43.098	20030912/20121207	Clean_ice	0.844	8.383
1139	KL094	94.277	43.102	20121207	Clean_ice	3.375	13.666
1140	KL095	94.355	43.110	20121207	Clean_ice	0.184	3.229
1141	KL096	94.360	43.095	20121207	Clean_ice	4.660	17.187
1142	KL097	94.248	43.109	20121207	Clean_ice	3.901	13.242
1143	KL098	94.338	43.099	20121207	Clean_ice	3.086	13.363
1144	KL099	94.329	43.106	20121207	Clean_ice	3.644	16.010
1145	KL100	94.320	43.128	20121207	Clean_ice	0.529	3.096
1146	KL101	94.261	43.122	20121207	Clean_ice	4.180	13.547
1147	KL102	94.226	43.132	20121207	Clean_ice	0.193	2.018
1148	KL103	94.270	43.135	20121207	Clean_ice	0.190	3.479
1149	KL104	94.260	43.137	20121207	Clean_ice	0.137	2.600
1150	KL105	94.305	43.121	20121207	Clean_ice	2.793	9.319
1151	KL106	94.337	43.137	20121207	Clean_ice	0.355	3.020
1152	KL107	94.249	43.138	20121207	Clean_ice	0.470	4.626
1153	KL108	94.287	43.127	20121207	Clean_ice	3.646	18.248
1154	KL109	94.238	43.140	20121207	Clean_ice	0.188	2.698
1155	KL110	94.319	43.140	20121207	Clean_ice	0.077	1.664
1156	KL111	94.262	43.139	20121207	Clean_ice	0.210	2.660
1157	KL112	94.325	43.138	20121207	Clean_ice	0.650	4.010
1158	KL113	94.231	43.140	20121207	Clean_ice	0.324	4.031
1159	KL114	94.263	43.142	20121207	Clean_ice	0.332	3.183
1160	KL115	94.218	43.145	20120929	Debris_covered	0.173	1.733
1161	KL116	94.274	43.144	20121207	Clean_ice	0.561	3.447
1162	KL117	94.206	43.151	20120929	Clean_ice	0.205	2.218
1163	KL118	93.411	43.369	20100426	Debris_covered	0.238	2.305
1164	KL119	93.400	43.375	20100426	Clean_ice	0.387	3.167
1165	KL120	93.408	43.376	20100426	Clean_ice	0.727	5.093
1166	KL121	93.393	43.379	20100426	Clean_ice	0.716	5.095
1167	KL122	93.354	43.385	20100426	Clean_ice	0.251	2.450
1168	KL123	93.385	43.387	20100426	Clean_ice	1.409	7.009

1169	KL124	93.363	43.389	20100426	Clean_ice	1.251	5.986
1170	KL125	93.321	43.400	2010	Clean_ice	0.901	5.303
1171	KL126	93.304	43.404	2004	Clean_ice	0.546	4.179
1172	KL127	93.326	43.418	2010	Clean_ice	3.038	10.184
1173	KL128	93.303	43.427	2003	Clean_ice	0.664	3.801

Appendix 2. Quartz weights, ^{9}Be carrier masses, AMS measured ^{10}Be/^{9}Be ratios, and measured chemical blanks for samples from the Urumqi River headwater area and the Haxilegen Pass, China

| Sample ID	Latitude (°N)	Longitude (°E)	Elevation (m)	Quartz weight (g)	^{9}Be carrier mass (mg)	^{10}Be/^{9}Be (10^{-15})	Error (10^{-15})
HDB-12-06	43.739	84.402	3484	100.22	0.3730	40.5	3.2
HDB-12-07	43.738	84.403	3485	99.93	0.3530	53.2	5.1
HDB-12-08	43.738	84.403	3481	90.03	0.3670	134.4	11.6
HDB-12-09	43.738	84.403	3483	50.81	0.3620	54.9	3.8
HDB-12-10	43.738	84.403	3485	90.04	0.3570	43.5	4.3
HDB-12-11	43.739	84.403	3477	69.12	0.3650	29.4	5.0
HDB-12-12	43.739	84.403	3475	51.00	0.3600	41.1	4.0
HDB-12-13	43.739	84.403	3473	99.80	0.3580	134.9	8.2
HDB-12-14	43.739	84.403	3473	100.10	0.3530	76.1	6.3
HDB-12-15	43.739	84.403	3477	99.91	0.3580	1141.5	29.5
HDB-12-16	43.737	84.407	3411	88.96	0.3670	43.6	9.4
HDB-12-17	43.737	84.407	3418	99.92	0.3560	25.5	4.0
HDB-12-18	43.737	84.407	3417	68.66	0.3800	31.1	4.7
HDB-12-19	43.737	84.406	3420	102.31	0.3640	58.0	10.3
HDB-12-20	43.737	84.406	3424	90.03	0.3640	37.8	5.7
HDB-12-21	43.727	84.412	3546	65.03	0.3580	159.2	10.1
HDB-12-22	43.727	84.412	3546	70.98	0.3693	1291.0	38.7
HDB-12-23	43.727	84.412	3542	70.23	0.3619	1012.2	31.2
HDB-12-24	43.726	84.413	3544	64.95	0.3590	552.1	37.4
HDB-12-25	43.726	84.413	3540	46.00	0.3565	193.4	5.9
WY-12-03	43.100	86.842	3638	80.91	0.3600	106.7	4.4
WY-12-04	43.099	86.842	3639	54.48	0.3620	526.1	13.2
WY-12-08	43.098	86.841	3653	99.94	0.3660	1005.2	24.3
WY-12-09	43.098	86.841	3656	45.52	0.3610	250.2	13.2
WY-12-21	43.118	86.821	3785	89.84	0.3610	54.3	6.6
WY-12-22	43.117	86.822	3764	66.20	0.3580	75.4	20.2
WY-12-23	43.117	86.822	3758	63.35	0.3640	28.6	2.6
Blank 1					0.3685	3.1	1.0
Blank 6					0.3600	0.7	0.6
Blank 7					0.3600	1.3	0.8
Blank 8					0.3620	2.9	0.8
Blank 9					0.3620	5.8	0.9
Blank 10					0.3704	1.4	0.6

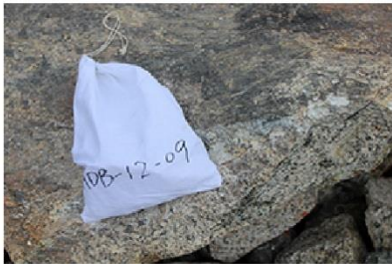**Appendix 3. Field photos for each sample**
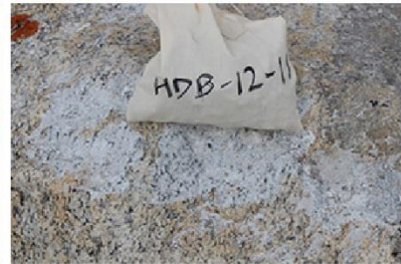

HDB-12-06

HDB-12-07
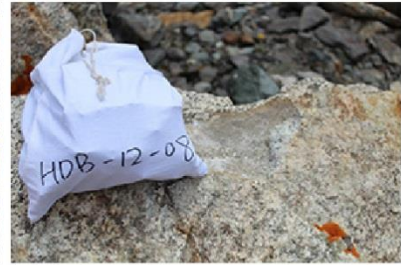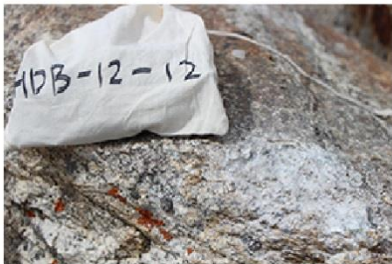

HDB-12-08

HDB-12-09

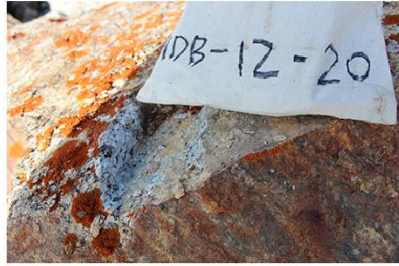HDB-12-10

HDB-12-11

HDB-12-12
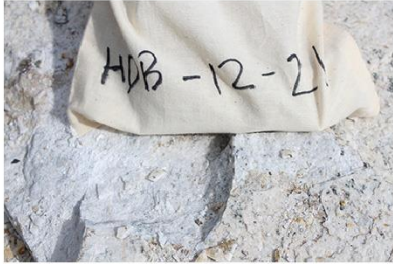
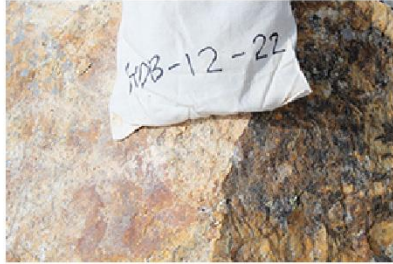
HDB-12-13

HDB-12-14

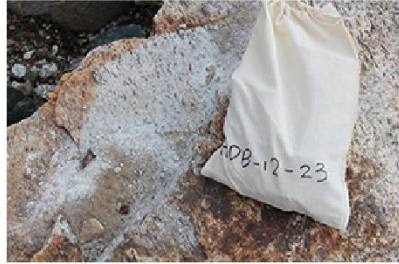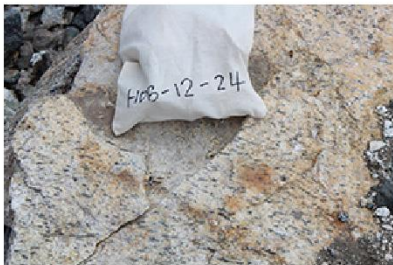HDB-12-15

HDB-12-16

HDB-12-17

HDB-12-18

HDB-12-19

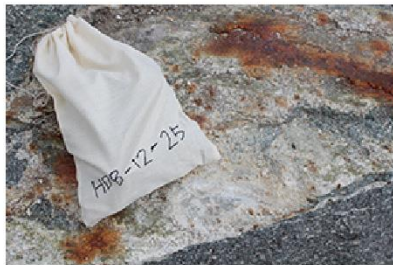HDB-12-20

HDB-12-21

HDB-12-22
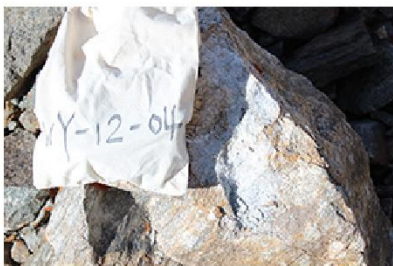

HDB-12-23

HDB-12-24

HDB-12-25
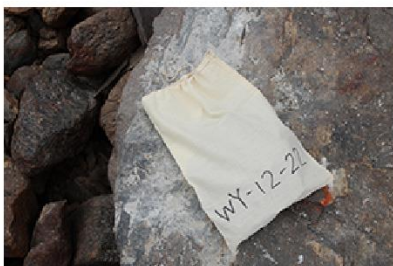

WY-12-03

WY-12-04

WY-12-08

WY-12-09

WY-12-21

WY-12-22

WY-12-23

Vita

Yanan Li comes from China. She grew up in Urumqi, Xinjiang Uyghur Autonomous Region. She received a Bachelor of Sciences degree in Geosciences from Beijing Normal University in 2008. During undergraduate years, she published a paper titled "*Precipitation in February–May Reconstructed from Tree-Ring since ca.1895 in Xiaowutai Mountains, China*" as the second author and completed a thesis about "*A Test on the Measuring Ability of LIGNOSTATION Wood Surface Scanner*". In fall 2008, Yanan was enrolled in the master's program of the University of Tennessee at Knoxville with concentrations of dendrochronology, biogeography, and climate change in the Department of Geography. She received a Master of Sciences degree in 2011, with a thesis focusing on "*Dendroclimatic Analysis of Climate Oscillations for the Southeastern United States from Tree-Ring Network Data*". From summer 2011 to summer 2015, Yanan continued her graduate study in a doctoral program in Knoxville, with fields of interests broadened to glacial geomorphology and terrain analysis using GIS. She was awarded the Doctorate of Philosophy degree in August 2015. She worked as a Graduate Teaching Assistant for the graduate years in the Department of Geography in a variety of courses, including World Regional Geography, Natural Hazards, Geography of the Natural Environment, and Quantitative Methods in Geography. She also actively participated in both local and international field trips, academic conferences, publishing peer-reviewed papers, and outreach activities. After graduation, Yanan seeks for a faculty position in some university or academic institution.